



Project Title:

## Innovative compact HYbrid electrical/thermal storage systems for low energy BUILDings

Project Acronym:

**HYBUILD**

Grant Agreement N°: 768824

Collaborative Project

# Deliverable Report

Deliverable number:

**D4.1**

Deliverable title:

## Smart System Algorithms

<b>Related task:</b>	4.1
<b>Lead beneficiary:</b>	ENG
<b>Authors and institutions:</b>	Alessandro Rossi (ENG), Giuseppe Paternò (ENG), Chiara Dipasquale (EURAC), Grazia Barchi (EURAC), Federico Trentin (EURAC), Valeria Palomba (CNR), Andrea Frazzica (CNR), Francesco Sergi (CNR), Nelson Koch (CSEM), Eduard Oró (UDL), Stratis Varvagiannis (NTUA), Yannis Mandilaras (NTUA), Werner Pink (PINK), Emhofer Johann (AIT)
<b>Due date:</b>	30/09/2018 (M12)

### DISSEMINATION LEVEL

PU	Public, fully open, e.g. web	X
CO	Confidential, restricted under conditions set out in Model Grant Agreement	
CI	Classified, information as referred to in Commission Decision 2001/844/EC.	

# Table of contents

<b>Publishable executive summary.....</b>	<b>4</b>
<b>Acronyms and Abbreviations.....</b>	<b>6</b>
<b>1 Introduction.....</b>	<b>7</b>
1.1 Aims and objectives.....	7
1.2 Relations to other activities in the project .....	7
1.3 Report structure .....	8
1.4 Contributions of partners .....	8
<b>2 Algorithms for smart control .....</b>	<b>10</b>
2.1 Introduction .....	10
2.2 Control strategies for HYBUILD.....	10
2.3 The model.....	11
2.3.1 Reinforcement learning: QLearning .....	12
2.3.2 Preliminary results.....	13
2.3.3 A distributed implementation of QLearning.....	16
2.4 Algorithms for high-level optimization .....	17
2.4.1 Mono-objective optimization .....	18
2.4.2 Multi-objective optimization .....	20
2.5 Simplified building model control implementation.....	22
<b>3 Mathematical representation of the building system.....</b>	<b>30</b>
3.1 Modelling approach.....	30
3.1.1 Methodology.....	30
3.2 Energy model of the Bordeaux demo building.....	31
3.2.1 Building Description .....	31
3.2.2 Building Geometry and envelope characteristics .....	33
3.2.3 Zoning.....	34
3.2.4 Boundary conditions / model inputs.....	36
3.2.5 Energy balance .....	38
3.2.6 Demands and peak loads .....	40
3.3 Energy model of the Cyprus demo building .....	41
3.3.1 Building Geometry .....	43
3.3.2 Zoning.....	44
3.3.3 Boundary conditions / model inputs.....	45
3.3.4 Energy balance .....	47
3.3.5 Demands and peak loads .....	48
3.4 Energy model of the Almatret demo building .....	48

3.4.1 Building Description .....	48
3.4.2 Building Geometry and envelope characteristics .....	49
3.4.3 Zoning.....	52
3.4.4 Boundary conditions / model inputs.....	53
3.4.5 Energy balance .....	58
3.4.6 Demands and peak loads .....	60
3.5 Models of the core components .....	62
3.5.1 Sorption storage.....	62
3.5.2 Chiller and latent storage.....	65
3.5.3 Electric battery .....	69
3.5.4 DC controller/inverter.....	70
3.6 Mediterranean system model .....	73
3.7 Continental system model .....	74
<b>4 Conclusions.....</b>	<b>77</b>
<b>5 References.....</b>	<b>78</b>

## Publishable executive summary

HYBUILD is an EU Horizon 2020-funded project, led by COMSA Corporación, which will develop two innovative compact hybrid electrical/thermal storage systems for stand-alone and district connected buildings.

Dynamic simulations of thermal and electric systems integrated into the building could become fundamental for analysis of complex systems. Especially when dealing with storages, both thermal and electric, static calculations are not enough for studying all the involved effects. Moreover, the influence that one technology’s behaviour has on the whole system can be analysed if all the parts of a system are simulated together. For these reasons, this report presents the modular structure used for developing the simulation environment where each component and sub-system of the HYBUILD integrated solution constitutes a module, building included. This approach allows for updating a sub-system numerical model, to develop the whole layout model before designing all the parts, or to replace a component/sub-system without losing the already created connections.

This report presents the sub-systems and core components numerical models as defined in the GA, developed within the project and used in the proposed systems layouts.

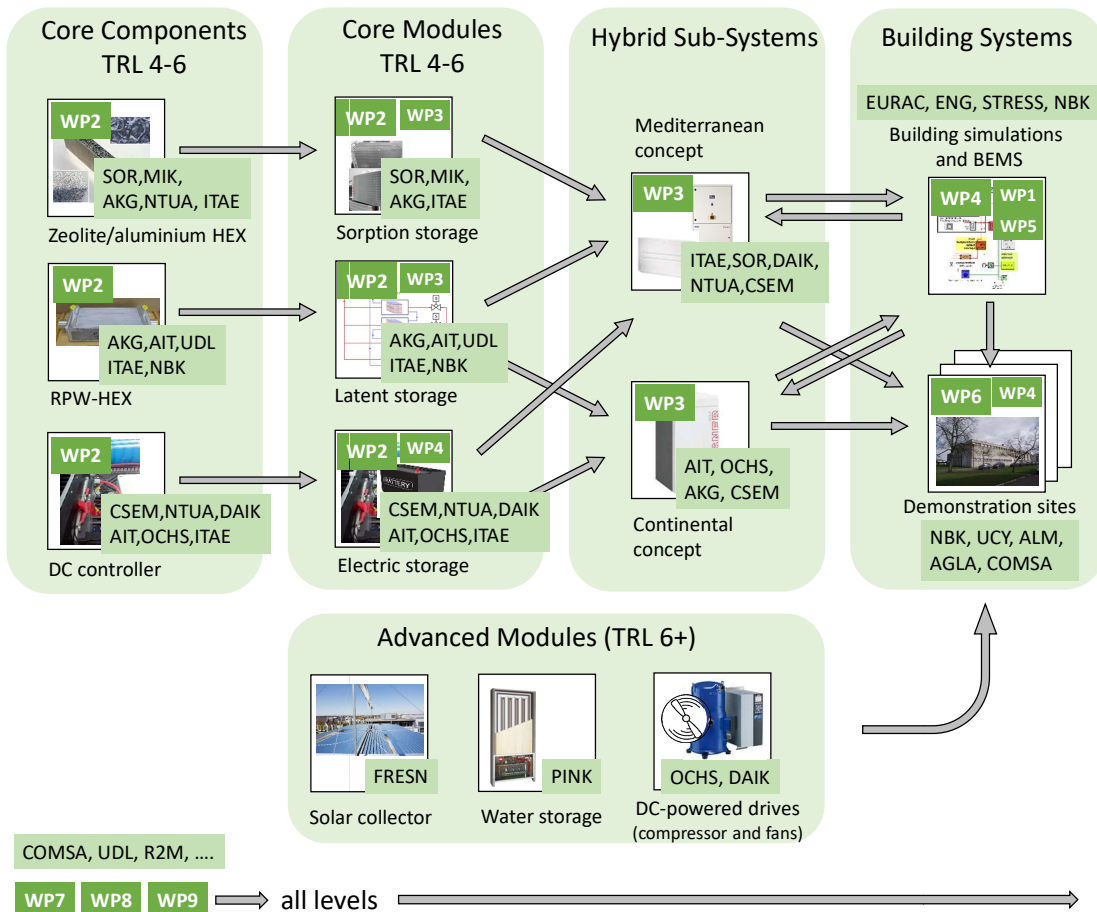


Figure 1 – HYBUILD core components, modules, sub-systems, building systems and work packages (also shown in D3.1)

For the sake of simplicity and due to the degree of detail adopted for estimating energy consumption, simplified models have been adapted in a suitable way for the thermal and electric analysis. The reduced models of the core components were developed, starting from more detailed models and experimental data, in order to carefully represent the performance

of each model, guaranteeing a high flexibility and easiness in integrating them in the overall system model. In particular, the model of the sorption storage was derived by the detailed simulation tool developed within WP3. Different operating boundaries were simulated, by varying ambient temperature and cycle time, in order to define a performance map, in terms of thermal Coefficient of Performance (COP) and cooling power. This performance map allows integrating, in the overall system simulation environment, the sorption storage to be connected to the vapour compression chiller for the Mediterranean climate. The model of the electrical battery was implemented by means of a simplified analytical approach, representing the battery with an equivalent electric circuit, which is calibrated by means of experimental data measured on a reference battery in the lab. This makes this model easily implemented in different simulation environments. The simplified implemented models were able to simulate with good accuracy the performance of the modules that will be integrated in the simulation model of the energy system for Mediterranean applications.

The unique simulation environment adopted for the whole system allows for performing energy and comfort analyses, on an hourly to a yearly basis. Finally, an additional advantage of using a numerical model of the overall system is the possibility to implement and test the adopted control strategies. The working scenarios for the two systems configurations, in the Mediterranean and in the Continental climate have been described as well. Depending on the external conditions and building loads, the generation sources or storages are used in order to minimize the energy consumption.

On top of that, a preliminary study of the background and possible control algorithm to adopt has been provided, as well, till an early overview of the main techniques in the fields of optimization processes in smart energy contexts. In particular, three types of predictive control algorithms have been proven, demonstrating they are a suitable class as well. Then, a high-level description of the main approaches and algorithms is provided in order to present the high-level energy flow optimization in contexts where several aspects have to be taken into account, thus requiring an optimization process for finding a suitable solution. A main categorisation has been adopted: after having introduced the main classes of optimization algorithms, they have been categorised in mono-objective and multi-objective processes.

This analysis provided a wide range of perspective solutions for tackling the problem of the energy flow optimization within smart energy environments, such as smart buildings. Depending on the number of aspects to be considered, the suitable approach will be selected accordingly. A first attempt of implementation has been conducted in order to provide a first proof of concept of the presented approaches. A simplified system has been used to apply the algorithms and provide the first early results. As most innovative part of the control process of the system, Demand Response (DR) has been taken into consideration as it will be further explored in the next months.

The outcomes of this activity will be used in the next phases of the project, when refined models from the components and subsystems become available, adapting the used techniques to the requirements of the system in both configurations.

## Acronyms and Abbreviations

<b>BMS</b>	Battery Management System
<b>COP</b>	Coefficient of Performance
<b>DC</b>	Direct Current
<b>DHW</b>	Domestic Hot Water
<b>DR</b>	Demand Response
<b>DSO</b>	Distribution Service Operator
<b>GA</b>	Genetic Algorithm
<b>HEX</b>	Heat Exchanger
<b>HP</b>	Heat Pump
<b>HVAC</b>	Heat, Ventilation & Air Conditioning
<b>KPI</b>	Key Performance Indicator
<b>MPC</b>	Model Predictive Control
<b>NSGA</b>	Non-dominated Sorting Genetic Algorithm
<b>OF</b>	Objective Function
<b>PCM</b>	Phase Change Material
<b>PI</b>	Proportional-Integral
<b>PLC</b>	Programmable Logic Controller
<b>PoC</b>	Proof of Concept
<b>PSO</b>	Particle Swarm Optimization
<b>PV</b>	Photovoltaic
<b>QL</b>	QLearning
<b>RL</b>	Reinforcement Learning
<b>RPW</b>	Refrigerant-PCM-Water
<b>SoC</b>	State of Charge
<b>TEXV</b>	Thermostatic Expansion Valve
<b>TSO</b>	Transport Service Operator
<b>WP</b>	Work Package

## 1 Introduction

### 1.1 Aims and objectives

The aim of this report is the presentation of the first outcomes of Work Package 4 - Smart control and System integration (WP4) in terms of study of the methodology and algorithms for the control of smart buildings, and the presentation of the first models and working scenarios of the HYBUILD system in both the Continental and Mediterranean cases. This report is the first one in WP4, which started at M3, and comes after 12 months from the beginning of the Project. The only task active in this first 10-month period of work in WP4 has been Task 4.1 - "Buildings model and system performance simulations". The same task will continue beyond the release of this report, and will end at M18. So, this report basically introduces the background, the methodology and the first outcomes of the work done about the study of the first basic algorithms and criteria of control of the system and its numerical representation for modelling and simulation, which will be finalized within WP4 in the following months.

A strong focus has been given to the clear definition of the input and outputs of the initial forecasted activities and the methodology. Basic control rules and optimization algorithms are intended to be implemented and tested in numerical models. To this aim, simplified models of each component or sub-system of both the Mediterranean and Continental cases have been received from WP3. Once received, all the parts have been put together for creating the model corresponding to each HYBUILD integrated system (Mediterranean and Continental). A clear distinction has been given to the top-down and bottom-up approach, and between the high level and low-level control: the top-down approach starts from the general overall targets, create a general approximated model of the overall system and iteratively tries to arrive at single component level having in mind what the system must do as a whole; the bottom-up, on the contrary, starts from the single components models, link, integrate and merge them in order to produce a model representative of the entire system. A top-down control will be used for the optimization algorithms, while bottom-up approach is suitable for the control rules of the overall HYBUILD integrated energy system. The first step was to individuate the control rules for each component (low-level) and the scenarios for each system layout (high level). Starting from the constraints of each device, in the next months we will try to integrate all the parts of the system and make it work properly (high level). For a better use of the system, in terms of energy consumption, comfort, environmental aspects and other KPIs (Key Performance Indicators), the optimization strategy will be able to read and forecast the loads and act for achieving the objectives.

Given the central role of the control unit within the overall the system, this report is a useful resource for the entire consortium according to the related activities described in the following section 1.2. Its dissemination level is "Public" for all external stakeholders potentially interested in a deeper understanding of the working scenarios of each HYBUILD storage system for Continental and Mediterranean applications, especially from the methodological point of view.

### 1.2 Relations to other activities in the project

Being the first report of WP4, this deliverable paves the way to the rest of the activities inside the WP. It is the starting point for the definition of the control strategies needed for the whole system operation. The control rules will be defined, together with the technologies provider partners, in Task 4.2 – "Operational function design" (starting at M12). For the aim of this report, here the working scenarios of each case are studied and presented.

As already briefly described in the previous paragraph, the low-level control will be exploited and integrated with the advanced high-level control which will be studied in Task 4.4 – “Building Energy Management System (BEMS) design”.

The simplified models of the sub-systems presented hereby have been studied with the collaboration of Task 3.1 – “Model Based Design and Control”. Detailed studies are carried out at technology level and reported in the deliverable D3.1. In this document, a reduced version of that models, which will be refined in the next months and integrated in the simulation accordingly, has been produced to be accurate enough for a representation of the component and subsystems, so as the model of the whole system can be built and described. In this sense, the interconnection and interdependency between Task 3.1 and Task 4.1 is very high, and the collaboration between the involved partners has been fostered and will be carried also beyond the end of the deliverable itself.

Finally, the developed refined models will be validated with monitoring data coming from WP6, in order to propose adjustments and refinements to the control strategies, as well.

### 1.3 Report structure

The deliverable is divided into five sections.

Section 1 describes the scope of the report, its purpose, structure, contributions and relationship with the rest of the project.

Section 2 introduces the algorithms among which the ones used for the control of the system are selected, as a brief summary of past experiences. The section ends with a first attempt of implementing one of these algorithms on a reduced simplified system.

Section 3 describes the methodology adopted for the system representation. In this section, the numerical models of sub-systems and single components are presented, along which the elaborated working scenarios for both HYBUILD hybrid storage configurations, in the Mediterranean and the Continental cases.

Section 4 concludes the report, and Section 5 provides the list of references.

### 1.4 Contributions of partners

ENG, as WP leader, coordinated the overall work and designed the structure of the deliverable. As responsible also of the next activities for the optimization, an overview of the main techniques in the fields of control and optimization processes in smart energy contexts has been provided. An analysis of the mono-objective and multi-objective algorithm families had been given, with a classification of them and a first early attempt of application to a simplified study scenario.

EURAC is responsible for the modelling of the demo case buildings and of the development of the whole system numerical model. Starting from the information provided by the demo managers on the geometry, physics and use of the buildings, energy models of the demo cases are created for assessing the building loads. This information is useful for other partners when sizing the system components. EURAC described the modelling approach and was in charge of the combination of all the partners’ components models.

ITAE proposed a simplified approach for simulating the sorption storage module, based on performance maps obtained out of the detailed simulation model implemented in Task 3.1. Similarly, also a simplified model of the electric storage (i.e. battery pack) was provided for the integration in the overall system simulation model. Finally, a detailed description of the

Mediterranean system operation was reported. In parallel, AIT studied and provided the operations for the Continental scenario.

CSEM contributed to the development of the Direct Current (DC) bus architecture as well as its associated control strategy which guarantees a stable operation of the electric system while following setpoints provided by an upper level controller.

UDL has been working on the predictive control algorithms and the detailed model of the latent storage, contributing both with a first analysis of the application of that class of algorithms and with the provision of a simplified model of the latent storage for the purposes of the deliverable.

NTUA is involved in the development of the sub-system referred to the latent storage together with the Daikin chiller.

PINK contributed at various levels for the definition of the models, as well.

## 2 Algorithms for smart control

### 2.1 Introduction

The systems layouts proposed in the HYBUILD project consist of different components and technologies that interact with each other to cover the building loads. A correct management of all the systems part allows to guarantee thermal comfort for the tenants and could lead energy savings with respect to a traditional Heat, Ventilation & Air Conditioning (HVAC) system.

Due to the complexity and novelty of the systems configuration, system performance assessment and control strategies definition are not an easy task. Studying the behaviour of one technology at time could neglect side effects due to the integration of different sub-systems.

For this reason, the modelling of the energy plant and the building as a whole is crucial for:

- assessing the system performance and energy consumption, included the share between renewable and not-renewable;
- developing and testing a comprehensive control strategy able to manage the whole system.

The used modelling environment is TRNSYS [1] as it allows for dynamically simulating:

- building energy model with internal gains schedule and energy contribution from the HVAC system;
- hydronic system in all its components as pumps, valves, pipes in addition to the energy generation devices and storages;
- control rules for managing each active component;
- different scenarios and working conditions.

### 2.2 Control strategies for HYBUILD

Three types of control algorithms will be described in this section, along with their potential applications in WP4 as well as their benefits and pitfalls, giving some results obtained in particular thermal storage systems.

#### ***Model Predictive Control***

Model Predictive Control (MPC) algorithms are suitable when the system models are linear or present few and particular non-linearities. As MPC performance is almost optimal, their utilisation can be highly recommended when systems fulfil the above mentioned linearity constraints. Examples of MPC applied to the control of thermal energy storage systems will be presented, with their corresponding performance results in Section 2.1.2.

#### ***Reinforcement Learning***

When system models are complex and/or highly non-linear some optimal control techniques fail in offering suitable solutions. In this sense, reinforcement learning algorithms have shown excellent performance for short- and long-term management of thermal energy storage systems. Even more, their easy distribution makes these algorithms particularly suitable to be implemented in cluster environments, speeding up learning times. Two implementations of reinforcement learning based on QLearning (QL) will be presented with application to complex thermal energy storage systems with their corresponding preliminary results. One of those solutions will be based on a naive and approximate version of a QLearning algorithm that

showed a good performance and an excellent scalability in supercomputer environments. The second implementation is an exact implementation of a QLearning algorithm for supercomputer environments using distributed memory stored structures that are currently being tested.

### Deep Learning

The same storage case studies used for reinforcement learning will be used to test some new deep learning implementations for control. Preliminary results will be presented as well as the best-found techniques so far.

The analysis performed for this deliverable contains a first approach to the utilisation of Reinforcement Learning (RL) algorithms to control HYBUILD-like systems.

## 2.3 The model

As the HYBUILD models needed to support learning strategies will be delivered in the current work package, a simple model was defined to simulate the Mediterranean system behaviour on winter operation. Even though knowing that the real model will surely present substantial differences, we think that the main aspects and tuning parameters of the control strategies derived from this first approach may result interesting for a definitive version of the HYBUILD control strategies.

Figure 2 depicts the simplified HYBUILD winter operation model.

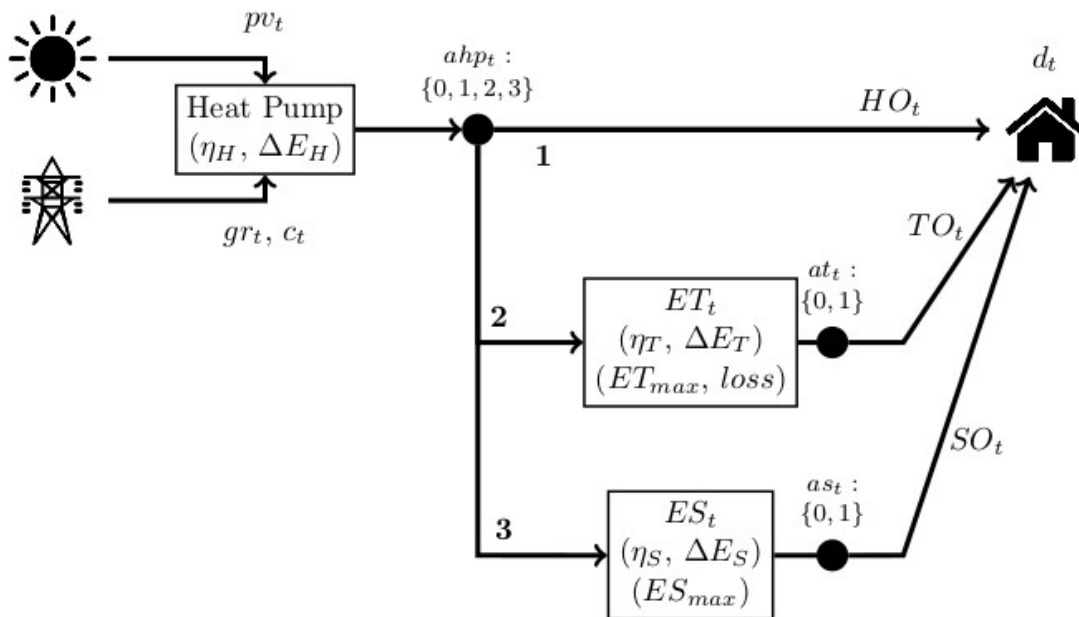


Figure 2 - HYBUILD Continental climate during winter operation simplified model

The model describes the system in discrete slot times (subscript  $t$ ). It is operated by a Heat Pump (HP) with efficiency and discrete energy output in a time slot of  $E_H$  (when required), driven either by photo-voltaic source ( $pv_t$ ) or electricity from grid ( $gr_t$ ) at cost ( $c_t$ ). Two energy storage systems are devised to buffer the energy provided by the HP. One of them is thermal energy storage and the other is sorption energy storage, each of them with their corresponding efficiencies, energy output capabilities per time slot and maximum energy storage.  $ET_t$  and  $ES_t$  denote, respectively, their storage status at any time  $t$ . Both storage systems operate identically in our model, with the difference that thermal energy storage presents some losses (loss) not considered in the sorption energy storage, modelling this way,

short- and long-range storage. Furthermore, the model has three activation valves (or actions):  $ahp_t$  set to 0 if no energy is required from HP, or set to 1, 2, or 3 if energy is to be sent directly to demand, thermal, or sorption energy storage, respectively. Actions  $at_t$  and  $as_t$  determines if energy is required from thermal and/or sorption energy storage to demand. Finally, the demand ( $d_t$ ) is fulfilled by outputs  $HO_t$ ,  $TO_t$  and/or  $SO_t$ .

The following figure shows the set of equations that describes the system dynamics:

$$gr_t = \mathbb{1}_{(ahp_t > 0)} \cdot \max\left(\frac{\Delta E_H}{\eta_H} - pv_t, 0\right), \quad (1)$$

$$ET_{t+1} = \min(\max(ET_t + \eta_T \cdot \Delta E_H \cdot \mathbb{1}_{(ahp_t=2)} - \Delta E_T \cdot \mathbb{1}_{(at_t=1)} - loss, 0), ET_{max}), \quad (2)$$

$$ES_{t+1} = \min(\max(ES_t + \eta_S \cdot \Delta E_H \cdot \mathbb{1}_{(ahp_t=3)} - \Delta E_S \cdot \mathbb{1}_{(as_t=1)}, 0), ES_{max}), \quad (3)$$

$$HO_t = \Delta_H \cdot \mathbb{1}_{(ahp_t=1)} \quad (4)$$

$$TO_t = \mathbb{1}_{(at_t=1)} \cdot \min(\Delta E_T, ET_t) \quad (5)$$

$$SO_t = \mathbb{1}_{(as_t=1)} \cdot \min(\Delta E_S, ES_t) \quad (6)$$

$$rew_t = \mathbb{1}_{(d_t > HO_t + TO_t + SO_t)} \cdot Penalty + gr_t \cdot c_t \quad (7)$$

Figure 3 - Set of equations describing the system dynamics

Eq. 1 determines the power grid requirement, being  $\mathbb{1}_{(x)}$  and indicator function. Eqs. 2 and 3 reflect the storage status. Eqs. 4, 5, and 6 reflect the energy requirements to demand. Finally, a RL strategy was implemented based on QLearning (QL). Eq. 7 describes the QL reward function, assuming a penalty reward. In our experimentation, it was always assumed as constant ( $c_t = 1$ ).

The demand profile ( $d_t$ ) was generated for two weeks, one week in summer time (to allow charging for the long-term sorption storage) and another in winter time, for a particular location (i.e. Paris). On week days, demand is on during two different time periods, namely, from 6:00 to 9:00 hours and from 17:00 to 23:30. On week-end days, activation is from 9:00 to 23:30 hours. During this activation periods,  $d_t$  is set to 1 when outside temperature falls below a given set-point (15 °C.) and set to 0 otherwise. All efficiencies are set to 1, but  $\eta_H = 1/400$ .  $\Delta E_H$ ,  $\Delta E_T$ , and  $\Delta E_S$  were chosen to be 0.8, and the maximum storage times for thermal and sorption were set to 2 hours and to 1 day, respectively, of maximum demand. Losses for the thermal energy storage were set to 10% for every time slot, with 30' as time slot value.

### 2.3.1 Reinforcement learning: QLearning

One can think on different control strategies for HYBUILD. MPC is a kind of strategy that has been probed to work efficiently for thermal energy storage systems, especially when coupled with Mixed Integer Non-Linear Programming solvers [2] [3]. For this type of control, models have to be almost linear, because the coupled minimising solvers only support a few type of non-linear functions. When models are numeric or far from linear, one should devise other strategies. Local search may be an option, admitting any type of models, but presents high computational requirements that may prevent from operating the control system in real time. Conversely, RL control algorithms, even though the learning process is time consuming, they can be done off line and using super-computing resources, which allows to perform real time

control operation based on look-up tables, easily implemented on small devices. As at the UDL we have designed and implemented different reinforcement learning strategies under distinct control scenarios [4] [5] [6] [7], here we propose a RL based on QLearning for HYBUILD.

A RL strategy involves a set of actions ( $A$ ) and states ( $S$ ). The  $A$  set is defined, in our case and for every  $t$ , by the triplet  $(ahp_t, at_t, as_t)$ .

$S$  is defined by the vector:  $(ET_t, ES_t, d_t, T_t, R_t, T_{t+1}, R_{t+1}, \dots, T_{t+NF}, R_{t+NF})$ , being  $T_t$  and  $R_t$  the environment temperature and solar radiation at time  $t$ , and being  $NF$  the number of future states (in time slots) to observe. As all state levels are continuous, we should discretize them with a predetermined number of discretization levels. A Q-table function is defined according to the following equation:

$$Q(s_t, a_t) = (1 - \alpha) \cdot Q(s_t, a_t) - \alpha \cdot (rew_t + \gamma \cdot \min_a Q(s_{t+1}, a)) \quad (8)$$

defining the value of a given action ( $a_t$ ) at a given state ( $s_t$ ), and being  $\alpha$  and  $\gamma$  the learning rate and discount factor parameters. Eq. 8 is computed iteratively over a repeated number of episodes. In our case, episodes consist of the two above mentioned weeks. When iteration is performed, a random action is chosen, instead of the best one, with some decay probability, in order to perform a large exploration of the space state.

### 2.3.2 Preliminary results

In order to test the performance of the QL algorithm developed, first a training set and a test set was defined, consisting of two weeks (summer and winter) of temperature, radiation and demand data. Figure 4 shows the total reward evolution according to the number of learning iterations (up to 15,000). One can observe an optimal reward for  $NF = 6$ , which seems to indicate that there is no advantage on taking more future states, in our case. We compared the performance against a simple control policy that obeys to some simplistic rules. In this case, the rules are the following:

- Provide the demand from thermal and/or sorption energy storage when possible.
- If solar radiation exists, then charge the thermal energy storage.
- If thermal energy storage is full, then charge the sorption energy storage.

As observed, QL control outperforms such a basic simple control operation for the trained set, but when checked for a test set, its performance is comparable (see Figure 5). Obviously, the reason relies on the fact that not enough training data was provided during the learning process.

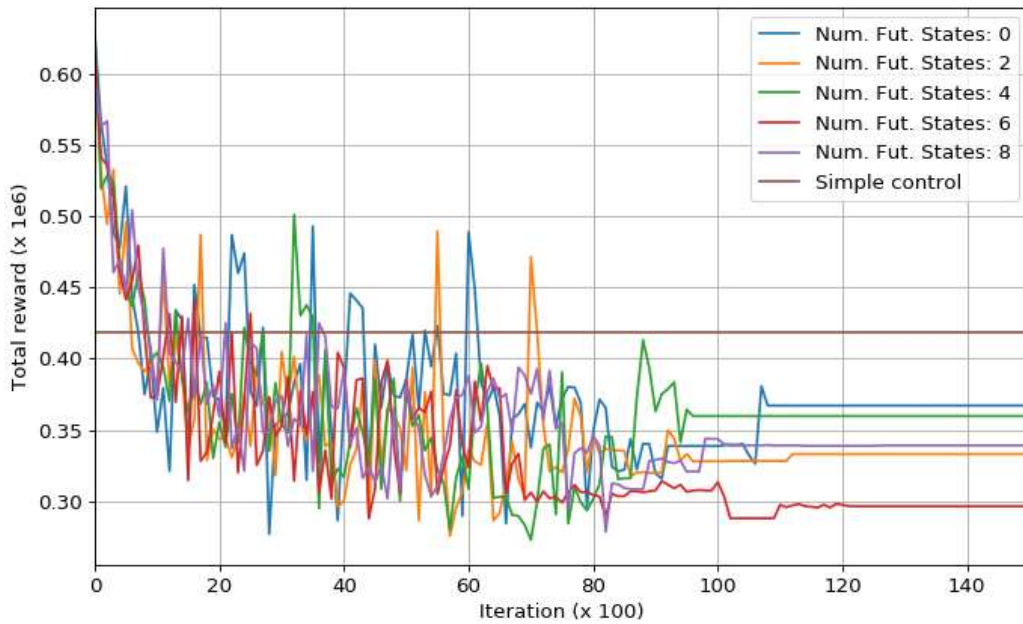


Figure 4 - Total reward for Penalty = 5000

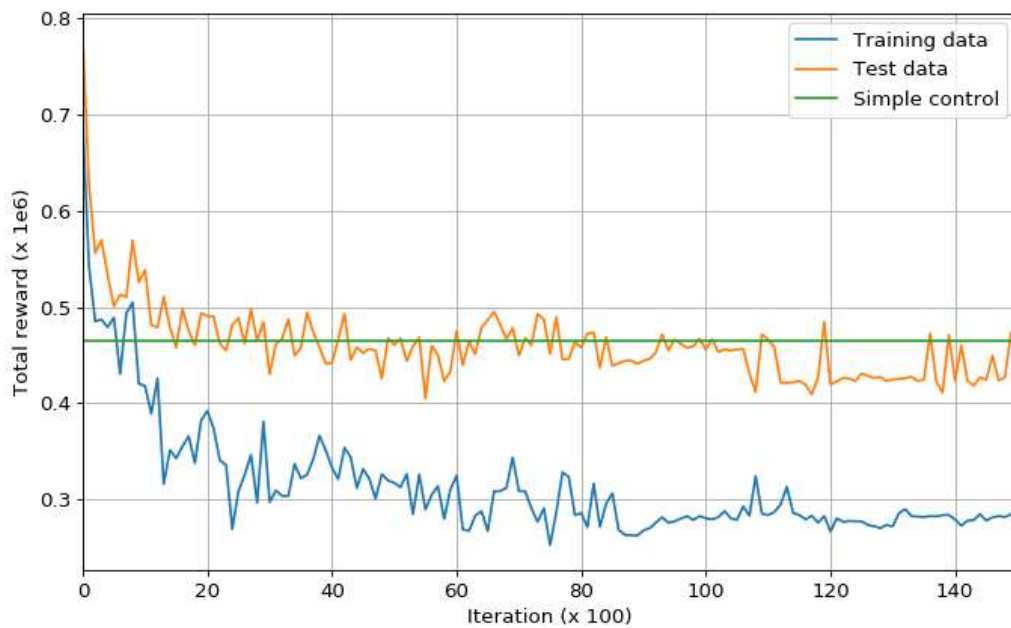


Figure 5 - Total reward for NF=6

To improve the learning, a larger training set of 16 weeks (8 summer and winter weeks) was built and their performances were compared for different values of NF. As shown in Figure 6 the performance over the test set has clearly improved. Actually, the best NF parameter has now changed, being low values of NF the more advantageous. This fact can be explained because on test set instances, some of the visited states are unknown, occurring more

frequently for higher values of NF. Of course, such an effect may change for a larger training set.

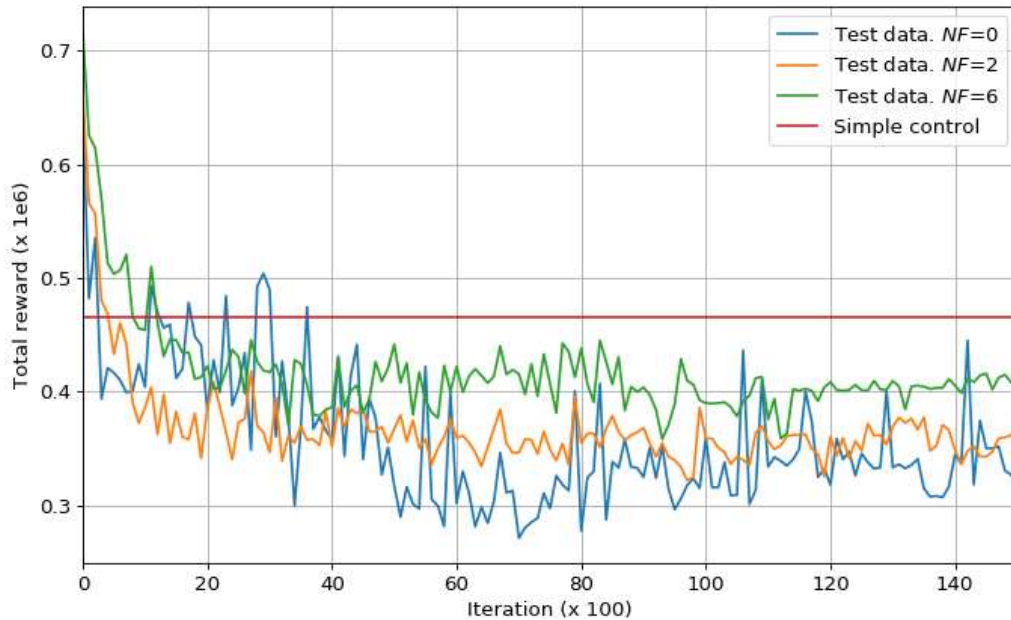


Figure 6 - Total reward training for 16 weeks

Figure 7 shows the behaviour of the QL on the test data set. The upper plot shows the thermal and sorption tanks status, and the demand profile as well. In this plot one can observe that QL decides to charge the sorption tank during the first week (summer) in order to use it during the second week (winter) with very low reward (energy from grid), by using photo-voltaic energy. This sorption storage is largely spent during the winter week, in order to minimise reward. One can also observe periodic charging phases on thermal energy storage during solar radiation peaks on winter that are discharged during demand requirements. The central plot shows the activation decisions on the HP and the storage tanks. The lower plot shows the radiation and outer temperatures of the test data.

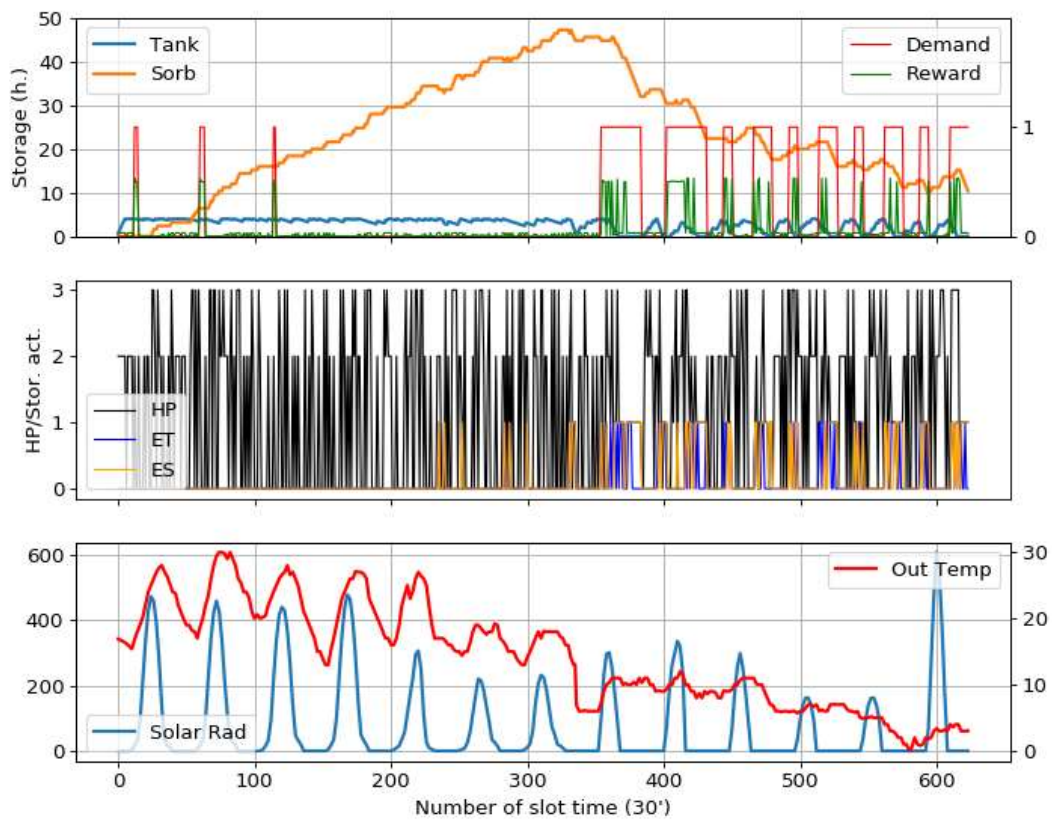


Figure 7 - Behaviour of QL algorithm

### 2.3.3 A distributed implementation of QLearning

To tackle with the dimensionality problems arising from such a complex problem, namely, the enormous search space to explore, a feasible approach for the training phase is to do it in a distributed way.

To such goal, we have designed a method to carry out the training using the supercomputing facilities existing in the University of Lleida. Some PoC (proof of concept) implementations of the learning algorithms are on the way.

On those initial PoC, the implementation of our distributed algorithm for QLearning requires the availability of some shared, distributed, and network-accessible data structures (primarily, as is the mainly needed one, a distributed dictionary/hash table) being accessed by all the agents exploring the search space to coordinate their search effort.

Our implementation relies on having several agents running independently (each one on a server on a cluster of machines), and, instead of having their local Q-Table, they access a remote implementation of a shared Q-Table. That way, although they all crawl the search space independently, all the values they learn are stored on the unique shared Q-Table, being immediately accessible for the remaining agents. The agents also use the shared data structures to create a set of locking semaphores to coordinate the access to Q-Table rows, to avoid concurrence updates. The current implementation (1 write lock / n read rows) is deadlock safe.

## 2.4 Algorithms for high-level optimization

The complexity of a typical smart energy scenario and of the related smart system architecture relies upon the high number of actors involved in the implementation of smart actions, the different parts of the energy chain addressed, and the several goals pursued by the manager of these smart scenarios. Moreover, a plenty of very diverse technology are interested and installed in these contexts, making their integration and operation very difficult, especially for the management of dynamic behaviours.

The actors responsible of the grid are in charge of managing both technical contingencies and power quality targets over an infrastructure that spans physically over several kilometres. In many cases, these grid operators have to deal with virtual actors addressing financial and market aspects, as well as entities dealing with regulatory and policy topics. Moreover, many entities are involved in production and injection of power into the power systems, gaining economic benefits from the sale of the produced energy and/or the incentives related to the exploitation of renewable energy. Also consumption actors present many differences, in terms of absorption features, flexibility, control capability, dynamic services provided. The modern technologies such as storage devices, electric vehicles, smart metering systems, etc. are changing the typical energy consumption patterns and features of the grids they are connected to. The operations and the dynamic features entailed by these actors require a high level of interdependency among them, especially in balancing the generation and absorption phases, in managing grid operations, and in addressing economic aspects.

In this view, the implementation of optimization processes permits to solve most of the issues related to the management of smart systems [8].

The most referenced and addressed optimization methods are listed in the following:

- Linear programming [9]
- Convex optimization [10]
- Heuristic optimization [11]
- Dynamic programming [12]
- Stochastic optimization [13]
- Robust programming [14]
- Machine learning [15]
- Game theory [16]
- Multi-agent systems [17]

In the following sections, an overview on the most adopted heuristic algorithms is provided. They have been appointed for their flexibility and adaptability in several different smart energy contexts. They implement non-exact procedures for the solution of many complex problems, due to the nature of the problem, for the mathematical complexity of their functions, for the variables involved, for the uncertainty of some parameters, or for the dimension of the solution space. Despite of the loss of exactness, the heuristic algorithms allow addressing a wide number of problems that could not be solved otherwise. Moreover, the heuristic approach allows implementing multi-objective optimization.

### 2.4.1 Mono-objective optimization

A typical mono-objective optimization problem refers to a mathematical formulation that models the energy environments under management, for instance by means of Objective Functions (OFs) and constraints. The most general definition of such a problem is as follow [18]. A general optimization problem is defined as minimizing (or maximizing) the function  $f(\mathbf{x})$  subject to inequality constraints, expressed by the functions:

$$g_i(\mathbf{x}) \leq 0, \quad i = \{1, \dots, m\}, \mathbf{x} \in \Omega$$

and equality constraints, expressed by the functions:

$$h_j(\mathbf{x}) = 0, \quad j = \{1, \dots, p\}, \mathbf{x} \in \Omega$$

where  $m$  is the number of inequality constraints, whilst  $p$  is the number of equality ones.

A solution minimizes (or maximizes) the scalar  $f(\mathbf{x})$ , where  $\mathbf{x}$  is a  $n$ -dimensional decision variable vector  $\mathbf{x} = (x_1, \dots, x_n)$  from some universe  $\Omega$ .

$g_i(\mathbf{x}) \leq 0$  and  $h_j(\mathbf{x}) = 0$  represent constraints that must be respected by the optimization of  $f(\mathbf{x})$ .  $\Omega$  contains all possible  $\mathbf{x}$  that can be used to satisfy an evaluation of  $f(\mathbf{x})$  and its constraints. Of course,  $\mathbf{x}$  can be a vector of continuous or discrete variables, as well as  $f(\mathbf{x})$  can be continuous or discrete.

The optimization of mono-objective problem is based on the mathematical formulation provided in the previous section. Here a list of the most referenced algorithms used on the field of smart energy systems:

- Genetic Algorithm [19] [20];
- Differential Evolution [21];
- Evolution Programming [22];
- Simulated Annealing [23] [24];
- Tabu Search [25] [26];
- Firefly [27];
- Shuffled Frog Leaping [28] [29];
- Particle Swarm Optimization (PSO) [30] [31];
- Artificial Bee Colony [32] [33];
- Ant Colony Optimization [34];
- Whale Optimization [35];
- Cuckoo Search Algorithm [36].

A typical mono-objective algorithm application could be reported describing the Particle Swarm Optimization (PSO) process, whose flow chart is shown in Figure 8. In this algorithm the population is modelled as a school of fishes or a swarm of birds in which the behaviour of each agent inside the group can be represented with simple vectors. In this logic each agent utilizes two important kinds of information in decision process. The first one is their own experience; that is, they have tried the choices and know which state has been better so far, and they know how good it was. The second one is other people's experiences; that is, they have knowledge of how the other agents around them have performed.

Modification of the agent position is realized by the position and velocity information. Each agent knows its best value so far (pbest) and its x, y position. This information is an analogy of the personal experiences of each agent. Moreover, each agent knows the best value so far in the group (gbest) among pbests. This information is an analogy of the knowledge of how the other agents around them have performed.

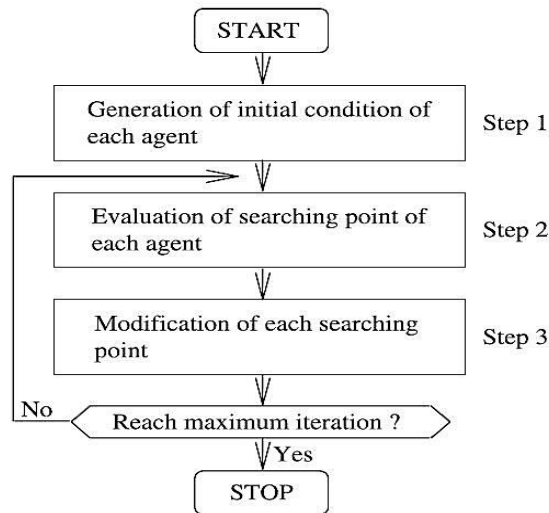


Figure 8 - Basic flow chart of PSO

Each agent tries to modify its position using the following information:

- the current position
- the current velocity
- the distance between the current position and pbest
- the distance between the current position and gbest

Velocity of each agent can be modified by the following equation:

$$v_i^{k+1} = wv_i^k + c_1rand1 * (pbest - s_i^k) + c_2rand2 * (gbest - s_i^k)$$

Where

- $v_i^k$  is the current velocity that generally weighs less than the other two terms;
- $s_i^k$  is the current position of the agent;
- $v_i^{k+1}$  is the modified velocity;
- $w, c_1, c_2$  are weight that can be chosen arbitrarily, generally  $c_1$  and  $c_2$  are equal to 2 and  $w$  is calculated by the following equation:

$$w = w_{max} - \frac{w_{max} - w_{min}}{iter_{max}} * iter$$

With typical value  $w_{max} = 0.9$  and  $w_{min} = 0.4$ .

The current position can be modified by the following equation:

$$s_i^{k+1} = s_i^k + v_i^{k+1}$$

The concept of the algorithm is shown in Figure 9.

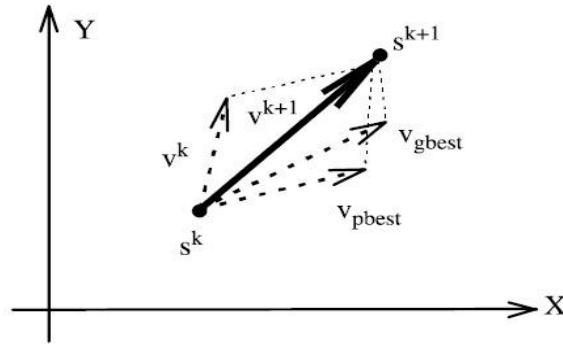


Figure 9 - Concept of modification of a searching point by PSO.

In case of binary variable, the PSO method must be modified as shown below. The model is modified adding a probability agent,  $v$ , to be able to make the decision ON or OFF. If  $v$  is higher, the agent is more likely to choose 1, and lower values favour 0 choice. Such a threshold requires staying in the range  $[0, 1]$ . One of the functions accomplishing this feature is the sigmoid function, which is usually utilized in artificial neural networks.

$$\text{sig}(v_i^k) = \frac{1}{1 + \exp(-v_i^k)}$$

Like the basic continuous version, the formula for the binary version of PSO can be described as follows:

$$v_i^{k+1} = wv_i^k + c_1 \text{rand1} * (pbest - s_i^k) + c_2 \text{rand2} * (gbest - s_i^k)$$

$$\rho_i^{k+1} < \text{sig}(v_i^{k+1}) \quad \begin{cases} \text{then} & s_i^{k+1} = 1 \\ \text{else} & s_i^{k+1} = 0 \end{cases}$$

Where  $\rho_i$  is a positive random number in the range  $[0.0 ; 1.0]$ .

## 2.4.2 Multi-objective optimization

As for smart energy scenarios implementation, the complexity of the contexts often address several goals to be pursued at the same for obtaining a comprehensive optimal management of the controlled system. For instance, the objective functions could refer to economics aspects, environmental issue, technical operations, etc. In this view, multi-objective optimization algorithms give great contribution to the setting up of such a complex optimization framework. These algorithms allow for taking into consideration two or more objectives function simultaneously.

The mathematical formulation of this kind of techniques is based on the Pareto-optimality theory [37]. The multi-objective optimization approach does not provide a unique solution, but a set of Pareto-optimal solutions. The solution that fits better the overall goal of the controlled system, for instance the one that offers the best trade-off conditions among the different criteria implemented, has to be chosen among the different solutions composing the Pareto-optimal solution front. This task is often performed by a decision support tool in order to simplify the choice.

The multi-objective optimization problem is formulated as follows [18]. Assuming that  $f_z(\mathbf{X})$  are  $k$  different objective functions, the multi-objective problem is defined as minimizing the vector of functions:

$$\mathbf{F}(\mathbf{X}) = [f_1(\mathbf{X}), \dots, f_k(\mathbf{X})]^T$$

which is subject to a set of inequality constraints, defined as:

$$g_i(\mathbf{X}) \leq 0 \quad i=1, \dots, m$$

and a set of equality constraints, defined as:

$$h_j(\mathbf{X}) = 0 \quad j=1, \dots, p.$$

The decision variables are the numerical values which are expected to be chosen, as solutions, by the multi-objective optimization. They are the independent variables of the objective functions and are used to minimise them; they are represented as the vector:

$$\mathbf{X} = [x_1, \dots, x_n]^T \quad \mathbf{X} \in \Omega$$

where  $\Omega$  is a n-dimensional vector space and represent the set of the feasible region of  $\mathbf{X}$ .

As already mentioned, the multi-objective optimization algorithms are based on Pareto-dominance and Pareto-optimality. A solution  $\mathbf{X} \in \Omega$  is said to be Pareto-optimal with respect to  $\Omega$  if and only if there is no  $\mathbf{X}' \in \Omega$  for which

$$\mathbf{v} = \mathbf{F}(\mathbf{X}') = [f_1(\mathbf{X}'), \dots, f_k(\mathbf{X}')]^T$$

dominates

$$\mathbf{u} = \mathbf{F}(\mathbf{X}) = [f_1(\mathbf{X}), \dots, f_k(\mathbf{X})]^T.$$

A vector

$$\mathbf{u} = [f_1(\mathbf{X}), \dots, f_k(\mathbf{X})]^T$$

is said to *dominate* another vector

$$\mathbf{v} = [f_1(\mathbf{X}'), \dots, f_k(\mathbf{X}')]^T$$

(denoted by  $\mathbf{u} \leq \mathbf{v}$ ) if and only if  $\mathbf{u}$  is partially less than  $\mathbf{v}$ , i.e.,

$$\forall i \in \{1, \dots, k\}, u_i \leq v_i \wedge \exists i \in \{1, \dots, k\}: u_i < v_i.$$

Therefore, the Pareto-optimal Set,  $\mathcal{P}^*$ , is defined as:

$$\mathcal{P}^* := \{\mathbf{X} \in \Omega \mid \neg \exists \mathbf{X}' \in \Omega: \mathbf{F}(\mathbf{X}') \leq \mathbf{F}(\mathbf{X})\}.$$

The most referenced and appointed multi-objective optimization algorithms implemented for managing such complex management systems are listed in the following:

- Indicator-Based Evolutionary Algorithm [38];
- Non-dominated Sorting Genetic Algorithm II (NSGA-II) [39];
- Strength Pareto Evolutionary Algorithm 2 [40];
- Pareto Archived Evolution Strategy [41];
- Multi-objective particle swarm optimization [42];
- Multi-Objective Bee Foraging Algorithm [43];
- Multi-Objective Dragonfly Algorithm [44].

One of the most referenced algorithms in this field is the Non-dominated Sorting Genetic Algorithm II (NSGA-II). This algorithm is based on Pareto-dominance and Pareto-optimality and many recent papers [45] [46] [47] [48] have proved that the NSGA-II is quite efficient, especially in the field of power distribution operation and planning.

This genetic algorithm separates and orders the population (the set of all the individuals) following a criterion based on non-dominance: individuals which are not dominated by any

other individual are labelled with a higher rank; individuals that do not dominate any other individual have a lower rank. Another sorting criterion is implemented within each rank, based on the concept of crowding distance, which is an index evaluating how an individual of the population is close to the neighbour elements in the solution space. By means of a Binary Tournament Selection, individuals with the best rank are chosen to be the parents of the offspring generation. Following the analogy with the biological phenomena, crossover and mutation actions are performed on the selected elements, through Simulated Binary Crossover and Polynomial Mutation mechanism. Now, the parent and the child population are mixed and only the best  $N$  individuals are chosen for the next generation, where  $N$  is the population size. This is one of the most innovative features of the NSGA-II, called elitism, which avoids possible losses of valuable solutions. After having repeated these steps for a prefixed number of generations, the algorithm results are an entire population of Pareto-optimal solutions.

In Figure 10, the flow chart of the algorithm and the elitism concept are shown.

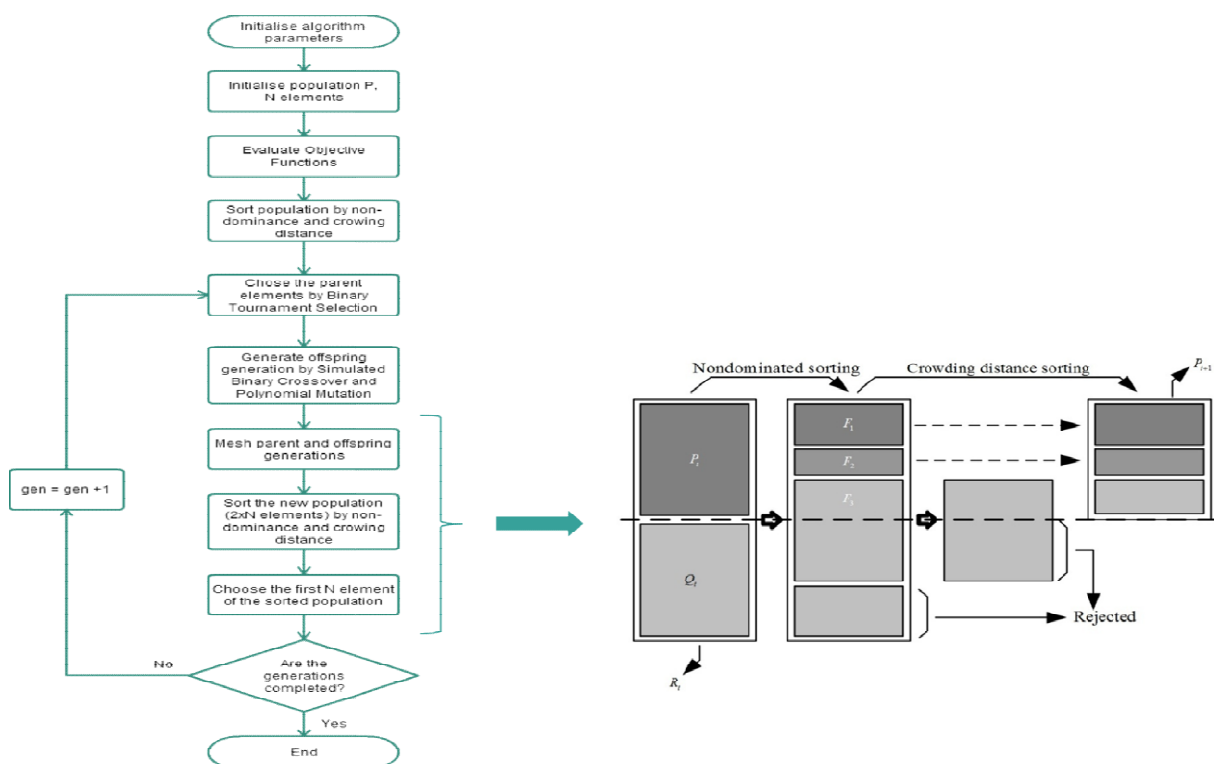


Figure 10 - Flow chart of the implemented NSGA-II algorithm and elitism block representation.

## 2.5 Simplified building model control implementation

In parallel with the bottom up approach followed for the production of the system models, thus starting from the low level models of components and subsystems (which will be addressed in Section 3), a top down approach has been attempted to provide a benchmark for the following optimization phases inside the WP. A very simplified building model has been used, with the only aim to describe and control the power flow inside the building. With this layout, it is possible to maximize energy efficiency, maximize local usage of renewables, minimize the costs and minimize CO<sub>2</sub> emissions. In addition, according to different protocol and interface, monitoring and asking request from Distribution/Transport Service Operators (DSO/TSO) for Demand Response (DR) can be implemented, providing to the energy retailer the possibility to manage the power flow and guarantee the safety and reliability of the network.

The core components of the HYBUILD overall integrated system are: low temperature latent storage, heat pump, sorption thermal storage, electric storage, water storage, Photovoltaic (PV) energy source and thermal collector energy source. The basic layout of the system is shown in Figure 11.

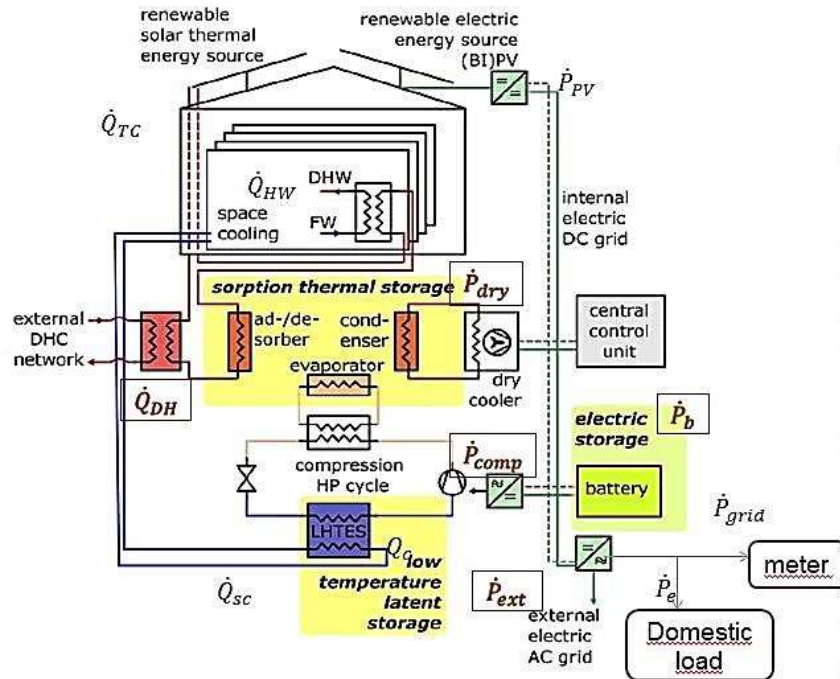


Figure 11 - Basic system layout with power/energy variables

With:

- $\dot{Q}_{TC}$  and  $\dot{P}_{PV}$  the power flows from thermal collector and PV;
- $\dot{Q}_{HW}$  the domestic demand of hot water;
- $Q_h$  the energy stored in the water storage;
- $\dot{Q}_{DH}$  the flow power came from district heating;
- $\dot{P}_{dry}$  the electric power to turn on the dry cooler;
- $Q_C$  the energy stored in the latent storage;
- $\dot{Q}_{sc}$  the cold demand of the house;
- $\dot{P}_{comp}$  the electric power absorbed by heat pump;
- $E$  energy stored in the electric storage;
- $\dot{P}_{ext}$  power exchanged with AC bus;
- $\dot{P}_b$  power exchanged from the battery;
- $\dot{P}_e$  electric demand;
- $\dot{P}_{grid}$  power exchanged with the grid.

These physical quantities are not independent because they are related to each other with the electric/thermal equations.

Before going into details of the algorithm, it is necessary to show the fundamentals hypothesis:

1. No power losses in the two thermal storages;
2. No power losses in the compression heat pump;
3. Battery is modelled with a resistance in series;
4. The components were implemented with their stationary models;

5. The problem is discretized in timestamps during which every control variable is constant;
6. Demand response service is provided as €/kW for each hour (no dependence on quantity);
7. The request of heating/cooling/electric loads is given with known accuracy.

Regarding equations, for the DC-bus, it is possible to write the following equations:

- $\Delta E = \dot{P}_b * \Delta t$
- $\dot{P}_{PV} \pm \dot{P}_{ext} \pm \dot{P}_b - \dot{P}_{comp} - \dot{P}_{dry} = 0$
- $\dot{P}_{grid} = \pm \dot{P}_{ext} + \dot{P}_{el}$

For the low temperature latent storage, it is possible to write the following equation with the hypothesis ideal component:

- $\Delta t [\dot{Q}_{sc} - \dot{P}_{comp} * COP] = \Delta Q_{cold}$

For the compression heat pump actually, the equation of the Coefficient of Performance (COP) is not known. In a logic of absolute optimization, the optimizer needs the function that ties the boundary temperature of heat pump and  $\dot{P}_{comp}$  to the power absorbed from the evaporator and the power leave to condenser but this function is often not given by manufacturer or is difficult obtain it. Sometimes, the manufacturer writes in the datasheet a table that relates the boulder temperature with the COP mask which is the algorithm they use. In this case it is necessary to implement the table in the algorithm of optimization.

Firstly, the COP is assumed constant in every condition with the consciousness that it is an unreal hypothesis but it can be changed simply in future. The electric power supplied to the dry cooler instead is assumed linear dependent from the power supplied to the heat pump. Such as:

$$P_{dry\ cooler} = k * P_{comp} \quad k \in \mathbb{R}$$

The last main component is the sorption thermal storage which, in first step, was modelled like a storage unit and, in a second time it has been modelled like two absorbers and two vacuum chambers for condenser and evaporator whose operating maps are known.

In this system, for each time interval there are 4 independent control variables: the heat pump, the power exchanged with the grid, the power exchanged from the battery (which is tied to the previous two from the equations of the DC-bus) and the heat coming from the district heating that in this step is assumed equal to zero with a view to increasing the self-consumption therefore the number of independent control variables is reduced to two. The target of the problem, thus, is finding when how these two controllable components have to work in each time interval. If the day is divided in steps of one hour the result is that the problem has  $24*2=48$  independent variables, if the step is 30 minutes the variables became 96. Another important aspect is that some variables are binary or discrete and some are continuous, so the analytical method cannot be applied. It is simple to understand that the problem has a high level of complexity whatever the objective functions are. To avoid the multi-objective optimization a method that embraces the target seen before is an optimization of the cost with a function expressed like:

$$OF = C_{in} * \dot{P}_{grid-} + C_{out} * \dot{P}_{grid-out}$$

Where

- $\dot{P}_{grid-out}$  and  $\dot{P}_{grid-in}$  is the power exchanged with the grid (assuming negative the power sold);
- $C_{in}$  and  $C_{out}$  are the hourly costs of selling and purchasing (€/kWh).

Minimise this function means finding the solutions that allow the minor energy consumption thus the better use of the resources. This function however can be seen as the product of two functions. One is the power exchanged and other is the profile cost which can represent the power profile of the DSO. For example, if in a specific hour  $t^*$  of the day, the DSO needs power injected to grid it can change  $C_{out}$  profile increasing  $C_{out}(t^*)$ , viceversa if it wants a consumption of energy it can change  $C_{in}$  profile reducing  $C_{in}(t^*)$ . Whether the rated power of the system will increase considerably the hourly costs of selling and purchasing could become dependent from quantity of the power and not only in direction but for this system the capacity of the components is too low for this representation.

In order to solve the objective function is necessary to find the correct method. The main algorithms to solve this problem are:

1. Analytical methods;
2. Linear programming;
3. Simulated Annealing;
4. Tabu Search;
5. Genetic Algorithm (GA);
6. Particle Swarm Optimization;
7. Ant Colony Optimization.

Basically the algorithm has to choose two independent variable of the system, compute the other variables and estimate  $\dot{P}_{grid}$  and the OF. The first problem is that the physical parameters of the problem are linked by non-linear equations thus the Linear Programming doesn't work.

As said before the analytical methods cannot be applied thus the research has been oriented to heuristics techniques. The second problem is that, obviously, the solution must satisfy the physical constraints:

1.  $0 > Q_{c0} + \Delta Q_c > Q_{cmax}(10kWh)$  Energy in Latent High Temperature Storage
2.  $E_{min} < E_0 + \Delta E < E_{max}(6kWh)$  Energy in Electric Battery
3.  $P_{ext}^{min} \leq \dot{P}_{ext} \leq P_{ext}^{max}(\pm 5kW)$  Power Flow in the inverter between DC-bus and AC-bus
4.  $P_b^{min} \leq \dot{P}_b \leq P_b^{max}(\pm 3kW)$  Power Flow in the electric battery
5.  $0 \leq \dot{P}_{comp} \leq P_n(6kW \text{ a passo } 0.6kW)$  Power supplying by heat pump
6.  $0 \leq \dot{Q}_{DH} \leq \dot{Q}_{DH}^{max}$  Heat coming from district heating (neglected in this step)
7. (obviously there is also a constraint in the water storage but actually is unknown the dynamic of this thermal section)

This means that the problem needs to pay close attention to the choice of independent variables in order to find as many solutions as possible. Thus, for a fastest solution, the Simulated Annealing and the Tabu Search have been rejected because the search ways for solutions of these methods are too random.

Finally, the research has moved to population-based strategies. Particular attention was paid to the choice of the initial population. In fact, as said before, given the great number of

variables, it is difficult to find a solution a priori that satisfies the constraints, so it was necessary to implement an algorithm as shown in Figure 12.

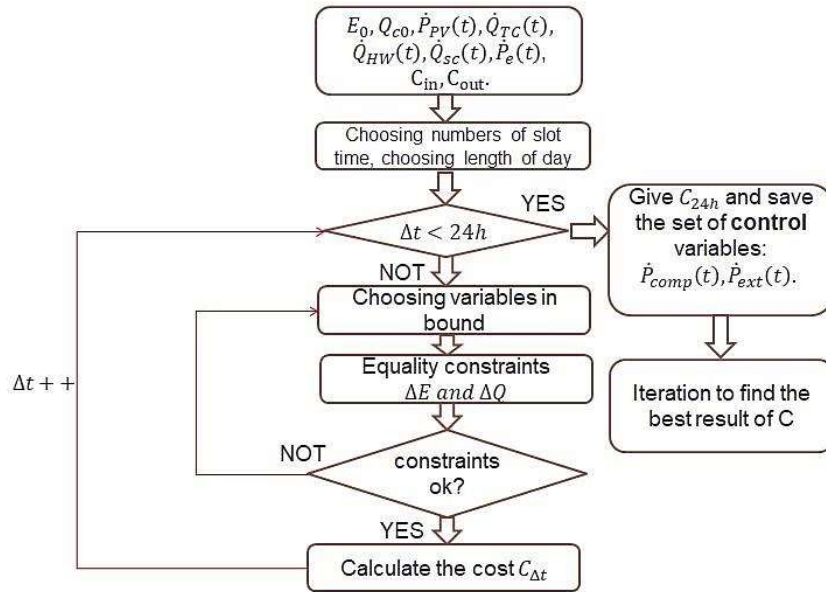


Figure 12 - Flow chart of the algorithm to find the initial population

This algorithm, basically, searches randomly, for each  $\Delta t$ , the two independent variables that satisfies the constraints and try again in case negative feedback of the constraints. The two input independent variables can be directly the two control variables,  $\dot{P}_{comp}(t)$  and  $\dot{P}_{ext}(t)$ , but in this case were chosen the two charge states of the accumulator,  $E(t)$  and  $Q_c(t)$ , in order to more easily implement these additional constraints:

$$E(0) = E(24) \pm \delta E$$

$$Q_c(0) = Q_c(24) \pm \delta Q_c$$

These further constraints ensure that the next day planning is not damaged, assuming that the thermal and electrical demands of the building between one day and another are similar. The two terms at right of the equations allow a certain variability between two days and can be chosen arbitrarily. For example, if  $\delta Q_c$  and  $\delta E$  are equal to zero the two days are equal; on the contrary, if they are equal to the capacity of the two storage the two days can be completely different.

Now, it is necessary to combine this population to find the sub-optimal solution. The algorithm chosen is the already presented PSO. First, this algorithm was applied into a system with only one electric storage unit with load profile and PV generation known, the battery is modelled with a resistance in series so as not to neglect losses (Figure 13). Also the initial battery SoC must be known.

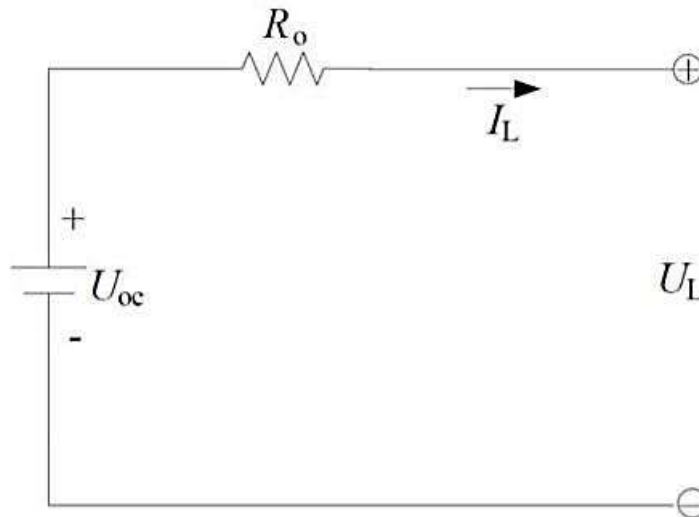


Figure 13 - Battery stationary model

Without the heat pump,  $\dot{P}_{ext}$  and  $\dot{P}_b$  are equal and there is only one control variable, thus only one independent variable. In this algorithm, the SoC of the battery was chosen, for the considerations previously exposed, and from this the other parameters were calculated.

The simulation starts with a discretization in time of one hour and it proceeds to a discretization of a quarter of an hour in which better results in terms of cost but also a greater dispersion of the parameters are given. Thus, this type of discretization could be necessary to try other methods (other algorithm, optimization in 6 hours instead 24). In this case the constraints are from 2 to 4 of generic case and also  $E(0) = E(24) \pm \delta E$ , as said before.

The results are shown in the following Figures. In Figure 14, the transformation from the best results of initial population (obtained with algorithm of Figure 9) to sub-optimal solution is shown, while Figure 15 shows the consequently power exchanged by battery. Figure 19 shows the cost variation at each iteration. Figure 17 and Figure 18 show the results of a discretization of a quarter of an hour ( $4 \cdot 24 = 96$  variable) and its spread distribution.

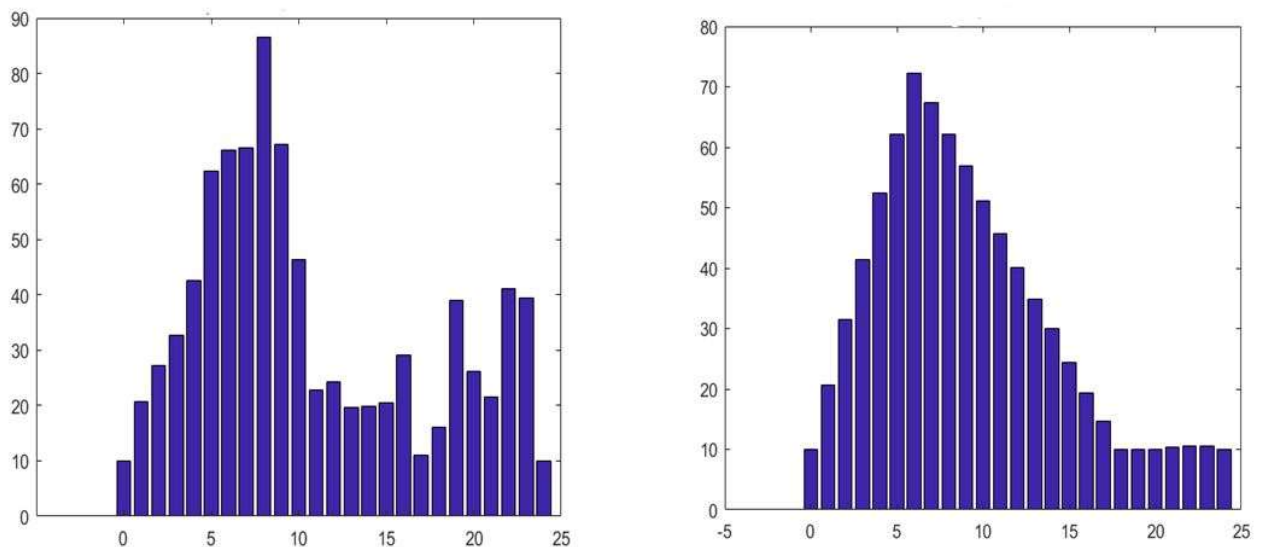


Figure 14 - Best results of SoC of initial population (left) and best results of SoC after optimization (right)

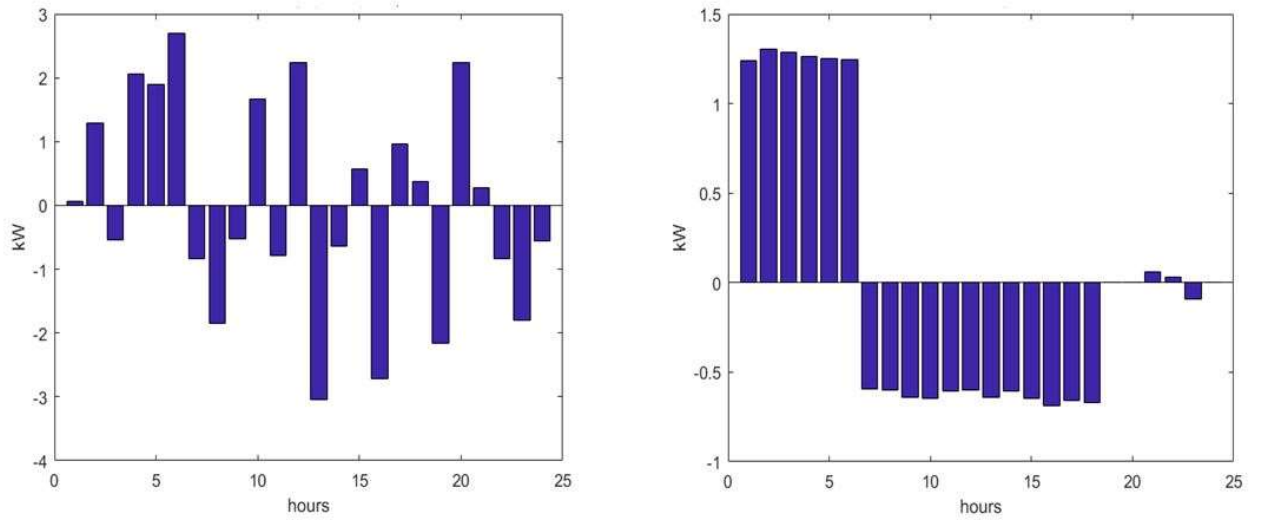


Figure 15 - Best result  $P_b$  of initial population (left) and best result of  $P_b$  after optimization (right)

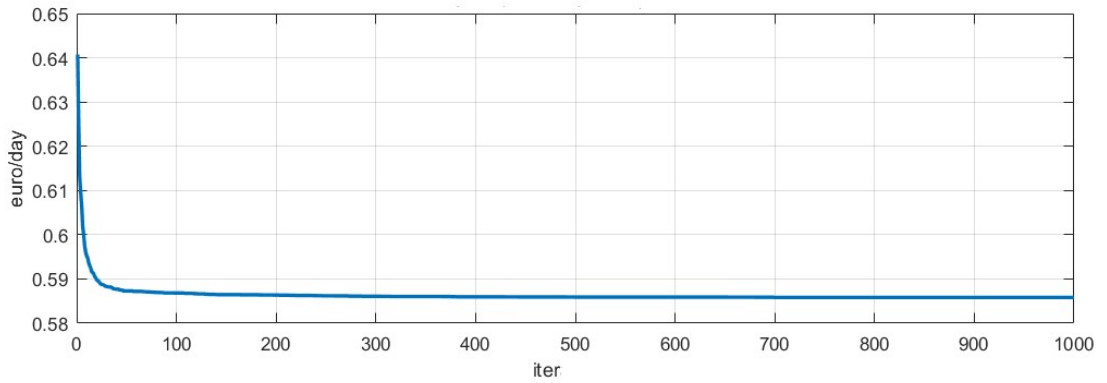


Figure 16 - Trend of the cost

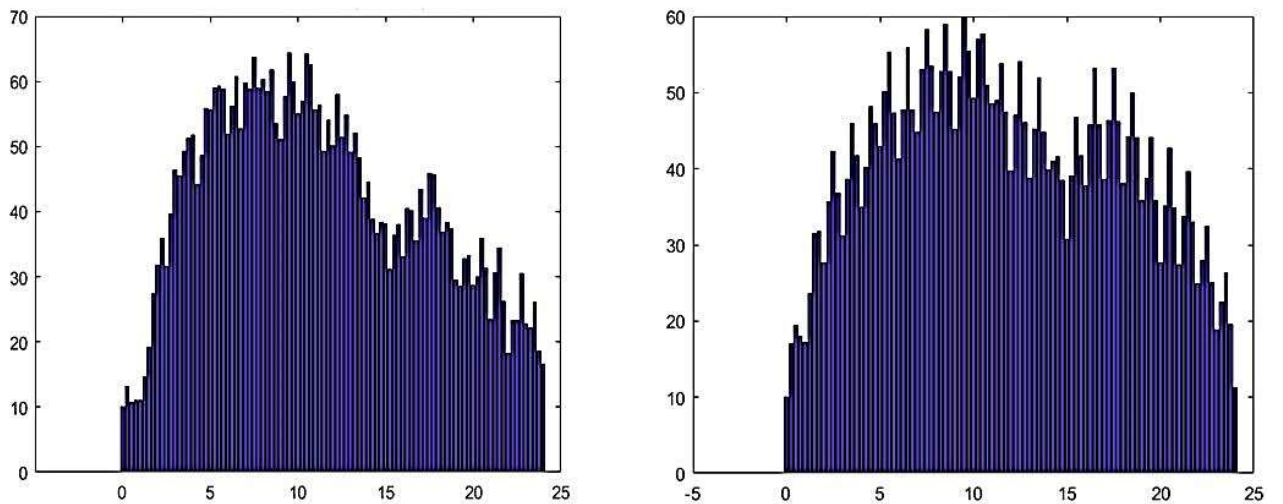


Figure 17 - Initial SoC best (left) and SoC best after optimization (right) with discretization of a quarter of an hour

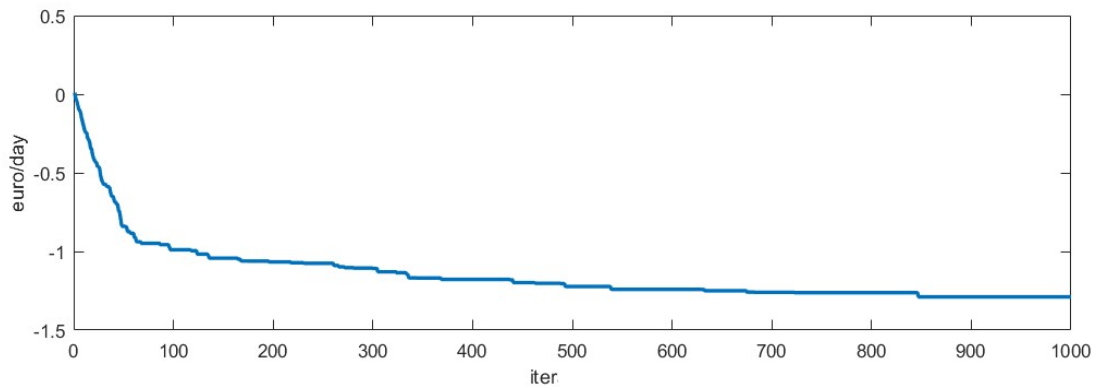


Figure 18 - Trend of cost with dt=0.25h

Figure 19 shows a demonstration of demand response request from DSO in which a profitable condition was simulated selling energy at the 10<sup>th</sup> hour,  $C_{out}(10)$  was multiplied by a factor of 2, and the battery asks discharges at maximum capacity (in this case the maximum capacity is 4kW).

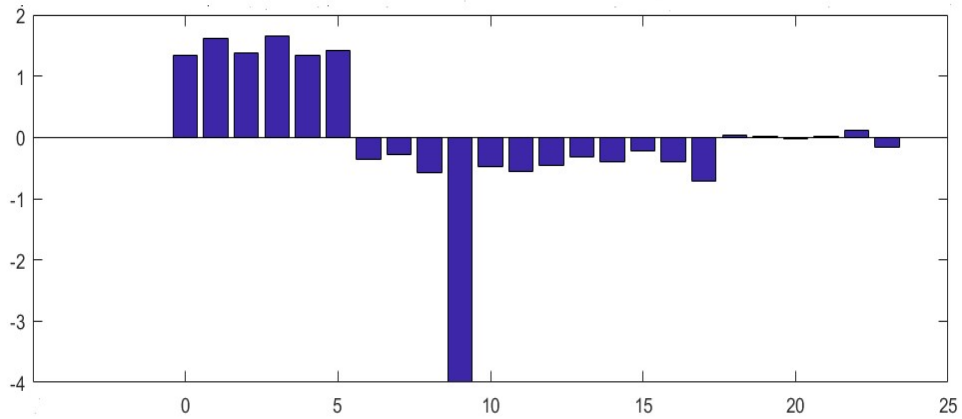


Figure 19 - Changing of flow power after request of DSO

## 3 Mathematical representation of the building system

### 3.1 Modelling approach

#### 3.1.1 Methodology

The system layouts suggested in the HYBUILD project, both the Mediterranean and the Continental one, are the result of the use of different technologies for the production and storage of thermal and electric energy. Each technology numerical model is developed by different partners. For this reason, a modular structure has been adopted for easing the development of complex systems models and facilitating the integration of different contributions.

The energy plant model is organized by sub-systems that are interconnected through interfaces. This structure allows to develop each module independently by different partners and, once ready, to be integrated in the main system. The numerical model of the technology solutions needs several revisions, tuning and validation process for having a trustable model. For this reason, the replacement of a sub-system with an updated version is possible in the adopted environment. Moreover, the replacement of a module does not affect the control rules.

The control rules, in particular, are defined with same structure as in the real case in a way that can be tested, and optimal setpoints identified, before being implemented in the field. As it can be understood, this feature gives several advantages on the system tuning and could reduce inconvenience to the tenants.

Finally, each component is modeled as a black, grey or white box, depending on the degree of detail of the system and simulation results resolution. In complex systems, computational effort can be high and the simplification of the numerical models is very relevant. Detailed numerical models of each solution are previously studied for ensuring a correct representation of the technology phenomena. Afterwards, a simplified numerical model is developed and included in the whole system.

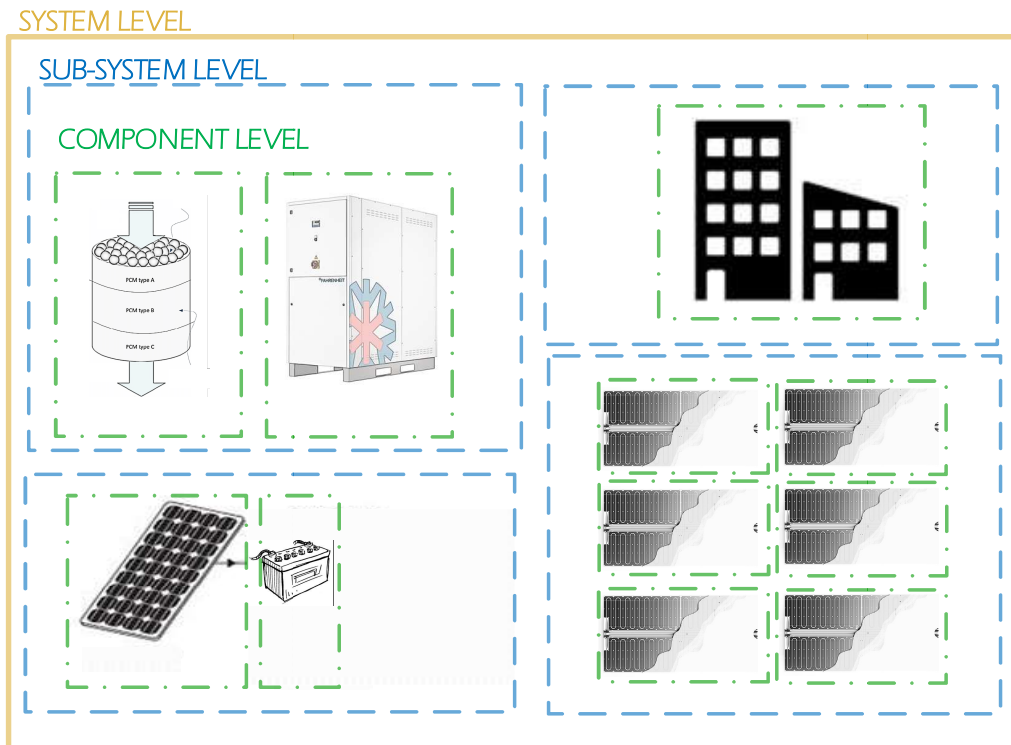


Figure 20 - Modular structure of the modelling approach

In the following paragraphs, each part of the whole system is described: first each component, device or building is presented as it is in the reality and then the adopted model and eventual simplification are reported.

## 3.2 Energy model of the Bordeaux demo building

### 3.2.1 Building Description

Bordeaux demo case is a multifunctional building located in Talence, Bordeaux. Perspectives from the satellite, east and north facades are reported in Figure 21 and Figure 22. The construction has been built around 1960 and no retrofit has been carried out up to now. Nevertheless, a renovation process is planned for the period 2018-2020 with the double objective of test a system with new integrated technologies and to demonstrate their validity for a possible spread of studied solutions. The part of the building studied in the HYBUILD project is currently used as an office (Figure 23) and an experimental workshop (Figure 24). Although the building use is not residential, its operation could be considered similar to residential one due to the fact that there is Domestic Hot Water (DHW) consumption.



Figure 21 - Satellite view of Bordeaux demo case



(a)



(b)

Figure 22 - Bordeaux demo case external view; (a) east façade, (b) north façade



Figure 23 - First floor, view of the offices



Figure 24 - Ground floor, view of the workshop

### 3.2.2 Building Geometry and envelope characteristics

The building is basically a parallelepiped with a total area of around 720 m<sup>2</sup> divided equally in two floors.

Regarding the envelope, there are three different walls stratigraphy: one for the external walls and two different for internal walls (made of concrete or plastic). Data regarding thermal conductivity and therefore thermal transmittance for vertical walls as well as ground floor, flat roof and external windows characteristics are reported respectively in Table 1, Table 2, Table 3 and Table 4. Data regarding internal walls' stratigraphy are not reported since they are not used in any further calculation.

Table 1. External wall stratigraphy

<i>External wall</i>					
Material	Thickness	Thermal conductivity	Density	Resistance	U value
	[m]	[W/(m*K)]	[kg/m <sup>3</sup> ]	[(m <sup>2</sup> *K)/W]	[W/(m <sup>2</sup> *K)]
Concrete	0.05	1.39	1300	0.04	
Air gap	0.03	0.31	1	0.10	
Concrete	0.25	1.39	1300	0.18	
Polystyrene	0.05	0.04	800	1.25	
<b>TOTAL</b>				<b>1.73</b>	<b>0.58</b>

Table 2. Flat roof stratigraphy

<i>Flat roof</i>					
Material	Thickness	Thermal conductivity	Density	Resistance	U value
	[m]	[W/(m*K)]	[kg/m <sup>3</sup> ]	[(m <sup>2</sup> *K)/W]	[W/(m <sup>2</sup> *K)]
Concrete	0.05	1.39	1300	0.04	
Air gap	0.03	0.31	1	0.10	
Glass wool	0.2	0.04	80	5.41	
<b>TOTAL</b>				<b>5.68</b>	<b>0.18</b>

Table 3. Ground floor stratigraphy

Ground floor					
Material	Thickness	Thermal conductivity	Density	Resistance	U value
	[m]	[W/(m*K)]	[kg/m <sup>3</sup> ]	[(m <sup>2</sup> *K)/W]	[W/(m <sup>2</sup> *K)]
Concrete	0.17	1.39	1300	0.12	
<b>TOTAL</b>				<b>0.33</b>	<b>3.03</b>

Table 4. Windows characteristics

Window					
Frame material	Frame thickness	Glazing type	Glass thickness	SHGC	U value
	[m]		[m]		[W/(m <sup>2</sup> *K)]
Wood	0.02	single	0.006	0.30	
<b>TOTAL</b>					<b>5.00</b>

### 3.2.3 Zoning

Only a part of the building total area is considered in the HYBUILD project, in particular, the north-east zone at ground floor and first floor for a total surface equal to 100 m<sup>2</sup>. For this reason, it has been decided to model the building in four different zones, two on the ground floor and two on the first floor. Each floor is composed by a “studied zone” that represents the part of the building that will undergo the renovation according to the HYBUILD Project and by a “non-studied zone” that represents the rest of the floor. The first floor studied zone includes a meeting room and two offices (as can be seen from Figure 25), while the ground floor studied zone is used as an experimental studio (Figure 26). The measures of the two zones are shown in Figure 27, while the values of the zones area are summarized in Table 5. The presence of a changing room on the ground floor is responsible of the DHW consumption and guarantees similar behaviours and comparison, as previously said, with respect to a residential building.

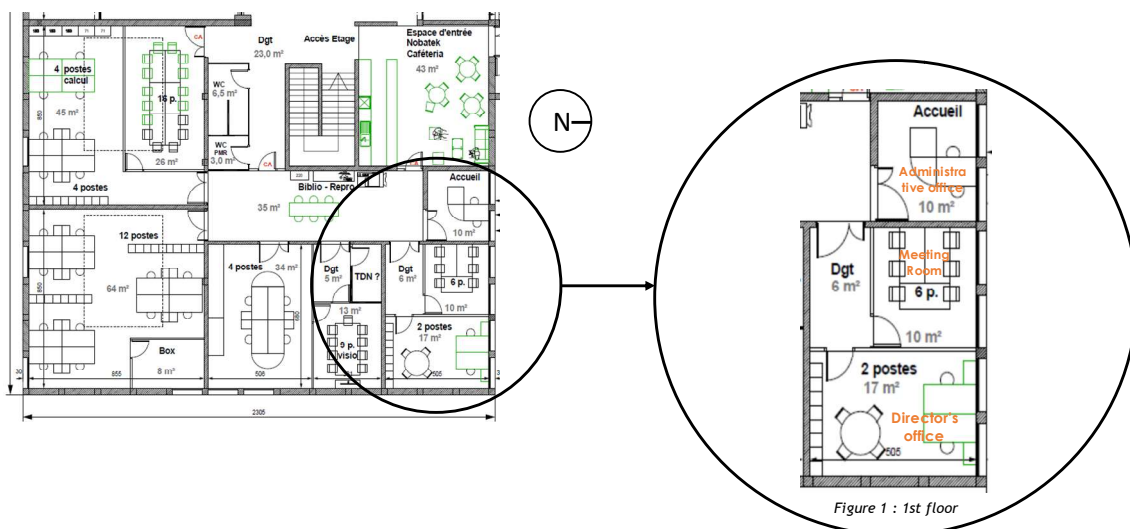


Figure 25 - Building first floor with zoom on the HYBUILD studied zone

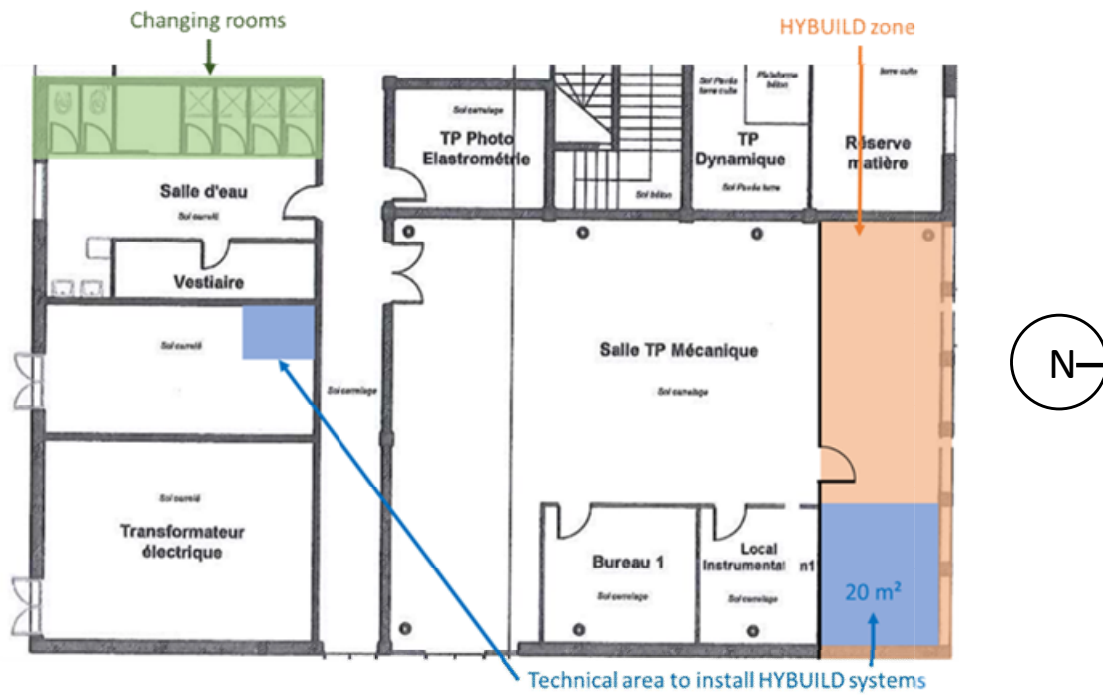


Figure 26 - Building ground floor architectural plan with additional information about the location of the HYBUILD systems installation

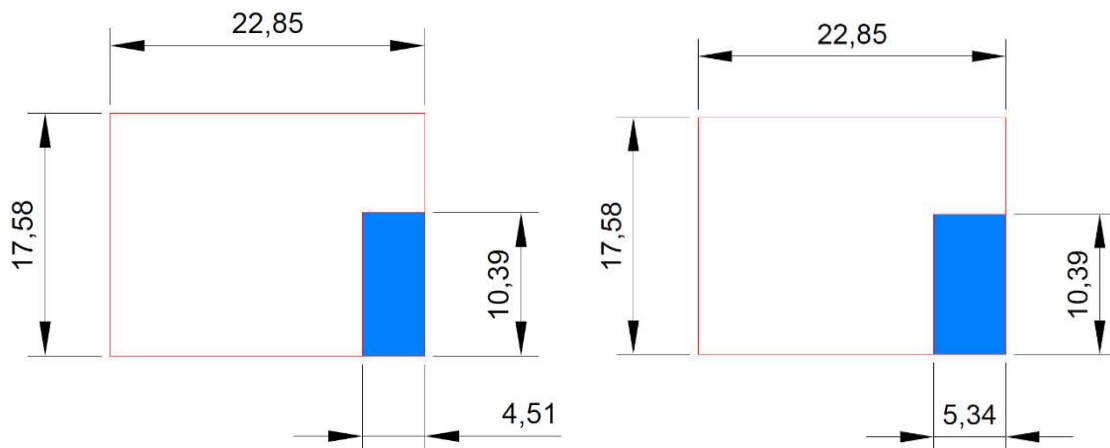


Figure 27 - Ground floor (left) and first floor (right) plant measures [m]

Table 5. Zones characteristics

Zones characteristics				
FLOOR	ZONE	LABEL	n° ZONE	AREA
				[m <sup>2</sup> ]
FIRST	Non-Studied Zone	1F_NS	1	314.0
FIRST	Studied Zone	1F_SZ	2	49.0
GROUND	Non-Studied Zone	GF_NS	3	315.2
GROUND	Studied Zone	GF_SZ	4	47.8

### 3.2.4 Boundary conditions / model inputs

As said in the section above, the building is modelled as one block composed by four independent zones. It is here important to remind that the presented simulations have been run on the actual state of the existing building. The model geometry has been created firstly using SketchUp Tool (Figure 28) and then it has been imported to TRNSYS where internal gains, ventilation and infiltration rates have been added to the model. The dimensions of the model have been taken as average between internal and external dimensions. Regarding the schedule used to identify internal gains and space heating and cooling, a distinction between weekdays, weekend days and holidays became necessary.

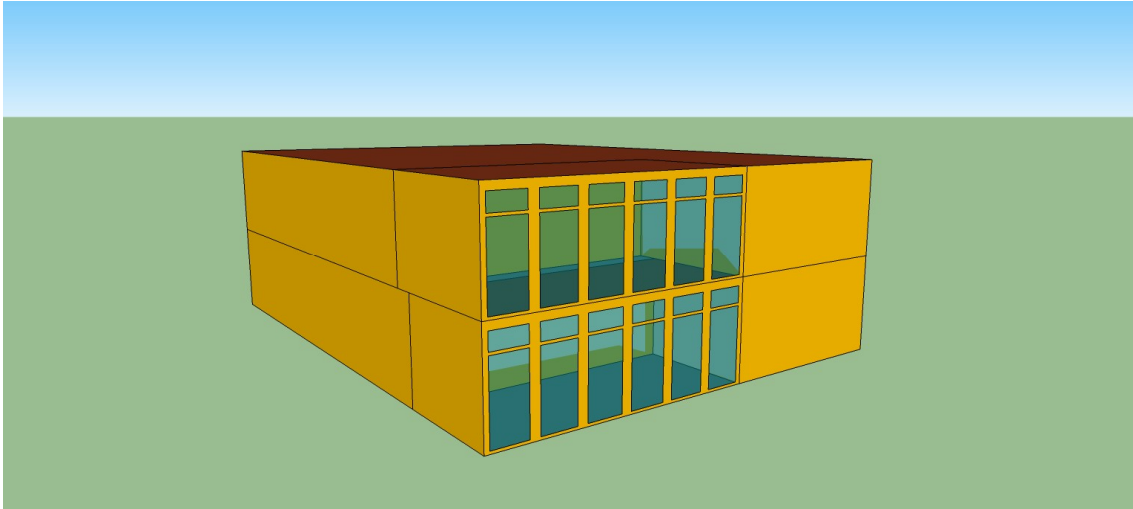


Figure 28 - SketchUp Tool model

#### Heating system

At now, only heating system is present in the building. The schedule of operation and the various set points have been modelled according to technical reports about the demo case and the used values are summarized in Table 6 and Figure 29. During the working hours, the two studied zones are heated up to 21°C while in the other periods the set-back temperature is 19°C. For simulation purposes, ideal heating system has been used. The presented system does not foresee any dehumidification or air humidity control.

Table 6. Heating schedule

<i>Heating schedule</i>		
	from	to
ON	7:00 AM	7:00 PM
OFF	7:00 PM	7:00 AM

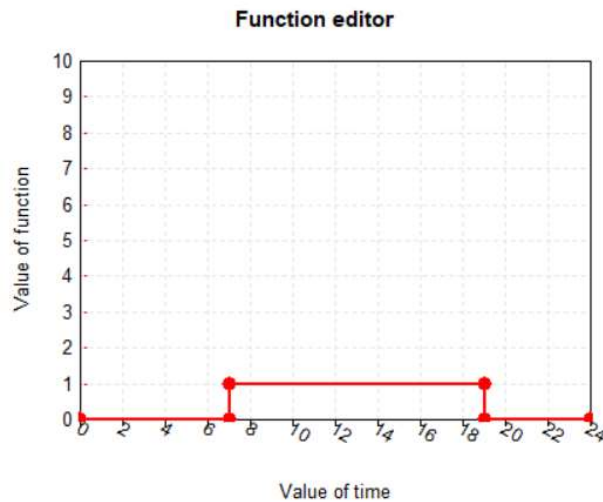


Figure 29 - Heating schedule

### Internal gains

Three different internal gains types have been considered in the building model: occupancy, appliances and lighting system. The schedule of occupancy, use of appliances and lights are equal to heating schedule profile (Table 6, Figure 29). The heat gain due to one person has been fixed to 80 [W/pers] (according to [49], Table 4. typical metabolic heat generation for standing, relaxed activities). This value is further divided in three main contributions: latent (40%), convective (42%) and radiative (18%).

The occupancy of the different zones has been decided based on the drawing of the floors plants (Figure 25 and Figure 26). In conclusion, being the ground floor composed by workshop and technical rooms with not well-defined occupancy level, two persons have been considered in each zone. On the contrary, the number of persons considered on the first floor has been calculated using the plant and assuming that the spaces are not fully occupied all the time but with a percentage of 80%. A further calibration process will define these assumptions with higher accuracy.

In Table 7 the number of occupants of the various building zones is reported, while the occupancy schedule is summarized in Table 8.

Table 7. Occupancy of the various zones

Occupancy			
FLOOR	ZONE		N° PERS
FIRST	Non-Studied Zone	1F_NS	48
FIRST	Studied Zone	1F_SZ	8
GROUND	Non-Studied Zone	GF_NS	2
GROUND	Studied Zone	GF_SZ	2

Table 8. Heating schedule

Heating schedule		
	from	to
ON	8:00 AM	7:00 PM
OFF	7:00 PM	8:00 AM

Regarding the appliances and lights, two different specific values of internal gains have been used. The specific contribution of appliances has been taken equal to 8 [W/m<sup>2</sup>] whereas the specific value for lights has been set to 5 [W/m<sup>2</sup>]. The schedule follows the occupancy ones (Table 8).

**Ventilation and Infiltration**

In the studied building, no mechanical ventilation system is installed and the user’s opening of windows is the only contribution to natural ventilation. Considering an average air change rate of 0.40 [m<sup>3</sup>/h/pers] and knowing the occupancy (Table 7) of the different zones, the ventilation contribution to energy balance can be calculated. The infiltration rate through the envelope has been instead considered constant during the year and the day with a value of 0.15 [vol/h].

**3.2.5 Energy balance**

Monthly thermal gains and losses during the year of the studied zones are summarized in the following graphs (Figure 30 for the ground floor and Figure 31 for the first floor). Internal gains are supposed to be constant for all the months; infiltration and ventilation contributions depend on the internal and external temperature as well as transmission losses. Heating energy is therefore defined for covering the energy losses.

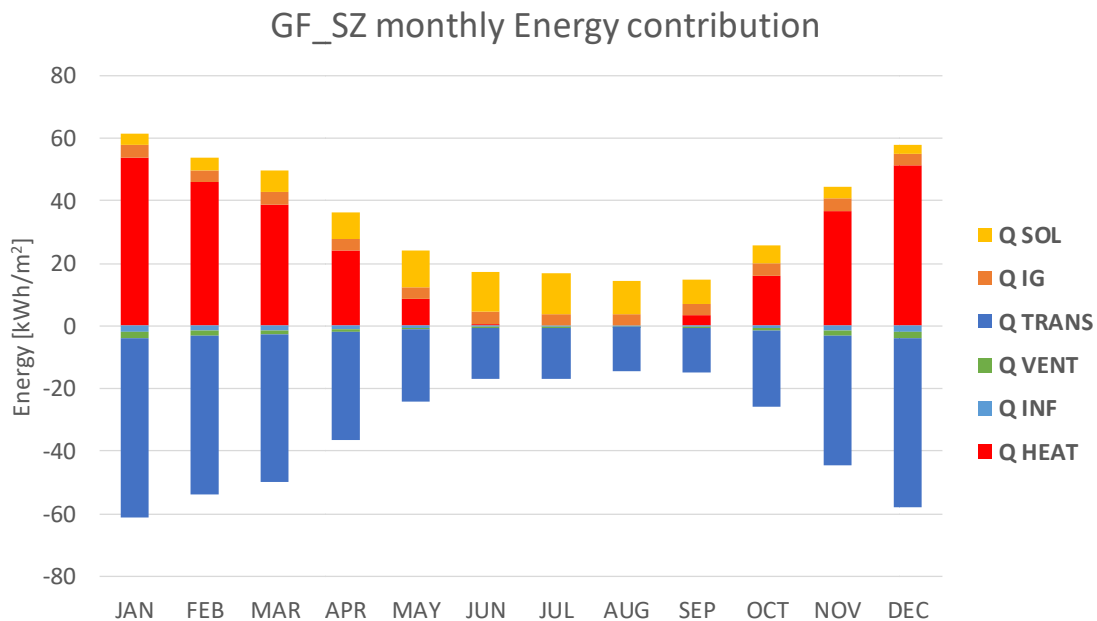


Figure 30 - Yearly energy balance of Ground Floor studied zone

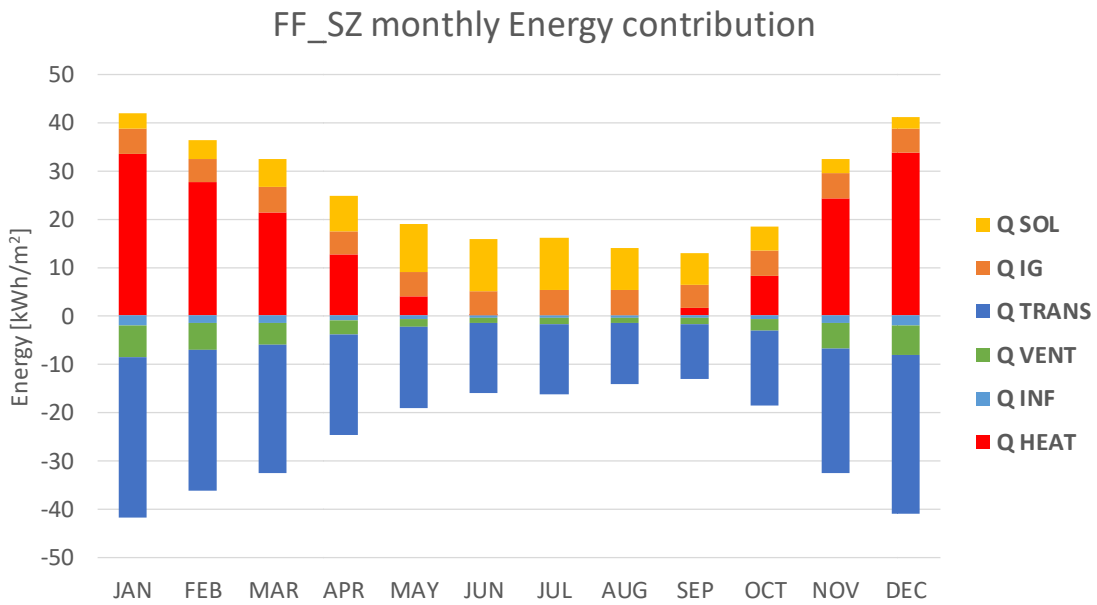


Figure 31 - Yearly energy balance of First Floor studied zone

Simulations do not foresee any cooling system as it is in the real case. Despite that, simulation results show as in around 5% of the working hours the zones temperature is above the comfort value of 26°C reaching a maximum temperature of 29°C in the first floor and 27°C in the ground floor.

Figure 32 shows the internal temperature of the two studied zones during the swing season and summertime. There could be noticed as temperature grows above 26°C for some hours during summertime keeping below 28°C almost for the whole period. Figure 33 reports on the frequency curve of the internal temperature in the two zones. As mentioned, temperature lies above 26°C for the 5% of the hours in the first floor and 1% of hours in the ground floor.

If any cooling system is installed in these zones, a night cooling strategy could help to improve the thermal comfort.

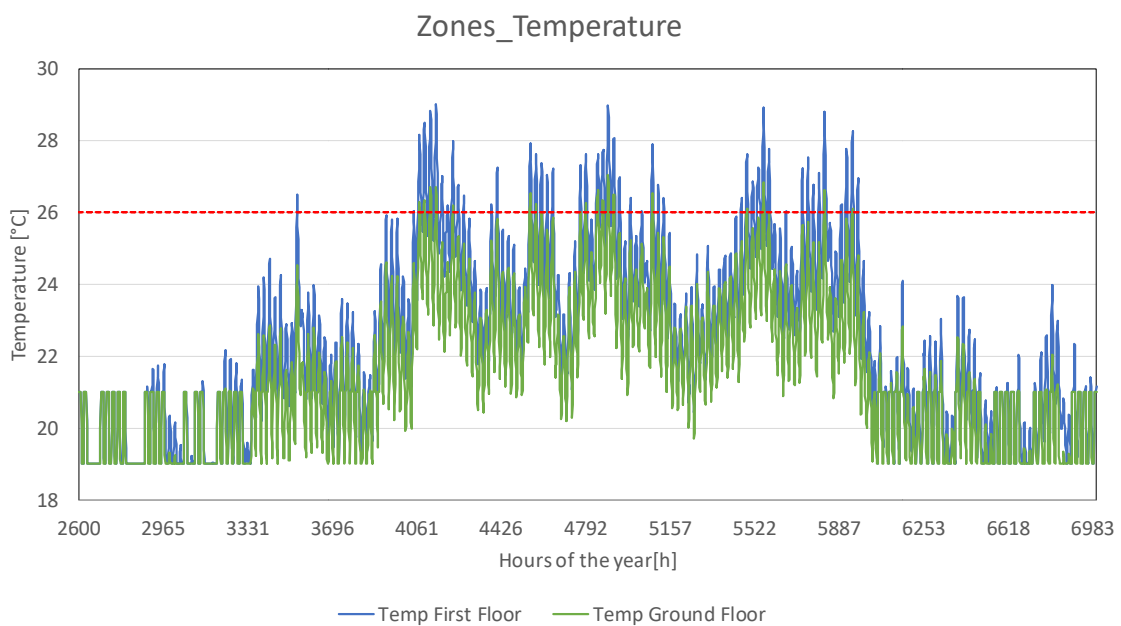


Figure 32 - Internal temperature of the two studied zones during no-heating season

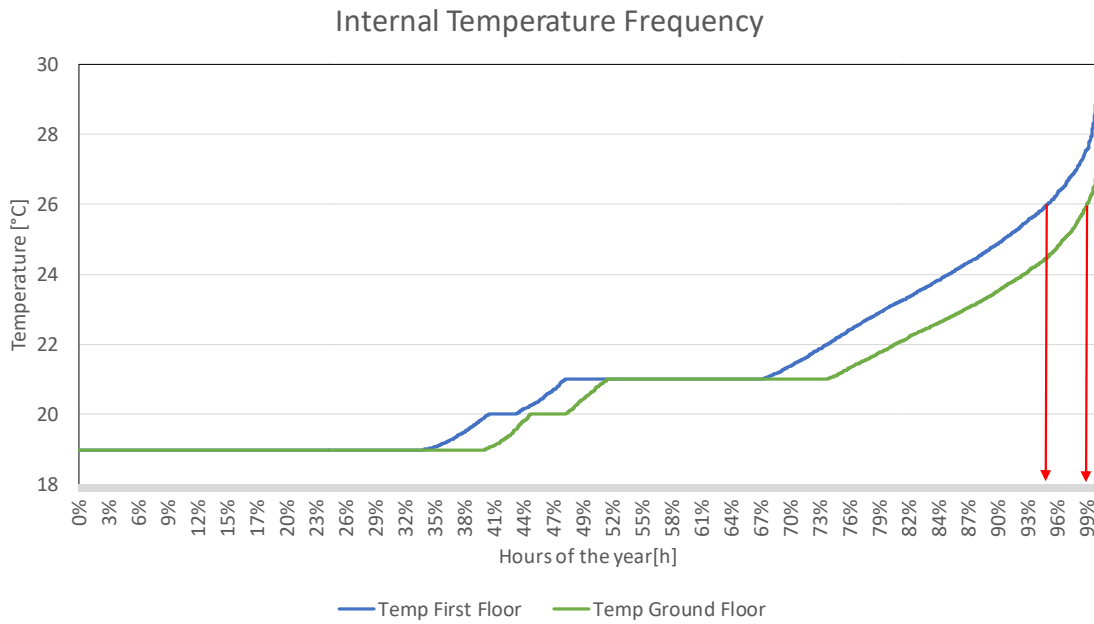


Figure 33 - Cumulative frequency of the two studied zones internal temperature over the year

### 3.2.6 Demands and peak loads

Space heating energy demands for the studied zones are summarized on a yearly base in Table 9. Heating demand of the ground floor results to be 40% higher than the one of first floor due to the walls constructions. In fact, the roof has an insulation layer that reduces the thermal losses through the outside while the ground floor is only a concrete slab that exchange heat with the ground. The average heating demand results 218 kWh/(m<sup>2</sup>year). The maximum peak power requested by the two zones together is around 12.5 kW.

Monthly heating demands are instead shown in Table 10, for the two zones separately, and together. December, January and partially February result to be the coldest months with, consequently, the highest heating demand; February, March and November have around one third less heating demand than the coldest months while October and April require very few space heating.

The maximum peak power for each zone and for the two zones simultaneously are reported in Table 11. As already mentioned, the maximum peak power is verified in December and January with a total value for the two zones of 12.5 kW.

Table 9. Resume HYBUILD studied zones thermal energy consumption for space heating and maximum peak load

HYBUILD studied zones summary			
Zone	Space heating demand	Specific space heating demand	Maximum peak load
	[kWh/y]	[kWh/m <sup>2</sup> /y]	[kW]
2	9301.0	167.6	6.8
4	13073.6	279.0	5.8
<b>TOTAL</b>	<b>22374.6</b>	<b>218.6</b>	<b>12.5</b>

**Table 10. Monthly specific space heating energy consumption of HYBUILD zones**

Zone	JAN	FEB	MAR	APR	MAY	JUN	JUL	AUG	SEP	OCT	NOV	DEC
	[kWh/m <sup>2</sup> ]											
<b>2</b>	33.5	27.8	21.4	12.7	4.1	0.2	0.0	0.0	1.6	8.4	24.2	33.8
<b>4</b>	53.7	45.9	38.8	24.1	8.5	0.6	0.0	0.0	3.3	16.0	36.8	51.3
<b>2 &amp; 4</b>	42.7	36.0	29.4	17.9	6.1	0.4	0.0	0.0	2.4	11.8	30.0	41.8

**Table 11. Monthly space heating peak demand of HYBUILD zones**

Zone	JAN	FEB	MAR	APR	MAY	JUN	JUL	AUG	SEP	OCT	NOV	DEC
	[kW]											
<b>2</b>	6.7	6.2	5.7	4.2	3.2	1.0	0.0	0.0	2.0	3.9	5.3	6.8
<b>4</b>	5.8	5.5	5.0	4.1	3.1	1.5	0.0	0.0	2.2	3.5	4.7	5.7
<b>2 &amp; 4</b>	12.4	11.7	10.7	8.3	6.3	2.5	0.0	0.0	4.1	7.4	10.1	12.5

### 3.3 Energy model of the Cyprus demo building

The case study is a building located in the square at Aglantzia's core (Figure 34, Figure 35). The traditional building will be refurbished in order to develop a destination that will be a cornerstone of social interaction and creative activities.

The building will become a benchmark for a permanent digital exhibition of renewable energy technologies and supportive equipment to serve as a space for informing the society about the use of smart technologies in our homes capable of offering the transition to a low carbon economy and high levels of energy savings.

In this context, the proposal aims at creating a multifunctional space which, apart from the promotion of smart technologies, will have the possibility of hosting events, seminars, artistic performances, etc. and at the same time it will function as a reading hall with a digital library for young citizens and students.



Figure 34 - Pictures of the current state of the building (outside)



Figure 35 - Pictures of the current state of the building (inside)

### 3.3.1 Building Geometry

The building total area is 140 m<sup>2</sup> divided in 7 rooms. Regarding the envelope there are two different wall configurations: one for the external walls and one for internal walls (made of limestone and rubble with or without plaster). The data regarding thermal conductivity and therefore thermal transmittance for vertical walls, ground floor, roof and external windows characteristics are reported respectively in Table 12 and Table 13.

Table 12. Wall (Internal/External), ground floor and roof specifications for Cyprus Demo Site

Surface	Material	Density	Thermal conductivity	Thickness	Uvalue
	[-]	[kg/m <sup>3</sup> ]	[W/(mK)]	[m]	[W/(m <sup>2</sup> K)]
External wall 1	Traditional stone (Limestone, very soft)	1600	0.85	0.55	1.17
	Internal coating gypsum plaster	1600	0.80	0.025	
External wall 2	External coating gypsum plaster	1600	0.80	0.025	1.13
	Traditional stone	1600	0.85	0.55	
	Internal coating gypsum plaster	1600	0.80	0.025	
Ground floor	Earth (clay)	1200-1800	1.50		0.68
	Tiles (marble)	2800	3.50		
Roof	Traditional barrel roof tiles	2000	1.00	0.02	0.219
	2 layers of bituminous waterproofing 4mm reinforced	1100	0.23	0.004	
	12mm OSB	600	0.14	0.012	
	120mm extruded polystyrene insulation	30	0.030	0.12	
	18mm MDF	600	0.14	0.018	
	Reed mat	190	0.056	0.01	

Table 13. Window specifications for Cyprus Demo Site

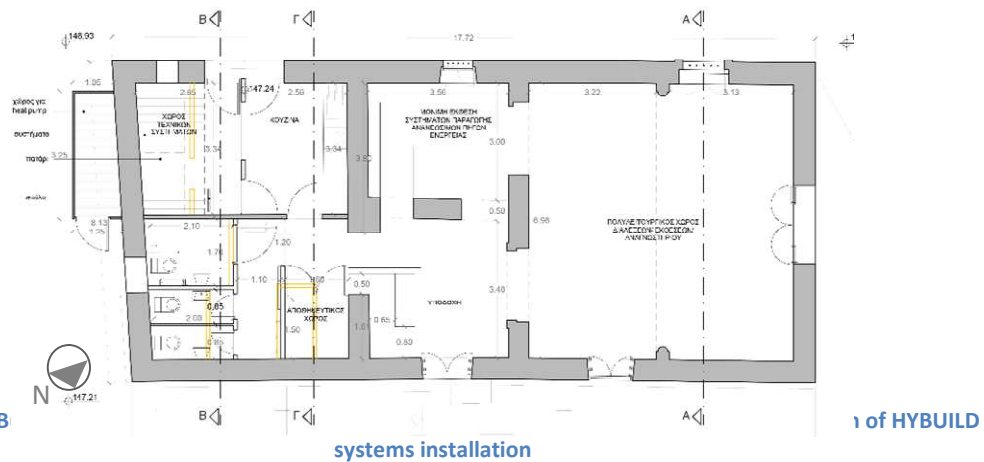
Surface	Frame material	Frame thickness	Glazing type	Glass thickness	g value	U value window	Area
		[mm]		[mm]	[-]	[W/(mK)]	[m <sup>2</sup> ]
Surface 1	wood	40-120	single	4	0.85	4.7	0.8x1
Surface 2	wood	40-120	single	4	0.85	4.7	1.7x1.1
Surface 3	wood	40-120	single	4	0.85	4.7	0.7x1.1
Surface 4	wood	40-120	single	4	0.85	4.7	1.45x1.05
Surface 5	wood	40-120	single	4	0.85	4.7	0.75x1.1
Surface 6	wood	40-120	single	4	0.85	4.7	0.45x0.8
Surface 7	steel	20	double	6-12-6	0.60	2.8	2x2.4

### 3.3.2 Zoning

One thermal zone is considered, and the behaviour of the building resembles a residential house. Zone information is shown below in Table 14 and detailed explanations of architectural plans are illustrated in Figure 36.

Table 14. Zone information for Cyprus Demo Site

Floor	Number of rooms	Gross area	Net area	Heated area	Cooled area	Height
	[-]	[m <sup>2</sup> ]	[m <sup>2</sup> ]	[m <sup>2</sup> ]	[m <sup>2</sup> ]	[m]
1	7	140	114	114	114	4.30 (average)



### 3.3.3 Boundary conditions / model inputs

The presented simulations have been run considering the renovated building. The model geometry has been created firstly using SketchUp Tool (Figure 37) and then it has been imported to TRNSYS where the behaviour regarding the envelope, internal gains, ventilation and infiltration rates have been added to the model. For the simulations the external dimensions of the building have been considered.

Regarding the schedule used to identify internal gains and heating and cooling systems a distinction between weekdays, weekend days became necessary.

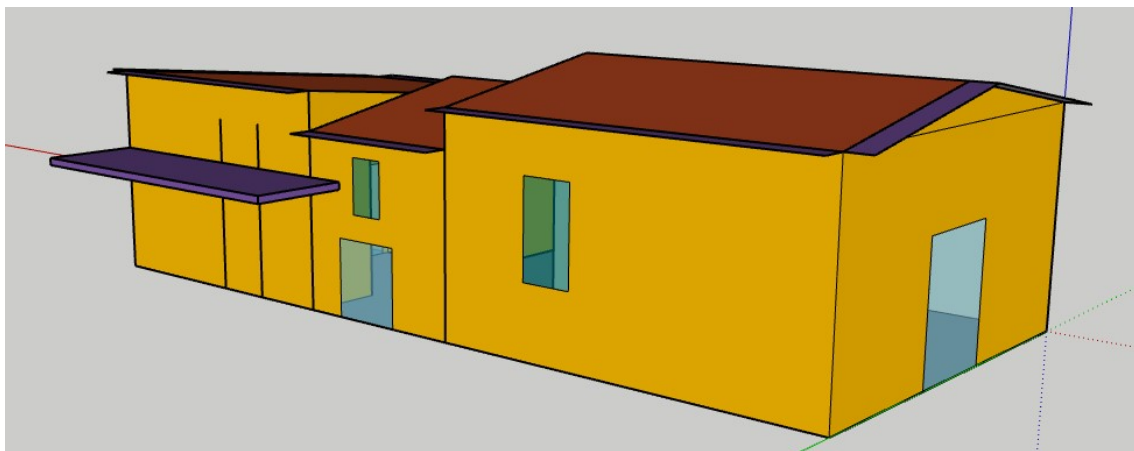


Figure 37 - SketchUp Pro building model

#### **Heating/Cooling System**

Heating and cooling demands are assessed assuming ideal capacity of the conditioning system in a way that the internal temperature is maintained between two set temperatures. The fixed temperature during winter time is 20°C while during summertime is 25°C.

#### **Internal gains**

Two different internal gains have been considered in the simulations. They are occupancy and lighting system. The schedule of occupancy, use of appliances and lights are shown in Table 15. The heat gain due to one person has been fixed to 120 [W/pers] (according to ISO 7730 and Figure 38). This value is divided in two main contributions, which are shown in the figure below.

No.	Degree of Activity	Typical Application	Total Heat Adjusted		Sensible Heat		Latent Heat	
			Watts	Btu/h	Watts	Btu/h	Watts	Btu/h
<input type="radio"/> 01	Seated at rest	Theatre, Movie	100	350	60	210	40	140
<input checked="" type="radio"/> 02	Seated, very light writing	Office, Hotels, Apts	120	420	65	230	55	190
<input type="radio"/> 03	Seated, eating	Restaurant	170	580	75	255	95	325
<input type="radio"/> 04	Seated, light work, typing	Office, Hotels, Apts	150	510	75	255	75	255

Figure 38 - TRNSYS Occupants Gains According to ISO 7730

In Table 15, the number of occupants is reported and visit schedule is explained.

Table 16 shows appliances and lighting gains. Moreover the schedule is described for each category.

Table 15. Occupancy profile and number of people living in the building

Operation	Day	Time	Number of people
Organized visits	Monday, Tuesday, Wednesday, Thursday, Friday	08:00-12:00	20
Free visits	Wednesday, Saturday, Sunday	08:00-19:00	20
Study Space / Library	Monday, Tuesday, Thursday, Friday	12:00-19:00	20
Lectures	Available all day	19:00-21:00	60

Table 16. Lighting and other electric loads (installed power and, if available, schedule of use).

Description	Average Watts	Schedule of use	
		Days	Time
7 screens	7*200	Available all day	08:00-21:00
7 headphones		Monday, Tuesday, Wednesday, Thursday, Friday	08:00-19:00
1 server	250	Available all day	08:00-21:00
20 pc (Laptops)	50	Monday, Tuesday, Thursday, Friday	12:00-19:00
1 projector	300	Available all day	19:00-21:00
Full audiovisual system for lectures	100	Available all day	08:00-21:00
1 alarm		Available all day	00:00-24:00
1 monitoring system	30	Available all day	00:00-24:00
5 CO <sub>2</sub> sensor		Available all day	00:00-24:00

5 fire alarm		Available all day	00:00-24:00
1 dishwasher	2400	Wednesday, Saturday	08:00-09:00
1 clothes dryer	2400	Saturday	08:00-10:00
1 washing machine	2400	Saturday	08:00-09:00
1 ironing equipment	1000	Saturday	08:00-12:00
1 microwave	1300	Available all day	08:00-08:30
1 kitchenette	2000	Available all day	08:00-09:00
1 oven	1800	Wednesday, Saturday, Sunday	08:00-11:00
1 fridge	150	Available all day	00:00-24:00
1 water cooler	90	Available all day	08:00-21:00
1 coffee maker	600	Available all day	08:00-21:00
1 toaster	600	Available all day	08:00-08:05
1 boiler	3000	Available all day	08:00-21:00
1 hairdryer	1000	Saturday	08:00-08:10
1 vacuum cleaner	1500	Saturday	08:00-09:00
LED lighting with wifi	6 or 15	Available all day	08:00-21:00
Building management system		Available all day	00:00-24:00
Controlled thermostats for heating / cooling and hot water		Available all day	00:00-24:00
Smart plugs µe wifi		Available all day	00:00-24:00

### ***Ventilation/ infiltration***

For the ventilation an average ACH rate of 0,40 is assumed. Regarding infiltration a constant value equal to 0,15 has been used as air change rate to evaluate the infiltration rate through the envelope.

### **3.3.4 Energy balance**

The various contributions entering the energy balance are reported in Figure 39.

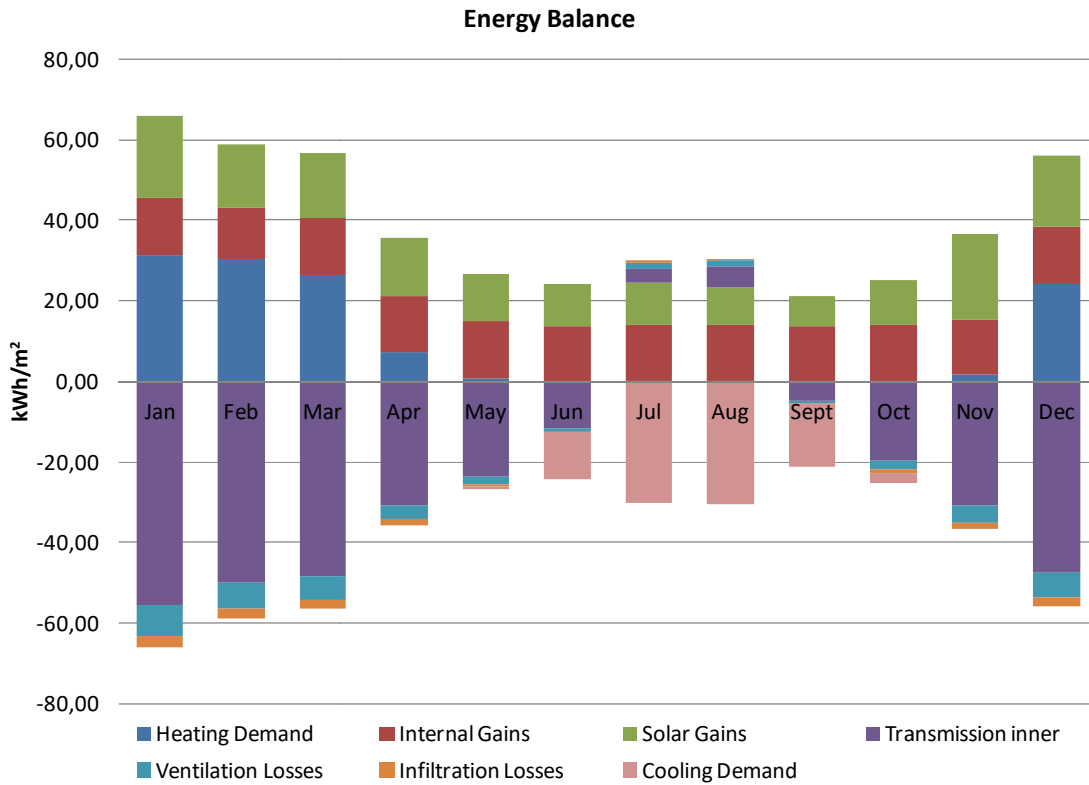


Figure 39 - Yearly energy balance of the Demo site

### 3.3.5 Demands and peak loads

Along the year, 5904 [kWh] are consumed for heating purposes and 4414 [kWh] are consumed for cooling purposes. In Table 17 instead, the specific demands are presented on a monthly basis.

Table 17. Monthly specific space heating energy consumption of Cyprus Demo building

Zone	JAN	FEB	MAR	APR	MAY	JUN	JUL	AUG	SEP	OCT	NOV	DEC
	[kWh/m <sup>2</sup> ]											
<b>Heating</b>	10.8	10.5	9.1	2.5	0.3	0	0	0	0	0	0.6	8.4
<b>Cooling</b>	0	0	0	0	0.3	4	10.4	10.6	5.4	0.8	0	0

## 3.4 Energy model of the Almatret demo building

### 3.4.1 Building Description

The second demo case where the HYBUILD Mediterranean concept will be installed is a house located in Almatret (Spain). Position from the satellite is visible in Figure 40. The building is a two floors single-family house built in 1970 and it has been partially renovated during the years (Figure 41 and Figure 42). In particular during the last intervention in 2014, windows, blinds and balcony doors on the North façade have been substituted with more insulating ones. In Figure 43 and Figure 44 one of the new balcony doors is reported. The two floors of the building present different usages, in fact, the ground floor is occupied by the medical office of the village whereas on first floor there is the apartment where the doctor lives with his family. To note that only the first floor of the construction will be used to test the HYBUILD Mediterranean system.



Figure 40 – Satellite view of Almatret demo case



Figure 41 – Almatret demo case external view: North facade



Figure 42 – Almatret demo case external view: South facade



Figure 43 – First floor: new balcony door detail



Figure 44 – First floor: new balcony door detail

### 3.4.2 Building Geometry and envelope characteristics

The building is basically a parallelepiped with a total area of around 250 m<sup>2</sup> divided in two floors. The first floor, the residential one, is subsequently divided in 8 rooms. In Figure 45 and Figure 46 schematic of North façade and vertical section are reported.



Figure 45 – Almatret demo building, schematic of North facade

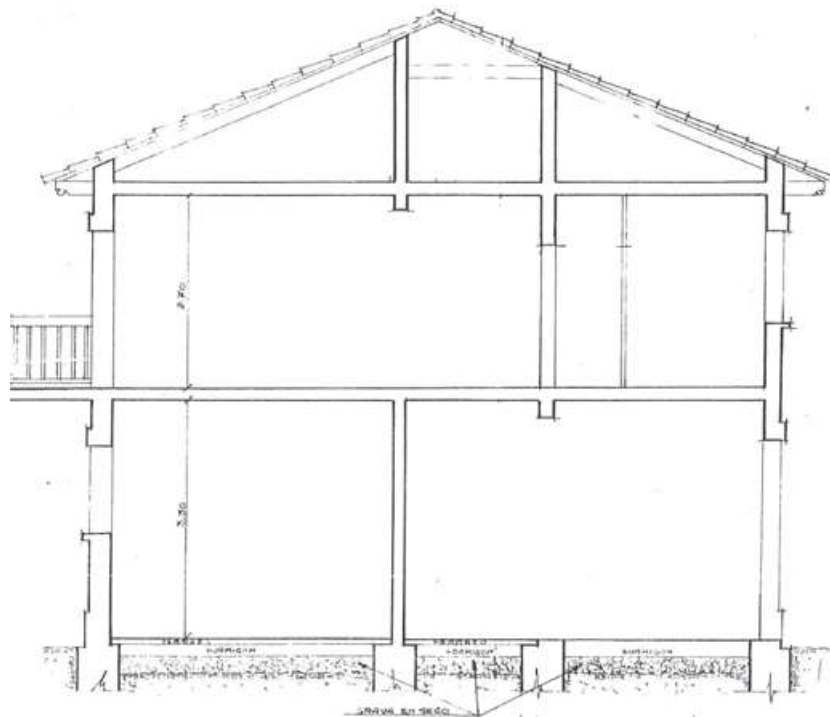


Figure 46 – Schematic of the house section

Data regarding thermal conductivity and therefore thermal transmittance for vertical walls as well as ground floor, ceiling, roof and external windows characteristics are reported respectively in Table 18, Table 19, Table 20, Table 21 and Table 22. Data regarding internal walls' stratigraphy are not reported since they are not used in any further calculation.

Table 18 – External wall stratigraphy

<i>External wall</i>					
Material	Thickness	Thermal conductivity	Density	Resistance	U value
	[m]	[W/(m*K)]	[kg/m <sup>3</sup> ]	[(m <sup>2</sup> *K)/W]	[W/(m <sup>2</sup> *K)]
R <sub>se</sub>	-	-	-	0.04	
Exterior mortar plaster	0.01	0.80	1525	0.01	
Perforated brick	0.15	0.37	900	0.41	
Air chamber	0.04	0.31	1	0.13	
Partition wall	0.04	0.45	1000	0.09	
Gypsum Plaster	0.02	0.57	1150	0.04	
R <sub>si</sub>	-	-	-	0.13	
<b>TOTAL</b>				<b>0.84</b>	<b>1.19</b>

Table 19 – Ground floor stratigraphy

<i>Ground floor</i>					
Material	Thickness	Thermal conductivity	Density	Resistance	U value
	[m]	[W/(m*K)]	[kg/m <sup>3</sup> ]	[(m <sup>2</sup> *K)/W]	[W/(m <sup>2</sup> *K)]
R <sub>si</sub>				0.17	
Terrazzo	0.04	1.3	1895	0.03	
Cement	0.03	0.55	1125	0.05	
Concrete beams + vaults + compression layer with mesh	0.25	0.91	1220	0.28	
Gypsum Plaster	0.02	0.57	1150	0.04	
R <sub>se</sub>				0.04	
<b>TOTAL</b>				<b>0.61</b>	<b>1.65</b>

Table 20 – Ceiling stratigraphy

<i>Ceiling</i>					
Material	Thickness	Thermal conductivity	Density	Resistance	U value
	[m]	[W/(m*K)]	[kg/m <sup>3</sup> ]	[(m <sup>2</sup> *K)/W]	[W/(m <sup>2</sup> *K)]
R <sub>se</sub>	-	-	-	0.04	
Concrete beams + vaults + compression layer with mesh	0.25	0.91	1220	0.28	
R <sub>si</sub>	-	-	-	0.10	
<b>TOTAL</b>				<b>0.42</b>	<b>2.41</b>

Table 21 – Roof stratigraphy

<i>Roof</i>					
Material	Thickness	Thermal conductivity	Density	Resistance	U value
	[m]	[W/(m*K)]	[kg/m <sup>3</sup> ]	[(m <sup>2</sup> *K)/W]	[W/(m <sup>2</sup> *K)]
R <sub>se</sub>	-	-	-	0.04	
Roof tile	0.05	1.00	2000	0.05	
Tongue and groove joint	0.04	0.44	1000	0.09	
Concrete beams + vaults + compression layer with mesh	0.25	0.91	1220	0.28	
R <sub>si</sub>	-	-	-	0.10	
<b>TOTAL</b>				<b>0.56</b>	<b>1.80</b>

Table 22 – Windows characteristics

<i>Window</i>					
Frame material	Frame thickness	Glazing type	Glass thickness	SHGC	U value
	[m]		[m]		[W/(m <sup>2</sup> *K)]
Aluminium	0.045	double-pane	4/14/4	0.76	
<b>TOTAL</b>					<b>3.00</b>

### 3.4.3 Zoning

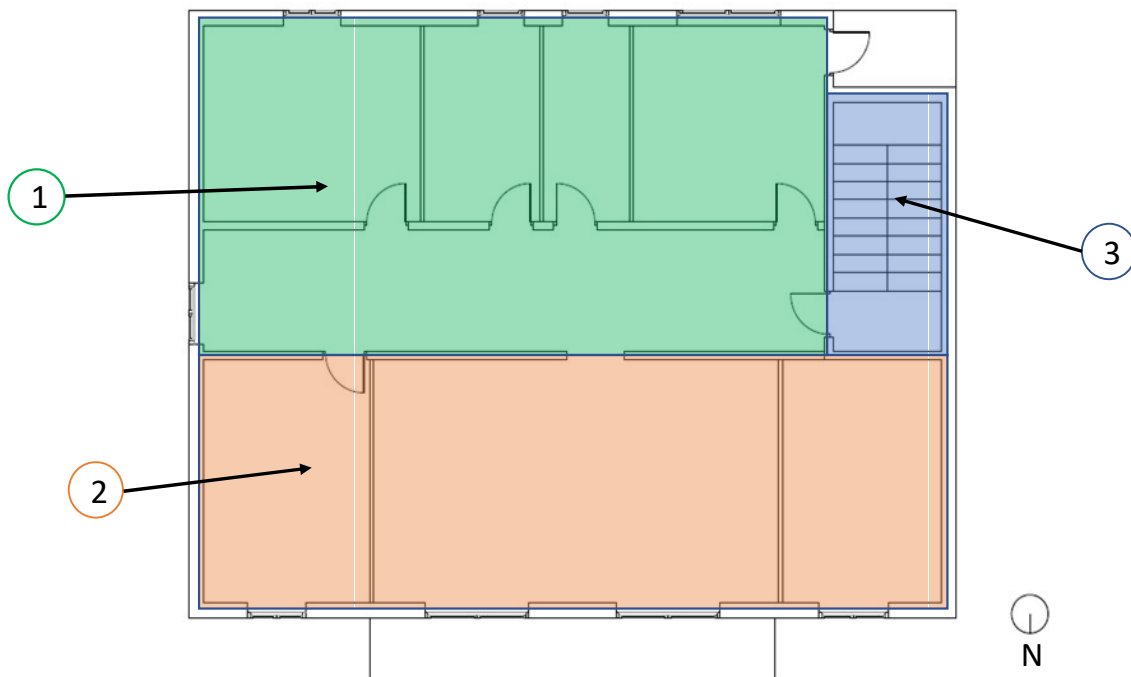
As previously said, only the first floor of the building is interested by the HYBUILD system installation in which the doctor apartment is located. More information about this zone are reported in Table 23 while Figure 47 presents the first floor plan. To determine in a realistic way heating and cooling demands of the building it has been decided to divide the building in five different zones as visible in Table 24. The ground floor and roof, being not interested by HYBUILD system installation, have been treated simply as two independent zones. The first floor has been subsequently divided in 3 different zones to take into account the fact that there is a stairwell that has been assumed as unheated space and the difference in solar gain of the rooms due to the different orientations. In Figure 47, the three zones representing the first floor divisions are highlighted. Moreover, it is important to notice that dimensions from mid-wall between inside and outside have been used. This motivates also the slightly difference in the area values of Table 23 and Table 24.

Table 23 - First floor information

First floor			
N° of rooms	Gross area	Net area	Height
	[m <sup>2</sup> ]	[m <sup>2</sup> ]	[m]
8	132.5	112.5	2.7

Table 24 - Zones characteristics

Zones characteristics				
FLOOR	ZONE	n° ZONE	LABEL	AREA
				[m <sup>2</sup> ]
GROUND	REST	0	GF	124.0
FIRST	HYBUILD	1	FF_1	61.0
FIRST	HYBUILD	2	FF_2	54.7
FIRST	HYBUILD	3	FF_3	8.3
ROOF	REST	4	ROOF	124.0



PLANTA PRIMER PIS

E: 1/100

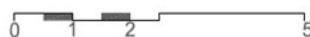


Figure 47 – First floor plan

### 3.4.4 Boundary conditions / model inputs

As previously said, five independent zones have been individuated to model the building. It is here important to remind that the presented simulations have been run on the actual state of

the existing building. The model's geometry has been created firstly using Sketch Up Tool (Figure 48) and then it has been imported to TRNSYS where internal gains, ventilation and infiltration rates have been added to the model. The dimensions of the model have been taken as average between internal and external dimensions. Regarding the schedule used to identify internal gains and space heating and cooling, a distinction between weekdays, weekend days and holidays became necessary in particular to model the ground floor.



Figure 48 – Almatret Sketch Up model

### **Heating system**

The heating system is a decentralized one, in particular a boiler that burns propane gas is used both to prepare DHW and to cover space heating demand sending the hot water to the 10 radiators of the apartment. As said before, the first floor zone FF\_3 is not heated and so the total heated area results equal to 112,5 m<sup>2</sup>. Regarding the operation schedule for the apartment the heating power has been considered as always available. For this reason, it has been considered that the temperature in the apartment's heated zones is maintained not lower than 21 °C for all the winter period. This temperature is fixed after a comparison with heating consumption obtained from bills (see paragraph 3.4.6).

Different considerations have been made on the contrary for the ground floor. Being this space used as medical office it has been supposed that the zone is heated to 21 °C only in the central hour of the week days (schedule visible in Table 25 and Figure 49) when it is used as ambulatory whereas the temperature is set to 19 °C for the rest of the time. For simulation purposes, ideal heating system has been used. The presented system does not foresee any dehumidification or air humidity control.

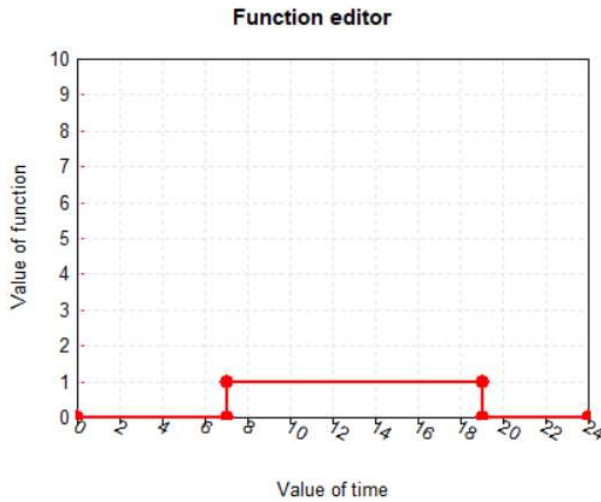


Figure 49 – Medical office heating schedule

<i>Heating schedule</i>		
	from	to
ON	7:00 AM	7:00 PM
OFF	7:00 PM	7:00 AM

Table 25 – Heating schedule

**Internal gains**

Two different kind of internal gains have been considered in the building model: occupancy and electrical (appliances and lighting). As apartment occupancy and electrical gains, typical profiles for a single-family house have been chosen (Figure 50, Table 26 and Figure 51, Table 27) whereas for the medical office it has been supposed that 5 people are present only when the clinic is open (see Table 29). Moreover, for this zone, a specific electrical contribution equal to 10 W/m<sup>2</sup> has been set when the clinic is open (Figure 52, Table 28) to consider the gain coming from electrical devices.

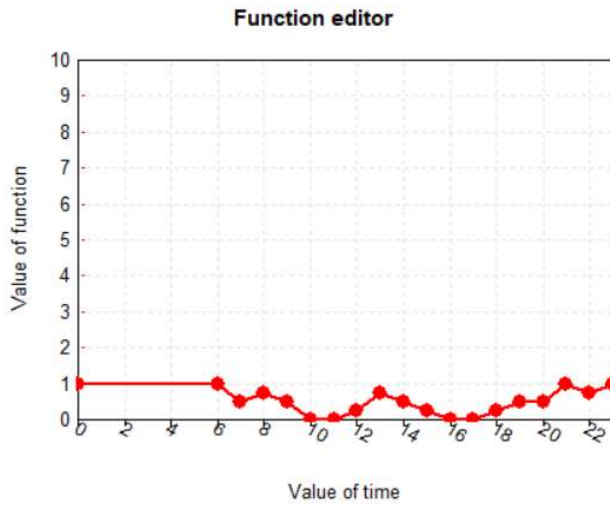


Figure 50 – Apartment occupancy profile

Occupancy apartment	
Time	Value
0	1
6	1
7	0.5
8	0.75
9	0.5
10	0
11	0
12	0.25
13	0.75
14	0.5
15	0.25
16	0
17	0
18	0.25
19	0.5
20	0.5
21	1
22	0.75
23	1

Table 26 – Ratio of apartment occupancy

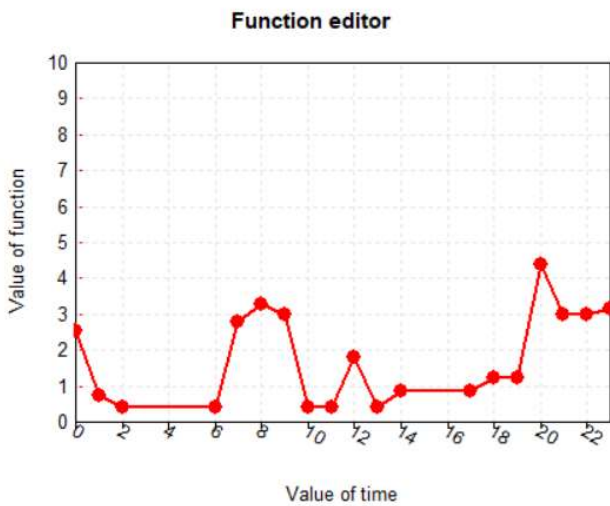


Figure 51 – El. gains apartment profile

El. gains apartment	
Time	Value
0	2.54
1	0.75
2	0.39
6	0.39
7	2.8
8	3.27
9	3
10	0.39
11	0.39
12	1.79
13	0.39
14	0.86
17	0.86
18	1.21
19	1.21
20	4.39
21	3
22	3
23	3.16

Table 27 – El. gains apartment (W/m<sup>2</sup>)

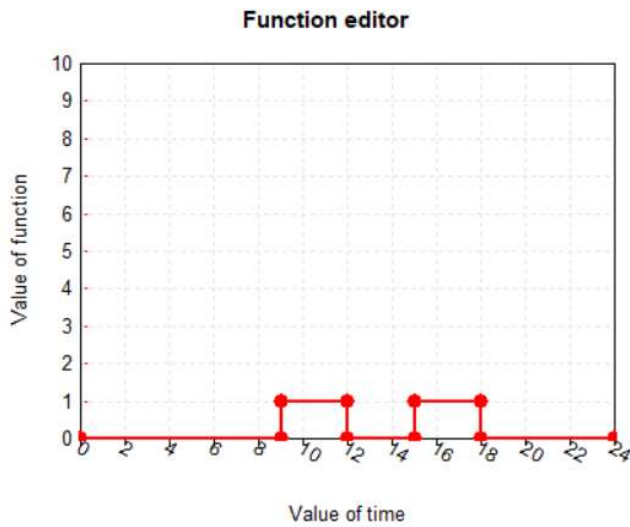


Figure 52- Medical office occupancy during week days profile

Occupancy medical office	
Time	Value
0	0
9	0
9	1
12	1
12	0
15	0
15	1
18	1
18	0
24	0

Table 28 – Ratio of medical office occupancy during week days

The heat gain due to one person has been fixed to 80 [W/pers] (according to [50], typical metabolic heat generation for standing, relaxed activities). This value is further divided in three main contributions: latent (40%), convective (42%) and radiative (18%).

The occupancy of the apartment has been decided based on hypothesis, considering a typical family of 4 persons equally divided between the two heating zones. A further calibration process will define these assumptions with higher accuracy.

In Table 29 the number of occupants of the various building zones is reported.

Table 29 – Number of occupants in the various HYBUILD zones

Occupancy		
FLOOR	ZONE	N° PERS
GROUND	GF	5
FIRST	FF_1	2
FIRST	FF_2	2
FIRST	FF_3	0

**Ventilation and Infiltration**

In the Almatret demo building, any mechanical ventilation system is installed and user’s opening of windows is the only contribution to natural ventilation. A ventilation rate of 0.3 vol/h has been used whereas the infiltration rate through the envelope has been set to 0.15 vol/h. Both these ventilation rates have been considered constant along the year.

### 3.4.5 Energy balance

In Figure 53 and Figure 54 the Energy balances of the HYBUILD zones are reported month by month for an entire average year. The components of the balances are internal gains (supposed to be constant for all the months), infiltration and ventilation contribution and thermal losses. These last four contributions vary along the year due to the variation of internal and external temperature. Heating energy is therefore defined for covering energy losses.

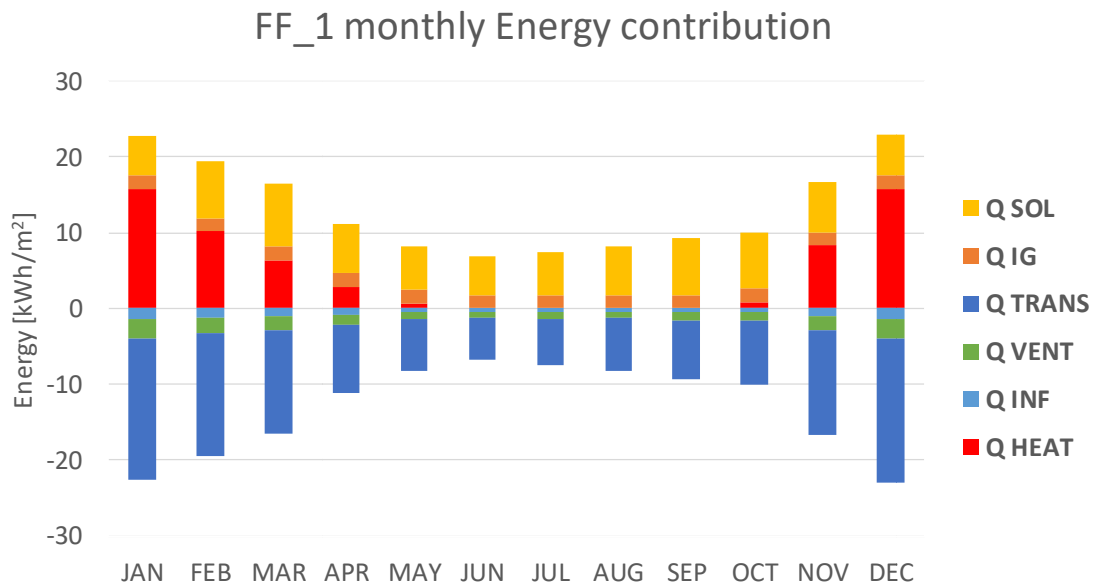


Figure 53 - Yearly energy balance of FF\_1 zone

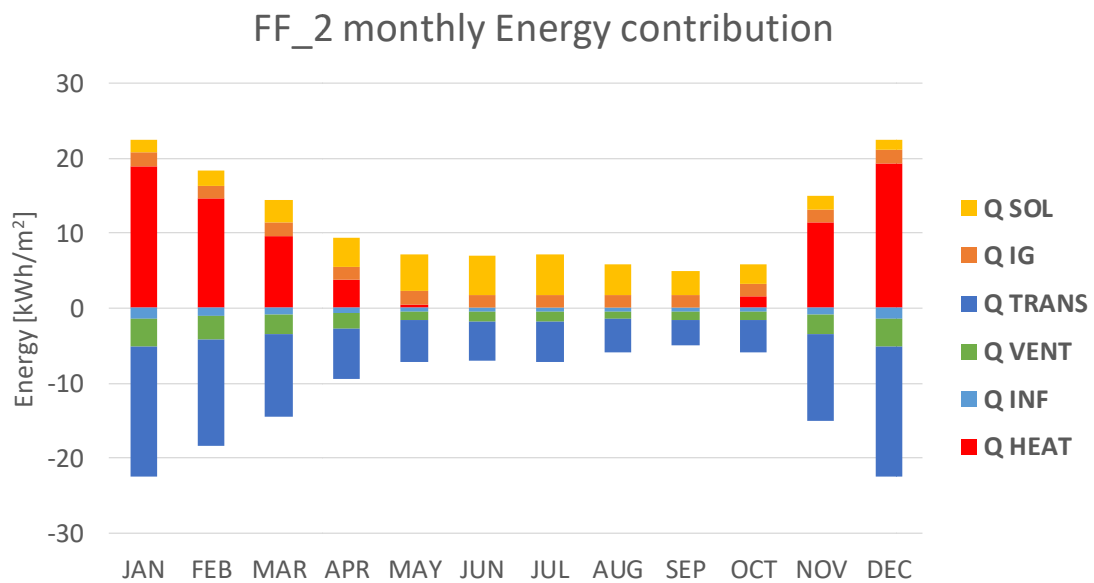


Figure 54 - Yearly energy balance of FF\_2 zone

Any cooling system has been considered in the simulations as it is at the moment in the real case. Despite that, being Almatret characterized by high ambient temperatures during the summer period an evaluation of the internal temperature and the number of hours in which

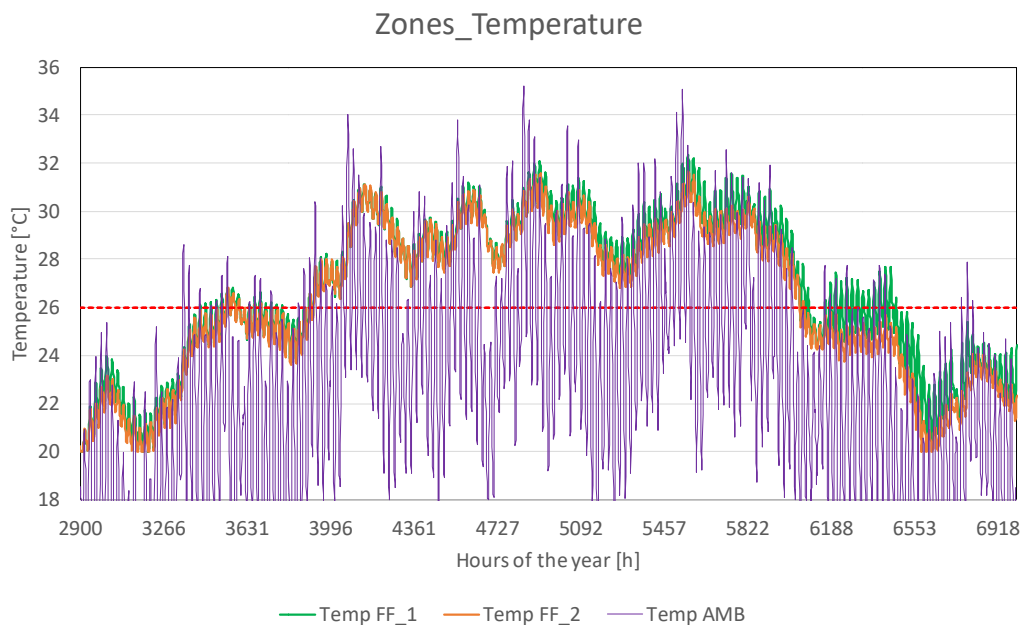
this value is above the comfort one (set equal to 26 °C) has been performed. Results of this analysis are visible in Figure 55 in which the temperature of the various apartment zones are reported. It can be noticed that a maximum temperature of 32 °C has been reached in the apartment.

Figure 56, instead, gives indication about the percentage of time in which the internal temperature is above the summer comfort one. Even if the various zones present slightly different temperature values an overheating problem is present and makes reasonable to think to the installation of a space cooling system. To have an evaluation of the space cooling demand a simulation considering also the presence of an ideal cooling system has been run. The calculated space cooling demand is equal to 2606.6 kWh/year whereas the cooling power peak is around 3.0 kW. Cooling results are summarized in Table 30.

**Table 30 – Summary of cooling demand and peak load in the existing case for guaranteeing the thermal comfort during summertime.**

<i>Resume HYBUILD zones</i>				
Zone	Space cooling demand	Specific space cooling demand	Maximum peak load	Specific maximum peak load
	[kWh/y]	[kWh/m <sup>2</sup> /y]	[kW]	[W/m <sup>2</sup> ]
FF_1	1465.4	24.0	1.8	16
FF_2	1141.3	20.9	1.4	12.5
FF_3	0.0	0.0	0.0	0.0
<b>TOTAL</b>	<b>2606.6</b>	<b>23.2</b>	<b>3.0</b>	<b>27</b>

If any cooling system is installed in the apartment a night cooling strategy could help to improve the thermal comfort. This comes from the notably decrease of the ambient temperature during the nights even in the summer period (Figure 55).



**Figure 55 – Internal temperature of the three apartment zones during summer period**

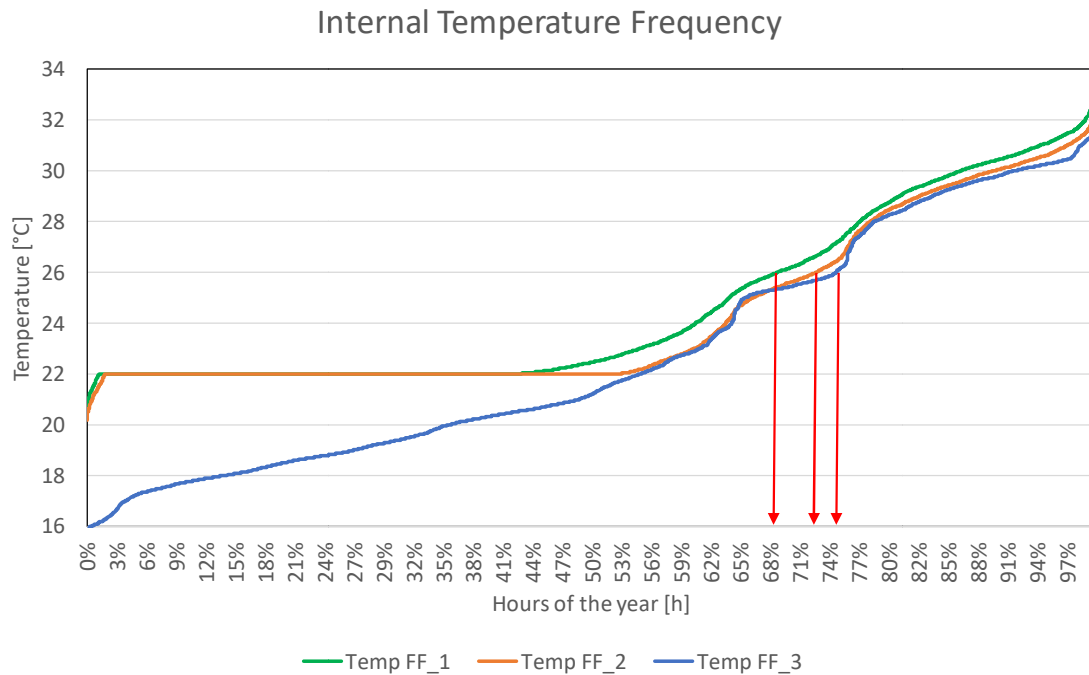


Figure 56 – Cumulative frequency of the three apartment zones internal temperature over the year

### 3.4.6 Demands and peak loads

Space heating energy demands for the studied zones are summarized on a yearly base in Table 31. In this, it can be noticed that heating demand of zone 2 is the highest. This is due to the North orientation of the major façade.

The average space heating demand results 68.8 kWh/(m<sup>2</sup>year) whereas the maximum peak power requested by the apartment is around 5.4 kW. To have a more realistic evaluation, data obtained from simulations have been compared with data coming from different technical papers reporting data measured on site. Being the total fuel consumption of the boiler the only comparable value, some assumptions have been made. Firstly, knowing the heated area, specific consumption values have been calculated. The second step instead consisted in dividing gas consumption for DHW preparation and for space heating. For doing so, the quantity of gas used during summertime has been assumed to be every month used for DHW uses. Consequently, a DHW consumption of 21 kWh/(m<sup>2</sup>y) has been obtained. Lastly, the remaining energy consumption has been multiplied by the boiler efficiency (0.8 considering an instantaneous propane boiler) for calculating heating demand. The just mentioned steps are summarized in Table 32 and give a final space heating consumption of 73.9 kWh/(m<sup>2</sup>year) in good agreement with the simulation value (68.8 kWh/(m<sup>2</sup>y)). In Figure 57 the monthly values of the boiler consumption (blue) and energy demand coming from simulation (orange) have been reported. The trends of the two demands are in line. To be noted that the simulation year is different from the one which consumption data refers to. A more detailed building validation will follow.

Table 31 - Resume HyBuild zones energy demand for space heating and maximum peak load

Resume HYBUILD zones			
Zone	Space heating demand	Specific space heating demand	Maximum peak load
	[kWh/y]	[kWh/m <sup>2</sup> /y]	[kW]
FF_1	3389.0	55.6	2.7
FF_2	4353.6	79.6	2.7
FF_3	0.0	0.0	0.0
<b>TOTAL</b>	<b>7742.6</b>	<b>68.8</b>	<b>5.4</b>

Table 32 – Consumption data, assumptions and calculation

Consumption data, assumption and calculation		
Energy consumption	12750.0	[kWh/y]
Net area	112.5	[m <sup>2</sup> ]
Specific En. consumption	113.3	[kWh/m <sup>2</sup> /y]
DHW cons. contribution	21.0	[kWh/m <sup>2</sup> /y]
SH cons. contribution	92.3	[kWh/m <sup>2</sup> /y]
Boiler efficiency	0.8	[-]
SH demand	73.9	[kWh/m <sup>2</sup> /y]

Boiler fuel consumption, heating demand and HDD

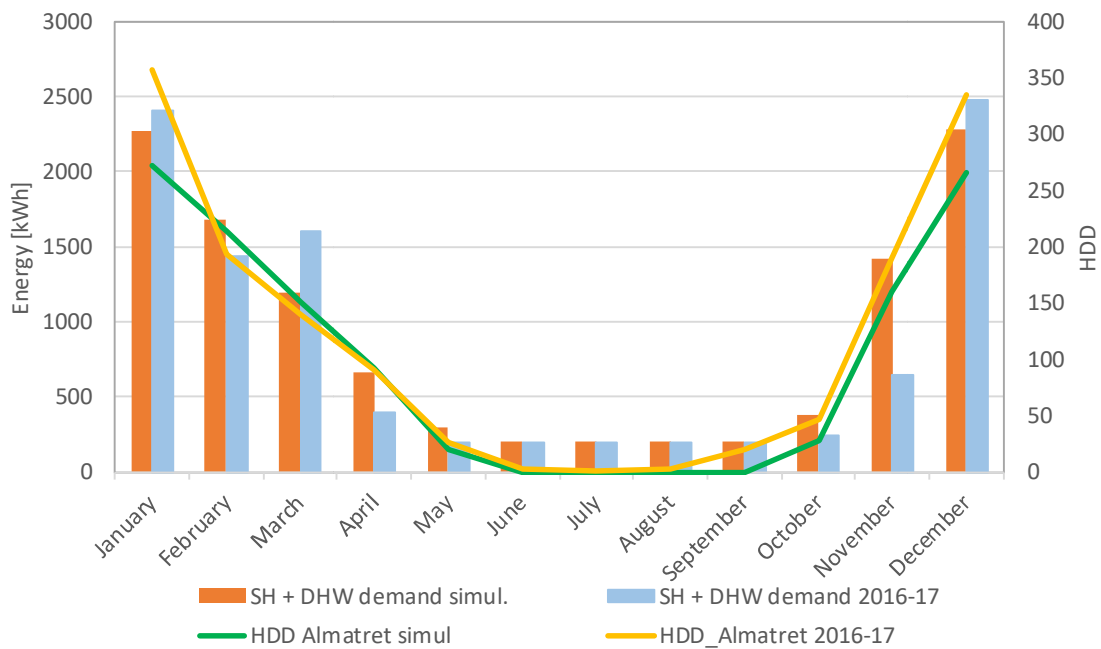


Figure 57 - Consumption of propane gas from October 2016 to September 2017

Monthly heating demands are instead shown in Table 33, for the three zones separately, and together. December and January result to be the coldest months with, consequently, the highest heating demand; February, March and November have around one third less heating demand than the coldest months while April, May and October require very few space heating.

The maximum peak power for each zone and for the three zones simultaneously are reported in Table 34. As already mentioned, the maximum peak power is verified in December with a total value for the apartment of 5.4 kW.

**Table 33 - Monthly specific space heating demand of HYBUILD zones**

Zone	JAN	FEB	MAR	APR	MAY	JUN	JUL	AUG	SEP	OCT	NOV	DEC
	[kWh/m <sup>2</sup> ]											
<b>FF_1</b>	15.1	9.6	5.6	2.1	0.3	0.0	0.0	0.0	0.0	0.5	7.4	14.9
<b>FF_2</b>	18.9	14.6	9.6	3.8	0.5	0.0	0.0	0.0	0.0	1.5	11.4	19.2
<b>FF_3</b>	0.0	0.0	0.0	0.0	0.0	0.0	0.0	0.0	0.0	0.0	0.0	0.0
<b>TOT</b>	15.8	11.2	7.0	2.7	0.4	0.0	0.0	0.0	0.0	0.9	8.7	15.8

**Table 34 - Monthly space heating peak demand of HYBUILD zones**

Zone	JAN	FEB	MAR	APR	MAY	JUN	JUL	AUG	SEP	OCT	NOV	DEC
	[kW]											
<b>FF_1</b>	2.6	2.2	1.9	1.1	0.7	0.0	0.0	0.0	0.0	0.8	1.8	2.7
<b>FF_2</b>	2.5	2.2	1.9	1.2	0.8	0.0	0.0	0.0	0.0	0.9	1.8	2.7
<b>FF_3</b>	0.0	0.0	0.0	0.0	0.0	0.0	0.0	0.0	0.0	0.0	0.0	0.0
<b>TOT</b>	5.1	4.4	3.8	2.2	1.5	0.0	0.0	0.0	0.0	1.7	3.6	5.4

### 3.5 Models of the core components

As previously introduced, reduced models for each components have been received from Task 3.1 where each new solution has been studied in detailed. Simplified numerical models have therefore been developed for modelling the whole system, distribution circuit and building included. In the following paragraphs, the description of the components and the developed models is reported.

#### 3.5.1 Sorption storage

##### 3.5.1.1 Description of the technology

The sorption storage module employed in the system is composed of two absorbers and two vacuum chambers for condenser and evaporator. In particular, the evaporator of the sorption storage will be connected to the condenser of the vapour compression chiller, in order to reduce the temperature lift and improve its performance. A schematic layout of the module and the integration in the overall system is shown in Figure 58, where the input parameters for each circuit are shown. The two absorbers work in counter-phase operation, in order to produce continuous cooling effect. During a typical working cycle, an absorber, which is completely saturated of water vapour (i.e. after having completed a previous adsorption

cycle), is connected to the heat source, in this case represented by the Fresnel solar collectors, which deliver the heating power to regenerate the adsorbent material. The heat flux is characterized by a defined mass flow rate,  $\dot{m}_{HT}$ , and an inlet temperature,  $HT_{in}$ . During the heating up phase, the pressure inside the absorber chamber increases as well. As soon as the pressure reaches the one existing in the condenser, the connecting valve between absorber and condenser is opened, and water vapour is desorbed against the condenser. The condensation heat in this phase is dumped into the ambient by means of a dry cooler. The cooled heat transfer fluid entering the condenser is then characterized by a mass flow rate,  $\dot{m}_{MT}$ , and an inlet temperature,  $MT_{in}$ . Once the regeneration of the adsorbent material is completed, the connection with the condenser is closed, and the absorber is connected directly to the dry cooler to be cooled down. As soon as the pressure inside the chamber reaches the pressure existing inside the evaporator, the valve between absorber and evaporator is opened, and the evaporation process starts. This guarantees the production of cooling effect. The chilled water entering the evaporator is characterized by a mass flow rate,  $\dot{m}_{LT}$ , and an inlet temperature,  $LT_{in}$ . In this phase, the absorber is continuously cooled down by means of the dry cooler, since it needs to reject the heat of adsorption caused by the exothermic reaction occurring between the water vapour and the adsorbent material. As already specified above, the second absorber is operating in the opposite mode.

### 3.5.1.2 Description of the reduced model

The reduced model of the sorption module is derived from the detailed model implemented in Dymola environment, whose details are reported in D3.1. The approach is to provide performance maps of the sorption module as a function of the most relevant boundary conditions, i.e. temperature of the heat source, ambient temperature and evaporator temperature. The mass flow rates are fixed according to the specifications of Fahrenheit, the adsorption machine provider. The simulated working conditions are reported in Table 35. The heating source temperature can vary from 90°C down to 75°C. Indeed, below this temperature, the adsorbent material is not effectively regenerated. On the contrary, no performance improvement can be achieved above 90°C, since the material gets almost completely regenerated at this temperature. The condensation temperature varies between 40°C and 25°C, to consider both extremely warm and cold ambient conditions. Finally, the operation is considered at a fixed cooling set-point of 15°C.

**Table 35. Boundary conditions employed for the sorption module simulations.**

	HT	MT	LT
$\dot{m}$ [kg min <sup>-1</sup> ]	27	29	41
T [°C]	90-75	40-25	15

Two main parameters are evaluated for the definition of the performance maps, namely, the thermal Coefficient of Performance,  $COP_{th}$ , and the cooling power,  $Q_{LT}$  [kW], defined as follows:

$$COP_{th} = \frac{Q_{LT}}{Q_{HT}}$$

$$Q_{LT} = \dot{m}_{LT} cp (LT_{in} - LT_{out})$$

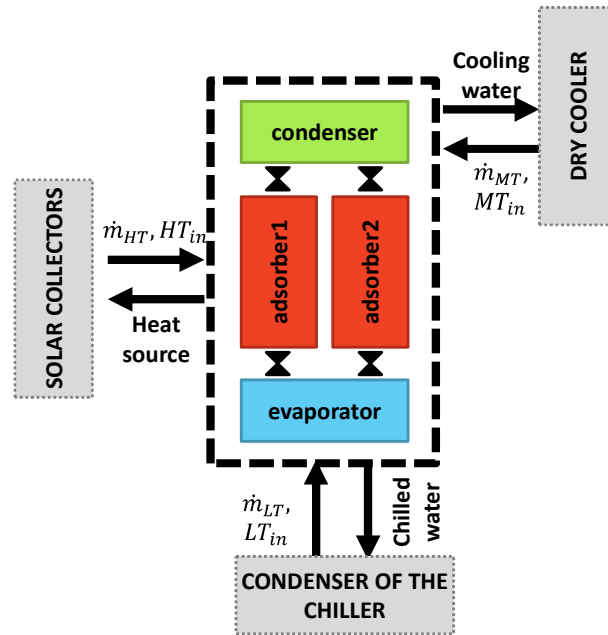


Figure 58 - Schematic layout of the sorption module and its integration with the other components in the system.

### 3.5.1.3 Description of the simplified model

The obtained performance maps as well as raw data are reported in Figure 59 and Table 36. It has to be highlighted that, simulations were performed by varying the cycle time, in order to optimize the cooling power produced by the sorption module. Consequently, varying this parameter, also the  $COP_{th}$  is affected, confirming in most of the cases a COP around 0.5. Of course, in case of heat source available at temperature below  $75^{\circ}C$ , the sorption module is not operated anymore, thus letting the vapour compression chiller to directly reject the heat of condensation towards the environment, by means of the dry cooler.

In the model of the overall system in the TRNSYS environment, the sorption chiller is modelled as a sort of *lookup table* that, depending on the working conditions, returns performance and exchanged heat. Inputting the three working temperatures,  $HT_{in}$ ,  $MT_{in}$  and  $LT_{in}$ , the exchanged heat,  $Q_{LT}$ , and the device performance,  $COP_{th}$ , are given.

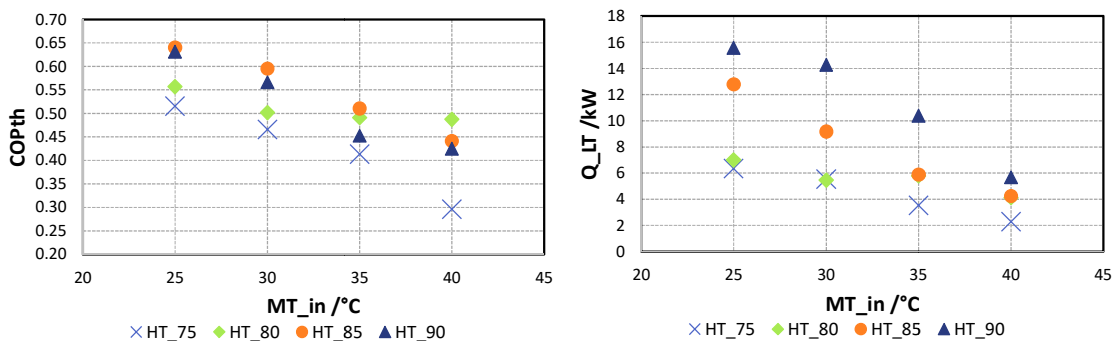


Figure 59 - Reduced performance maps of the adsorption module, derived by detailed simulations implemented in Dymola. On the left-hand side, the thermal COP ( $COP_{th}$ ) as a function of ambient temperature,  $MT_{in}$ , by varying the driving temperature from the solar collectors,  $HT_{in}$ . On the right-hand side, the cooling power delivered by the sorption module, at a fixed evaporation temperature of  $20^{\circ}C$ , by varying the other boundary conditions.

**Table 36. Raw data of the adsorption module performance maps**

$HT_{in}$	$MT_{in}$	$LT_{in}$	$Q_{LT}$	$COP_{th}$	cycle time
°C	°C	°C	kW	-	s
75	25	15	6.4	0.52	500
75	30	15	5.5	0.47	700
75	35	15	3.5	0.41	800
75	40	15	2.3	0.30	1000
80	25	15	7.0	0.56	500
80	30	15	5.5	0.50	600
80	35	15	5.8	0.49	700
80	40	15	4.1	0.49	900
85	25	15	12.8	0.64	500
85	30	15	9.2	0.60	500
85	35	15	5.9	0.51	600
85	40	15	4.2	0.44	700
90	25	15	15.6	0.63	400
90	30	15	14.3	0.57	450
90	35	15	10.4	0.45	500
90	40	15	5.7	0.43	600

### 3.5.2 Chiller and latent storage

The chiller of the Mediterranean concept is a conventional vapour compression machine consisting of two heat exchangers (evaporator and condenser), a hermetic scroll compressor and a Thermostatic Expansion Valve (TEXV). The analytical model was developed in Task 3.1 using the Moving Boundary methodology for the heat exchangers and steady state models for the rest of the components, while the TEXV is controlling the superheating temperature by means of a PID controller. Since the standard evaporator of the chiller will be replaced by the Refrigerant-PCM-Water Heat Exchanger (RPW-HEX), it was decided to implement a simplified model for both components.

As the chiller dynamics are in general faster compared to the inertia of the Phase Change Material (PCM), the former can be modelled using polynomial expressions that correlate the cooling capacity and the compressor power to the evaporation and condensation pressure, which is quite common in literature [51]. On the other hand, in order to model the behaviour of the PCM, a simplified procedure proposed by UDL was followed.

Firstly, in order to develop the simplified model three possible scenarios were defined:

- Scenario 1: Refrigerant is charging the PCM. There is no water circulation.
- Scenario 2: Water is discharging the PCM. There is no refrigerant circulation.
- Scenario 3: Refrigerant cooling the water. In this situation the PCM will be partially charged/discharged.

The model developed for control strategies will calculate the refrigerant conditions at the outlet (point 1) of the HEX while the state of charge of the PCM will be also calculated.

The PCM behaviour is deeply studied in Dymola, while a simplified model that integrates the chiller too is used in the model of the whole system. The reported equation are therefore implemented in the TRNSYS environment.

### 3.5.2.1 Scenario 1: Refrigerant is charging the PCM

The PCM energy capacity is calculated in Eq.1.

$$E_{PCM} = E_{PCM,latent} + E_{PCM,sensible} \quad \text{Eq. 1}$$

Since no water circulation exists, the energy stored in the PCM is equal to the energy provided by the chiller, which is:

$$E_{PCM,t} = E_{PCM,t-1} + Q_{evap,t} \cdot \Delta t \quad \text{Eq. 2}$$

where  $E_{PCM,t}$  is the energy stored in the PCM at the moment  $t$  and  $Q_{evap,t}$  the power of the evaporator.

Since the condensation pressure is usually unknown during the simplified simulation of a chiller, the cooling capacity and the compressor power were correlated to the water temperature in the inlet of the condenser instead (assuming fixed water flow through the condenser).

As a result, by utilizing the analytical model developed for Task 3.1 the performance maps depicted in Figure 60 and Figure 61 respectively were created:

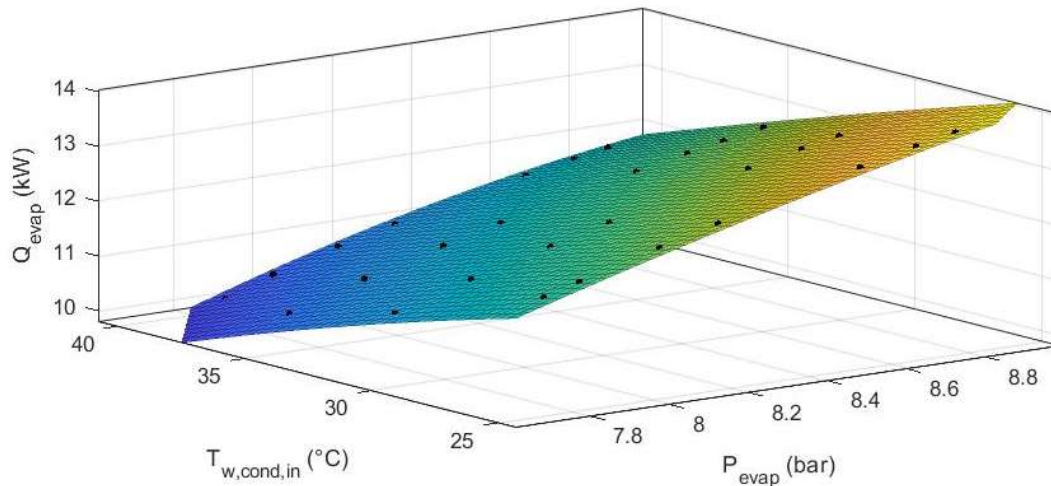


Figure 60 - Chiller cooling capacity performance map and fitted surface

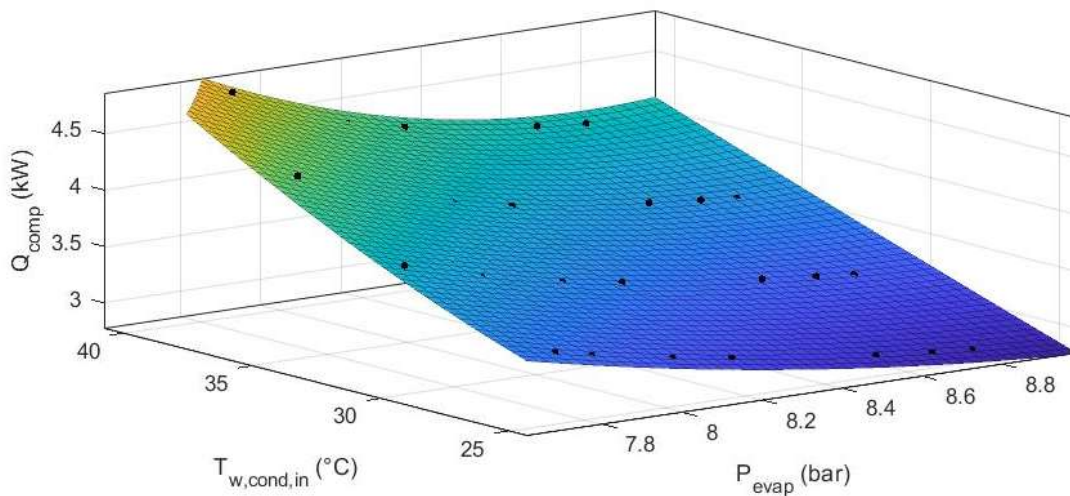


Figure 61 - Chiller compressor power performance map and fitted surface

The above performance surfaces were fitted by a surface resulting in the following correlations (where  $p_{evap}$  in bars and  $T_{w,cond,in}$  in °C):

$$P_{evap}(kW) = -94.99 + 24.21 \cdot p_{evap} - 1.303 \cdot p_{evap}^2 + 6.059 \cdot T_{w,cond,in} - 0.1207 \cdot T_{w,cond,in}^2 - 0.1207 \cdot p_{evap} \cdot T_{w,cond,in} + 0.0833 \cdot p_{evap}^2 \cdot T_{w,cond,in} + 0.0281 \cdot p_{evap} \cdot T_{w,cond,in}^2 - 0.0016 \cdot p_{evap}^2 \cdot T_{w,cond,in}^2 \quad \text{Eq. 3}$$

$$P_{comp}(kW) = 77.21 - 16.97 \cdot p_{evap} - 0.9449 \cdot p_{evap}^2 - 5.37 \cdot T_{w,cond,in} + 0.128 \cdot T_{w,cond,in}^2 + 1.24 \cdot p_{evap} \cdot T_{w,cond,in} - 0.7066 \cdot p_{evap}^2 \cdot T_{w,cond,in} - 0.0294 \cdot p_{evap} \cdot T_{w,cond,in}^2 + 0.0017 \cdot p_{evap}^2 \cdot T_{w,cond,in}^2 \quad \text{Eq. 4}$$

Since  $p_{evap}$  should be unknown as well, it was correlated to the average PCM temperature  $T_{PCM}$  (lumped model), over the operating range tested:

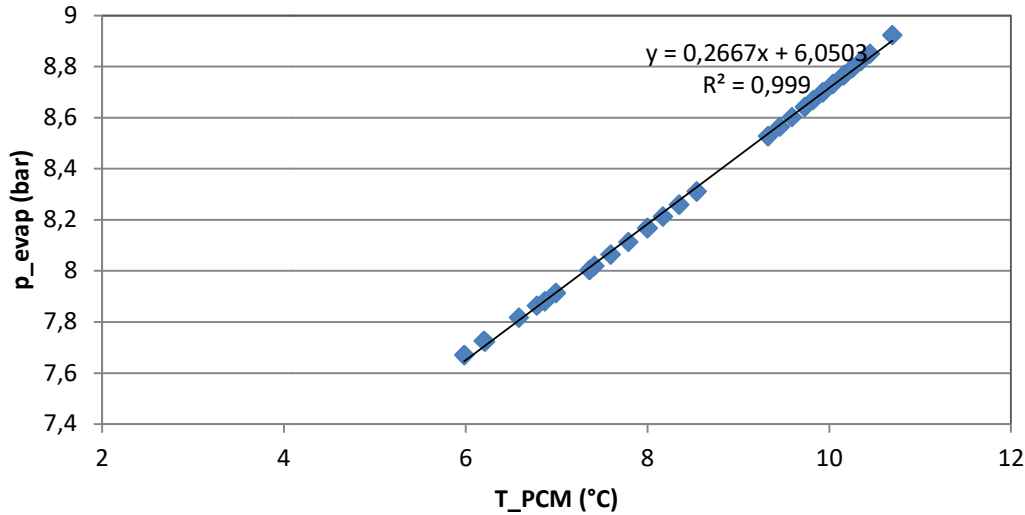


Figure 62 - Correlation between  $T_{PCM}$  and evaporation pressure

which yields to the following expression:

$$p_{evap}(\text{bar}) = 0.2667 \cdot T_{PCM,t} (\text{°C}) + 6.0503 \quad \text{Eq. 5}$$

While  $T_{PCM,t}$  can be explicitly found by the following expression:

$$T_{PCM,t} = \begin{cases} -0.002 \cdot E_{PCM,t} + 12, & \text{if } E_{PCM,t} \leq 5082 \text{ kJ} \\ -0.000037 \cdot E_{PCM,t} + 2.1875, & \text{if } E_{PCM,t} > 5082 \text{ kJ and} \\ -0.003 \cdot E_{PCM,t} + 96, & \text{if } E_{PCM,t} \geq 32186 \text{ kJ} \end{cases} \quad \text{Eq. 6}$$

The electrical consumption of the compressor can be directly calculated by the compression power, assuming a fixed electric motor efficiency equal to 0.93:

$$W_{comp}(KW_{el}) = \frac{Q_{comp}}{0.93} \quad \text{Eq. 7}$$

while the chiller COP is calculated immediately as:

$$COP = \frac{Q_{evap}}{W_{comp}} \quad \text{Eq. 8}$$

The condenser output power is also known, since:

$$Q_{cond} = Q_{evap} + Q_{comp} \quad \text{Eq. 9}$$

Finally, the State of Charge of the latent heat storage can be calculated from the following expression (see Figure 63):

$$SOC = \begin{cases} -0.0101 \cdot T_{PCM} + 0.9697, & \text{if } T_{PCM} \leq 1^{\circ}C \\ -0.8081 \cdot T_{PCM} + 1.7677, & \text{if } T_{PCM} > 1^{\circ}C \text{ and } T_{PCM} < 2^{\circ}C \\ -0.0152 \cdot T_{PCM} + 0.1818, & \text{if } T_{PCM} \geq 2^{\circ}C \end{cases} \quad \text{Eq. 10}$$

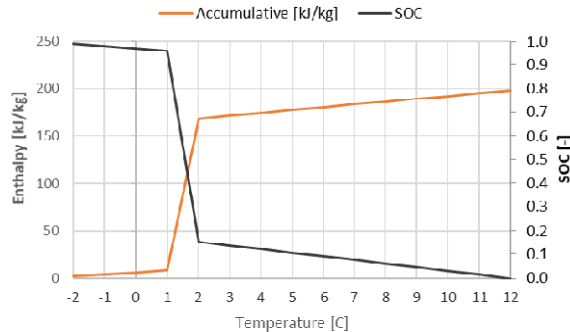


Figure 63 - Enthalpy and SOC in function of PCM temperature.

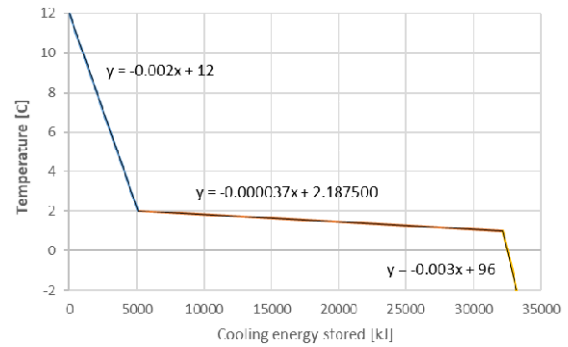


Figure 64 - Cooling energy stored by the PCM function of the PCM temperature.

### 3.5.2.2 Scenario 2: Water is discharging the PCM

Table 37 shows the inlet and the outlet parameters for the three fluid HEX. Notice that in this scenario, the characteristics of the refrigerant are not required since there is no refrigerant circulation.

Table 37. List of inlet and outlet parameters for the PCM storage tank

Inlet parameters		Outlet parameters	
Water flow rate [kg/s]	$\dot{m}_{in}$	Water outlet temperature [°C]	$T_{w,out}$
Water inlet temperature [°C]	$T_{w,in}$	SOC [%]	SOC [%]
Initial energy stored	$E_{PCM,o}$	PCM temperature [C]	$T_{PCM}$
PCM temperature [C]	$T_{PCM} (t-1)^1$	Total energy stored	$E_{PCM,t}$

<sup>1</sup> (t-1) means the previous time step.

The relationship between PCM temperature and SOC and energy stored showed before is also useful for this scenario, so the relations presented before are also playing an important role in this scenario.

In this scenario, water is the heat transfer fluid (HTF) which discharges the PCM. Water is entering the HEX at a certain temperature ( $T_{w,in}$ ) and flow rate ( $\dot{m}_{in}$ ). Both are inlet parameters for the model. For the model, the discharge process is assumed to behave as an internal flow through a constant temperature surface (phase change temperature).

In order to avoid any iterative method that will result in a high computational cost, the isothermal model makes use of an explicit scheme to discretize the time. Therefore, if the power of discharge of the PCM is assumed to be the same during the time step between the instant “n” and the instant “n+1” the amount of energy release by the PCM can be integrated through the time step as Eq. 18 shows:

$$E_{PCM,n \rightarrow n+1} = \int_n^{n+1} \dot{Q}_{PCM} \cdot dt \quad \text{Eq. 18}$$

Once the energy that the PCM has exchanged with the water is determined, the SOC of the PCM at the new instant “n+1” can be calculated. Initially, the available cooling energy in the storage tank is calculated using Eq. 19:

$$E_{PCM,t} = E_{PCM,o} - E_{PCM,n \rightarrow n+1} \quad \text{Eq. 19}$$

### 3.5.3 Electric battery

#### 3.5.3.1 Description of the technology

The electric battery technology which will be integrated in the HYBUILD system belongs to the family of lithium-titanate (LTO). Indeed, they are considered very promising for domestic applications, both for their quick charging rate as well as their safety in operation.

#### 3.5.3.2 Description of the reduced model

The modelling approach followed for the battery simulation is based on the implementation of a set of equations, deriving from an equivalent electric circuit that allows for evaluating voltage and current as a function of a set of parameters experimentally measured.

The equations are the following, as detailed in the D3.1:

$$V = E_0 - J \frac{C_{max}}{C_{max} - C(t)} i + H \exp[-P \cdot C(t)] - R_0 i$$

$$V = E - R_0 i$$

- V, cell voltage [V],
- E<sub>o</sub>, the Open Circuit Voltage(OCV) [V],
- J, the polarization factor [Ah<sup>-1</sup>],
- C<sub>max</sub>, the maximum capacity of the battery [Ah],
- C(t), the charged/discharged capacity at time t [Ah],
- i, the cell current [A],
- H, [V], P [Ah<sup>-1</sup>], R<sub>0</sub> [Ω], some parameters that can be derived from experimental results.

A battery charge regulator will be then implemented in TRNSYS to control the operation of the battery inside the overall system.

The parameters used to implement this model were taken from the literature, for similar battery technology (Table 38) [52]. Once completely characterized the selected batteries, the parameters will be updated for the refinement of the overall model.

**Table 38. Parameters for the battery modelling [52].**

C <sub>max</sub> [Ah]	E <sub>0</sub> [V]	R <sub>0</sub> [Ω]	H [V]	P [Ah <sup>-1</sup> ]	J [Ah <sup>-1</sup> ]	C(t) [Ah] @ V <sub>nominal</sub>
43	3.2326	0.001	0.4574	1.5	0.00034902	37

### 3.5.3.3 Description of the simplified model

In a first stage where measured data is not available, in the TRNSYS environment the electric battery is modelled with a standard type, type 47, based on the the equations devised by Shepherd [REF] and recommended by Hyman [REF]

The model's parameters are defined following Table 38.

More details on the battery numerical model can be found in [53].

### 3.5.4 DC controller/inverter

Before the control algorithm is presented, the system on which this algorithm will be applied is described. The developed Direct Current (DC) bus is meant to interface an external distribution grid, a local renewable energy source, a heat pump and a storage system. The architecture is depicted in Figure 65.

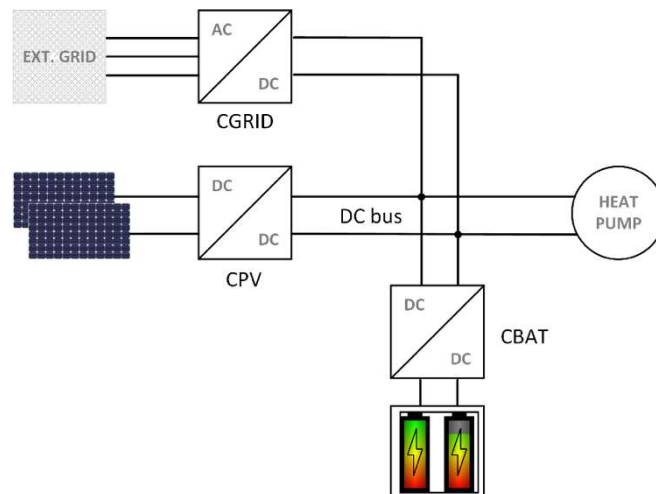


Figure 65 - DC Bus architecture

A voltage-controlled AC/DC grid-tie converter (CGRID) interfaces the DC bus with the external distribution grid. The photovoltaic modules are connected to the DC bus through DC/DC power optimizers (CPV) which guarantee the operation of the modules at their maximum power point. As for the DC/DC battery converter (CBAT), it is current-controlled and manages the interface between the storage system and the DC bus. Finally, the heat pump is directly connected to the DC bus. If a DC supply is not possible, an additional inverter will be added in-between.

In the TRNSYS environment, the DC controller is initially not modelled as, for the sake of the simulation aim, the effect of its use is not kept. The outputs of the simulations are, in fact, accounted in terms of thermal and electric energy, hourly to yearly-based. The degree of detail of a DC controller cannot therefore be appreciated in this kind of simulation. However, the control logics for managing the different electric devices are implemented in the overall system model.

#### 3.5.4.1 Control and measurement system architecture

The purpose of the developed electric controller is to regulate the SoC of the storage system while guaranteeing a stable operation of the DC bus. Its topology is illustrated in Figure 66.

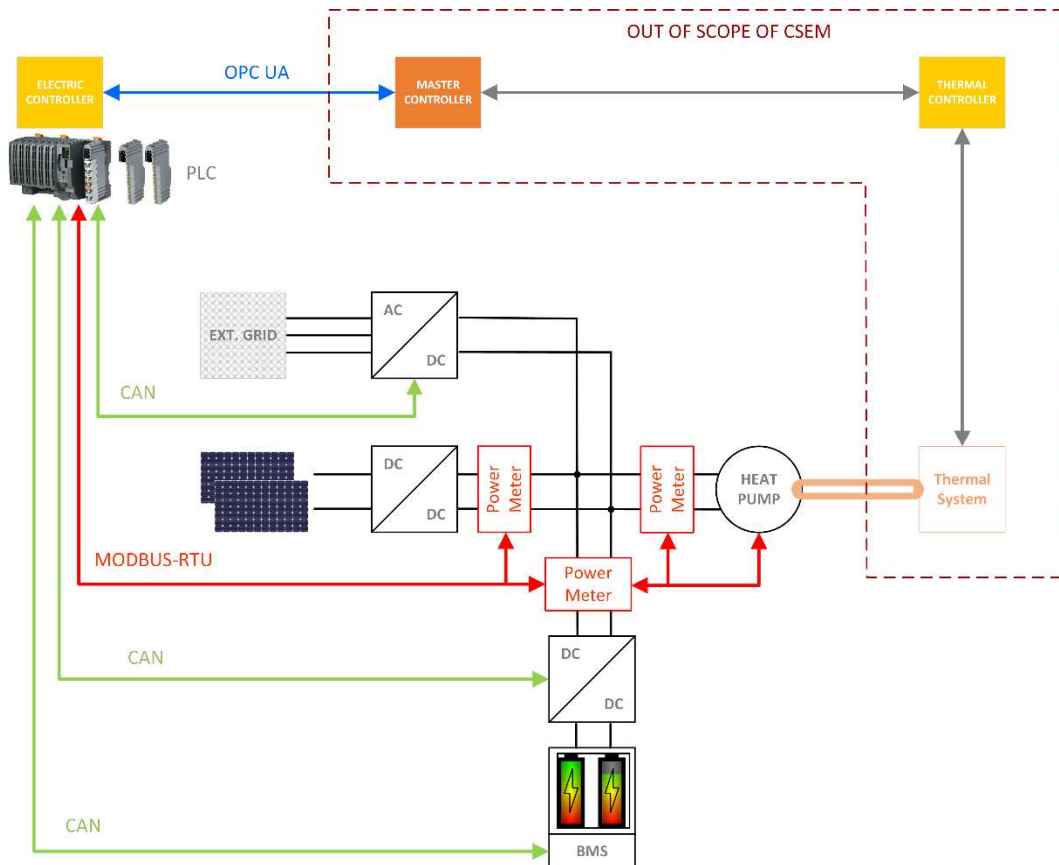


Figure 66 - Control and measurement system architecture

The control system consists of three controllers:

- the master controller, which manages the overall system by reading the system's state through the electric and thermal controller and by sending them setpoints;
- the thermal controller, which manages the thermal system;
- the electric controller, which manages the electric system.

The work provided focuses on the electric controller. Its main device is a Programmable Logic Controller (PLC) with several communication interfaces which allows it to communicate with the various components of the system as well as with the master controller.

The PLC monitors and controls the system in the following way:

- the photovoltaic production, the heat pump consumption and the power exchanged with the storage system are monitored with power meters;
- the SoC of the storage system is monitored by its Battery Management System (BMS);
- the states of the heat pump are also eventually monitored;
- the grid-tie converter and battery converter are controlled by respectively sending them voltage and current setpoints.

The states of the system are then reported to the master controller which feeds back a SoC reference. This SoC reference is the value which enters the electric controller.

#### 3.5.4.2 Control loops

The electric controller is composed of two control loops: the first one regulating the DC bus voltage and the second one regulating the storage system SoC. These control loops are illustrated in Figure 67.

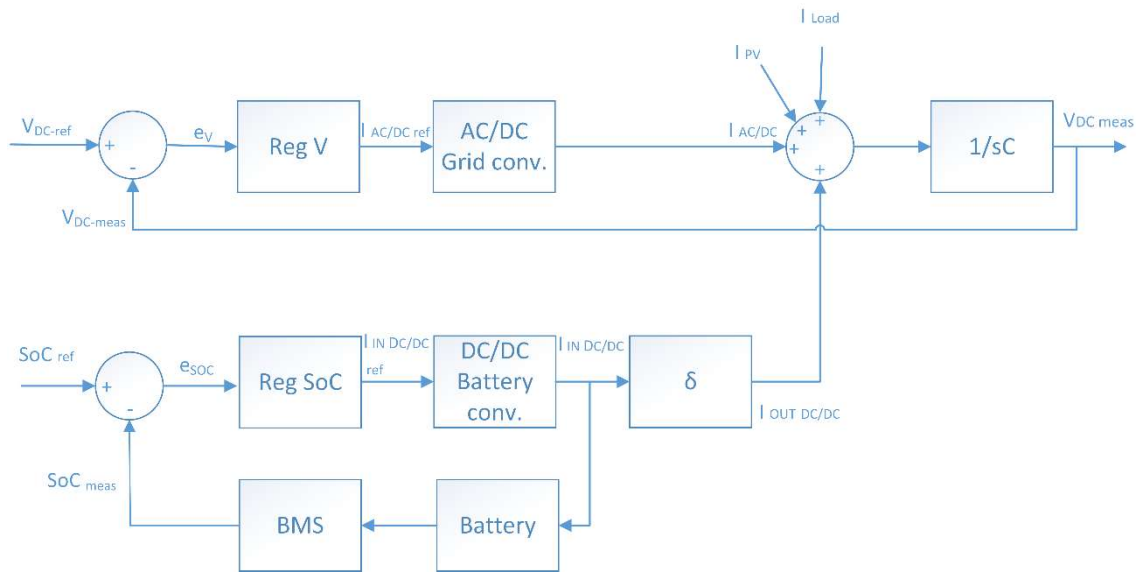


Figure 67 - Control loops topology

The upper loop is meant to regulate the DC bus voltage by controlling the grid-tie converter. The error on the bus voltage  $e_v$ , defined as the difference between the setpoint  $V_{DC-ref}$  (set constant) and the measured one  $V_{DC-meas}$ , enters the voltage regulator *Reg V*. This regulator computes the control variable  $I_{AC/DC-ref}$  which actuates the AC/DC grid-tie converter. The resulting current  $I_{AC/DC}$ , as well as the current linked to the PV production  $I_{PV}$ , load consumption  $I_{Load}$  and battery exchanges  $I_{OUT DC/DC}$ , are added into the DC bus. The voltage of the DC bus is then linked to the integral of the total current flowing through the DC bus' equivalent capacity  $C$ , divided by the value of this capacity.

The purpose of the lower control loop is to regulate the battery SoC by controlling the DC/DC battery converter. As for the first control loop, the error on the SoC ( $e_{SoC} = SoC_{ref} - SoC_{meas}$ ) feeds the SoC regulator *Reg SoC*. This regulator then provides the input current reference  $I_{IN DC/DC-ref}$  to the battery converter. This input current will be exchanged with the battery which will affect its SoC. The SoC is estimated by the BMS and fed back at the beginning of the loop. At the output of the converter, a current  $I_{OUT DC/DC-ref}$  is injected in the DC bus. This current is defined as the input current multiply by  $\delta$ , the ratio between the input voltage (i.e. battery voltage) and the output voltage (i.e. DC bus voltage).

Both regulators consist of a PI controller with saturation. The topology of such a controller is illustrated in Figure 68.

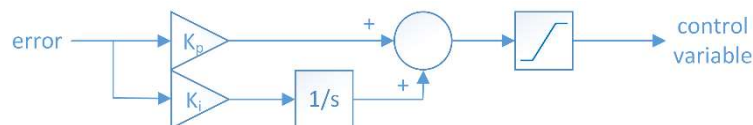


Figure 68 - Topology of a PI controller with saturation

The output of the PI controller (i.e. the control variable) is the sum of a proportional error and an integral error. The proportional error is linked to the error on the regulated state variable multiplied by a proportional gain  $K_p$ . The integral error is the integral of the error multiplied by an integral gain  $K_i$ . To comply with the physical limitations of the actuated devices, the output is saturated.

The gains of the two regulators will be tuned accordingly when all the hardware components will be defined.

### 3.6 Mediterranean system model

The Mediterranean system as a whole, including all the main components, is reported in Figure 69. The core of the hybrid thermal/electric storage solution is represented by a vapour compression chiller (1 in Figure 69) which is directly connected to a three-fluids latent storage on the evaporator side (2) and to a sorption module on the condenser side (3). An electric storage (4) is integrated to enhance the share of renewables and is managed by a DC bus controller (5). The main sources are represented by Fresnel solar collectors (6) and PV panels (7), with the external AC grid that can supply power when the storages are empty and no renewable source is available. Finally, a sensible water storage (8) is installed for storing and providing domestic hot water.

Since the system is primarily meant for providing space cooling in warm climates, its operation is drawn for enhancing the performance of the vapour compression chiller. When the renewable source is available, high temperature heat (e.g. in the range 75-90°C) is provided by the solar collectors to drive the sorption module while at the same time, the electricity produced by the PV panels is used to operate the vapour compression chiller. The sorption module cools down the condenser of the compression chiller, thus keeping the condenser at controlled temperature quite below the ambient temperature, while the process heat of the sorption module is rejected towards the ambient, by means of a dry cooler. In this way, since the temperature lift between evaporator and condenser of the vapour compression chiller is reduced, the work needed to drive the compressor is lower and the electric COP is enhanced. Depending on the thermal load demand, the produced cooling effect can be either directly provided to the building or partially stored in a latent storage integrated in the evaporator side of the chiller. In parallel, according to the power consumption of the compressor, part of the electric energy produced by the PV, can be stored in the batteries. In this way, once the renewable source is not anymore available, the latent storage can directly provide cooling energy to the load avoiding the operation of the compression chiller. When also the latent storage is fully discharged, the electric energy stored in the batteries can be used to drive the compressor, thus producing the requested cooling effect. Furthermore, a sensible water heat storage is connected to the solar thermal collectors, to take advantage of the renewable source also for the provision of domestic hot water. In such a way, the self-consumption of renewables at building scale is maximized, thus reducing the needs of exchanging power with the grid.

The implementation of proper control strategy is mandatory to operate the system. Indeed, there are some constraints that must be taken into account to maximize the efficient operation of the overall concept.

- The sorption module can be driven only when temperature above 75°C is provided by the solar thermal collectors,
- Below 75°C, the sorption module is not operated and the vapour compression chiller needs to directly dump the condensation heat into the ambient by means of the dry cooler,
- The main operating condition of the vapour compression chiller consists in satisfying the cooling load of the building. Once the cooling power production is higher than the load, it can be stored in the latent storage,
- Similarly, only the excess of electric energy produced by the PV is stored in the batteries.

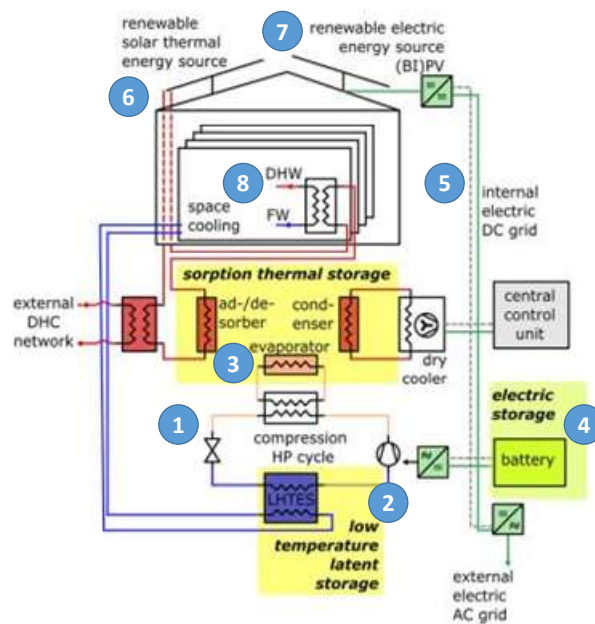


Figure 69 - Schematic of the HYBUILD solution for Mediterranean climate

### 3.7 Continental system model

In Task 4.1 models of the thermal subsystem of the Continental climate are being developed. The focus is on the generation of reduced order and simple models to be integrated in an entire Continental building simulation. The purpose is the development and optimization of high-level control strategies. For doing so, performance maps for different operating modes in the steady state will be derived from the detailed dynamic component models of the thermal sub-system in T3.1 (see Figure 70 and section 3.2 in D3.1). These detailed models (heat pump and RPW-HEX) are being developed in Dymola/Modelica for the design of the sub-system and the low-level control. Figure 70 shows the system sketch of the Continental system at the current state and implemented in the Dymola/Modelica simulation environment.

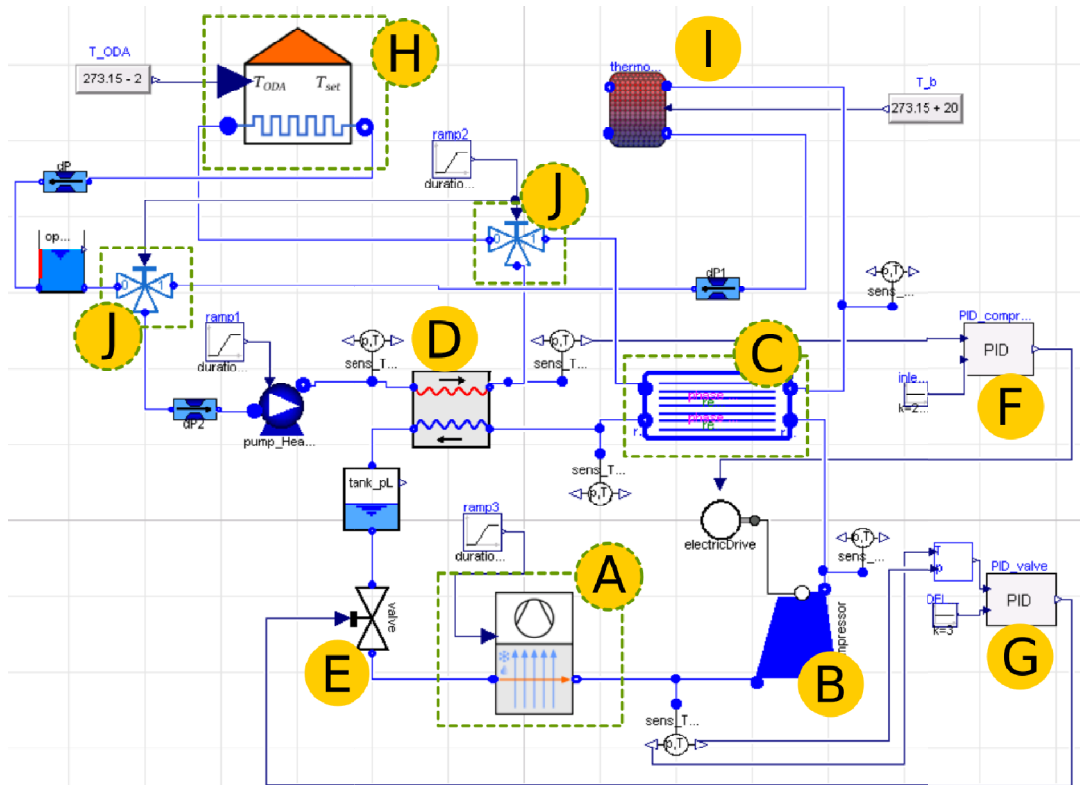


Figure 70 - Schema of Continental thermal sub-system implemented in the Dymola environment in Task 3.1 (taken from Section 3.2 in D3.1). (A) Continental outdoor unit (evaporator), (B) compressor, (C) RPW-HEX, (D) condenser, (E) expansion valve, (F) PID controller compressor, (G) PID controller expansion valve, (H) simplified building model, (I) decentralized DHW storage in the apartment, (J) three-way valves.

The Continental sub-system can provide heating, moderate cooling and DHW. The thermal energy of the DHW is stored in decentralized water storages in the apartment (I, in Figure 70) and in the centralized latent storage (RPW-HEX - C, in Figure 70). The same pipes for DHW and heating/cooling are used to deliver the thermal energy to the apartment. During heating/cooling operation, the RPW-HEX is charged, whereas during DHW generation the RPW-HEX is mainly discharged by the secondary water flow and provides the extra thermal energy to lift the temperature from heating level to DHW level. Hence, the heat pump is able to generate DHW with the same efficiency as for heating.

Different performance maps will be generated which account for the different operating modes of the thermal subsystem. These maps account for the latent storage charging level, the storage operation, i.e. storage charging and discharging, as well as the heat pump operation, i.e. heating, cooling and direct generation of DHW by the HP.

Table 39 summarises the three different operating modes.

Table 39. Operating modes for the Continental performance maps of the thermal sub-system

Mode#	Heat Pump			RPW-HEX	
	Heating	Cooling	DHW	Refr. Charging	Water discharging
1	X			X	
2		X		X	
3			X	X	X

For each mode (each line in Table 39), one performance map will be delivered by T3.1 for the continental thermal sub-system to T4.1. Note that the following limitations have to be considered by using performance maps with the Continental thermal sub-system in T4.1:

- The thermal system will operate slightly different dependent on the exact charging level (state of charge- SoC) of the RPW-HEX. The performance map reproduces/predicts quasi-steady state conditions, derived from the detailed model if the RPW-HEX is charged. Therefore, it represents an average over a range of SoCs (e.g. between 20% and 80%)
- For outdoor temperatures close to and below 0°C, the heating operation will be repeatedly interrupted by a defrost cycle to get rid of the aggregated frost on the evaporator. The defrost cycle is initiated by the low-level controller (heat pump controller) and cannot be influenced by the high level controller. Therefore, the overall performance maps at operating points where frost aggregation will include defrost cycles.
- The SoC of the RPW-HEX has to be calculated/monitored by the high-level controller. It needs to be discussed if the SoC will be monitored by the heat pump controller, too.

In addition, the following points are open and need to be discussed:

- Is the mass flow rate of the heating/cooling distribution system controlled by the high-level (guarantees fixed temperature differences) or the heat pump controller?
- Is the mass flow rate of the DHW distribution system controlled by the high-level controller or the heat pump controller?

Every single performance map consists of the following information:

- Ambient temperature
- Heat load
- Inlet temperature to the heating/cooling/DHW distribution system
- Thermal energy dissipated in the condenser
- Thermal energy dissipated in the RPW-HEX
- Electric energy consumption of the compressor
- Electric energy consumption of the fan

The integration of the thermal subsystem in the building system requires that the high-level controller should communicate either, a set-point temperature for the inlet temperature of the heating/cooling-distribution system or a heating/cooling power to the low level (heat pump) controller. Furthermore, the high-level controller has to decide in which operating modes the thermal sub system should run and should communicate this to the low level (heat pump) controller. Furthermore, there will be a limit of maximum changes of certain operating modes per hour to give the thermal sub-system enough time to establish energy efficient operation. E.g. it should be avoided to turn off the heat pump system (operating mode #7, nearly zero changes/hour) whereas changing between operating mode #1 and #2 will not cause any performance losses if limited by an appropriated number (about 3 changes/hour).

## 4 Conclusions

In complex systems as the ones proposed in HYBUILD, the assessment of the energy consumption and the tuning of control strategies set values are not an easy task. For this reason a numerical model of the overall system, building included, could help to estimate the system consumption, the building loads and test the control strategies before being implemented in the field.

In a first step, detailed models of the single technologies or sub-systems are needed for better understanding the functioning and phenomena at a lower level. However, when dealing with complex systems, the interaction between the different parts becomes crucial and an overview of the whole system is fundamental. Depending on the analysis degree of detail, in this case hourly to yearly basis, simplified models can be also used especially when a common simulation tool is used. For this reason, one of the main aims of the performed activities was to develop simplified models of each component, to be implemented in the overall system simulation model. In particular, the model of the sorption storage was based on a simplified performance map, which covers its main operating conditions. It was derived by the detailed modelling activity in WP3 and will be integrated with the vapour compression chiller for the Mediterranean climate system. The model of the battery was implemented as an equivalent electric circuit, whose main parameters were derived by experimental testing in the lab. The DC bus architecture and its dedicated control strategy proposed for the electric part of the HYBUILD system has been presented, as well: the developed control strategy allows for guaranteeing stable operation of the electric system while following a SoC setpoint provided by an upper level controller. The solution consists of two control loops regulated by two PI controllers.

As for the three predictive control algorithms analysed in the document, the results obtained from the described model prove that RL could be a promising control strategy when appropriately trained. The presented QL implementation can deal with any system model defined in the future, independently of its linearity, as long as it can be computed in a reasonable small time during the iterative learning process. Furthermore, the obtained Q-table can be easily implemented in any small control machine, with low computational resources, making it ideal for real time control.

In the following steps of the project, not only the low level control will be refined but also the high level one. The most significant management strategies have been discussed in order to clearly define the approach towards the optimization process. The first early solutions presented here gave the possibility of exploring a wide set of smart control algorithms, both for mono objective and multi objective optimization problems. The analyses here conducted showed that the techniques adopted for medium or large smart energy contexts, such as urban neighbourhood or industrial facilities, are suitable to smaller ones, like the smart building field, if the system can be represented in a simplified way. In this view, the presented techniques have to be adapted for considering different time scales, users' comfort profiles and field devices equipment.

Further details about the progress of the activities introduced hereby will be given later, as well as the final results of the work presented, and will be reported in the upcoming WP4 deliverables.

## 5 References

- [1] S. Klein, W. Beckham and D. Mitchell, "TRNSYS 17.1: A Transient System Simulation Program," *Solar Energy Laboratory*, 2010.
- [2] G. Gohar, J. Tarragona, A. d. Gracia, C. Fernández, L. F. Cabeza and M. M. Farid, "Model predictive control strategy applied to different types of building for space heating," *To be published*, 2018.
- [3] J. Tarragona, C. Fernández and A. d. Gracia, "Model predictive control applied to a heating system with PV panels and thermal energy storage," *To be published*, 2018.
- [4] A. d. Gracia, R. Barzin, C. Fernández, M. M. Farid and L. F. Cabeza, "Control strategies comparison of a ventilated facade with PCM energy savings, cost reduction and CO<sub>2</sub> mitigation," *Energy and Buildings*, pp. 130:821--828, 2016.
- [5] A. d. Gracia, C. Fernández, A. Castell, C. Mateu and L. F. Cabeza, "Control of a PCM ventilated facade using reinforcement learning techniques," *Energy and Buildings*, Vols. SI: IEA-ECES Annex 31 Special Issue on Thermal Energy Storage, pp. 106:234--242, 2015.
- [6] C. Fernández, F. Manyà, C. Mateu and F. Sole-Mauri, "Approximate dynamic programming for automated vacuum waste collection systems," *Environmental Modelling & Software*, pp. 67:128--137, 2015.
- [7] C. Fernández, F. Manyà, C. Mateu and F. Sole-Mauri, "Modeling energy consumption in automated vacuum waste collection systems," *Environmental Modelling & Software*, vol. Thematic issue on Modelling and evaluating the sustainability of smart solutions., pp. 56:63--73, 2014.
- [8] X. A. Sun and D. Phan, "Some Optimization Models and Techniques for Electric Power System Short-term Operations," in *Wiley Encyclopedia of Operations Research and Management Science*, Wiley, 2014, pp. 1-17.
- [9] N. Ruiz, I. Cobelo and J. Oyarzabal, "A Direct Load Control Model for Virtual Power Plant Management," vol. 24, no. 2, pp. 959-966, May 2009.
- [10] A.-H. Mohsenian-Rad, V. W. Wong, J. Jatskevich, R. Schober and A. Leon-Garcia, "Autonomous Demand-Side Management Based on Game-Theoretic Energy Consumption Scheduling for the Future Smart Grid," *IEEE Transactions on Smart Grid*, vol. 1, no. 3, pp. 320-331, December 2010.
- [11] Z. Zhao, W. C. Lee, Y. Shin and K.-B. Song, "An optimal power scheduling method for demand response in home energy management system," *IEEE Transactions on Smart Grid*, vol. 4, no. 3, pp. 1391-1400, September 2013.
- [12] Y. Liu, N. U. Hassan, S. Huang and C. Yuen, "Electricity cost minimization for a residential smart Grid with distributed generation and bidirectional power transactions," in *2013 IEEE PES Innovative Smart Grid Technologies (ISGT)*, Washington, DC, USA, 2013.
- [13] B. Jiang and Y. Fei, "Smart Home in Smart Microgrid: A Cost-Effective Energy Ecosystem With Intelligent Hierarchical Agents," *IEEE Transactions on Smart Grid*, vol. 6, no. 1, pp. 3-13, January 2015.

- [14] A. J. Conejo, J. M. Morales and L. Baringo, "Real-Time Demand Response Model," *IEEE Transactions on Smart Grid*, vol. 1, no. 3, pp. 236-242, October 2010.
- [15] X. Fang, D. Yang and G. Xue, "Online Strategizing Distributed Renewable Energy Resource Access in Islanded Microgrids," in *2011 IEEE Global Telecommunications Conference (GLOBECOM 2011)*, Kathmandu, Nepal, 2011.
- [16] C. Ibars, M. Navarro and L. Giupponi, "Distributed Demand Management in Smart Grid with a Congestion Game," in *2010 First IEEE International Conference on Smart Grid Communications (SmartGridComm)*, Gaithersburg, MD, USA, 2010.
- [17] W.-D. Zheng and J.-D. Cai, "A multi-agent system for distributed energy resources control in microgrid," in *2010 5th International Conference on Critical Infrastructure (CRIS)*, Beijing, China, 2010.
- [18] C. Coello Coello, G. B. Lamont and D. A. van Veldhuizen, *Evolutionary Algorithms For Solving Multi-Objective Problems*, 2 ed., New York, NY, USA: Springer US, 2007, p. 800.
- [19] M. Alonso, H. Amaris and C. Alvarez-Ortega, "Integration of renewable energy sources in smart grids by means of evolutionary optimization algorithms," *Expert Systems with Applications*, vol. 39, no. 5, pp. 5513-5522, April 2012.
- [20] A. Arabali, M. Ghofrani, M. Etezadi-Amoli, M. S. Fadali and Y. Baghzouz, "Genetic-Algorithm-Based Optimization Approach for Energy Management," *IEEE Transactions on Power Delivery*, vol. 28, no. 1, pp. 162-170, January 2012.
- [21] J. Wang, L. Li, D. Niu and Z. Tan, "An annual load forecasting model based on support vector regression with differential evolution algorithm," *Applied Energy*, vol. 94, pp. 65-70, June 2012.
- [22] K. Po Wang and J. Yuryevich, "Evolutionary programming based algorithm for environmentally constrained economic dispatch," *IEEE Transactions on Power Systems*, vol. 13, no. 2, pp. 301-306, May 1998.
- [23] R. Velik and P. Nicolay, "Grid-price-dependent energy management in microgrids using a modified simulated annealing triple-optimizer," *Applied Energy*, vol. 130, pp. 384-395, October 2014.
- [24] T. Sousa, H. Morais, Z. Vale, P. Faria and J. Soares, "Intelligent Energy Resource Management Considering Vehicle-to-Grid: A Simulated Annealing Approach," *IEEE Transactions on Smart Grid*, vol. 3, no. 1, pp. 535-542, March 2012.
- [25] K. Tanaka, A. Yoza, K. Ogimi, A. Yona, T. Senjyu, T. Funabashi and C.-H. Kim, "Optimal operation of DC smart house system by controllable loads based on smart grid topology," *Renewable Energy*, vol. 39, no. 1, pp. 132-139, March 2012.
- [26] S. A. Arefifar, Y. A.-R. I. Mohame and T. H. El-Fouly, "Comprehensive Operational Planning Framework for Self-Healing Control Actions in Smart Distribution Grids," *IEEE Transactions on Power Systems*, vol. 28, no. 4, pp. 4192-4200, November 2013.
- [27] R. Khorshidi, F. Shabaninia and T. Niknam, "A new smart approach for state estimation of distribution grids considering renewable energy sources," *Energy*, vol. 94, pp. 29-37, January 2016.
- [28] M. H. Athari and M. M. Ardehali, "Operational performance of energy storage as function

- of electricity prices for on-grid hybrid renewable energy system by optimized fuzzy logic controller," *Renewable Energy*, vol. 85, pp. 890-902, January 2016.
- [29] G. Derakhshan, H. A. Shayanfa and A. Kazemi, "The optimization of demand response programs in smart grids," *Energy Policy*, vol. 94, pp. 295-306, July 2016.
- [30] P. Faria, Z. Vale, J. Soares and J. Ferreira, "Demand Response Management in Power Systems Using Particle Swarm Optimization," *IEEE Intelligent Systems*, vol. 28, no. 4, pp. 43-51, August 2013.
- [31] M. A. A. Pedras, T. D. Spooner and I. F. MacGill, "Coordinated Scheduling of Residential Distributed Energy Resources to Optimize Smart Home Energy Services," *IEEE Transactions on Smart Grid*, vol. 1, no. 2, pp. 134-143, September 2010.
- [32] M. Marzband, F. Azarnejadian, M. Savaghebi and J. M. Guerrero, "An Optimal Energy Management System for Islanded Microgrids Based on Multiperiod Artificial Bee Colony Combined With Markov Chain," *IEEE Systems Journal*, vol. PP, no. 99, pp. 1-11, May 2015.
- [33] Y. Zhang, P. Zeng and C. Zang, "Optimization algorithm for home energy management system based on artificial bee colony in smart grid," in *2015 IEEE International Conference on Cyber Technology in Automation, Control, and Intelligent Systems (CYBER)*, Shenyang, China, 2015.
- [34] T. Ghanbarzadeh, S. Goleijani and M. P. Moghaddam, "Reliability constrained unit commitment with electric vehicle to grid using Hybrid Particle Swarm Optimization and Ant Colony Optimization," in *2011 IEEE Power and Energy Society General Meeting*, Detroit, MI, USA, 2011.
- [35] D. P. Reddy, V. V. Reddy and G. T. Manohar, "Optimal renewable resources placement in distribution networks by combined power loss index and whale optimization algorithms," *Journal of Electrical Systems and Information Technology*, p. In Press, June 2017.
- [36] M. Bhoje, S. N. Purohit, I. N. Trivedi, M. H. Pandya, P. Jangir and N. Jangir, "Energy management of Renewable Energy Sources in a microgrid using Cuckoo Search Algorithm," in *2016 IEEE Students' Conference on Electrical, Electronics and Computer Science (SCEECS)*, Bhopal, India, 2016.
- [37] M. Ehrgott, *Multicriteria Optimization*, 2 ed., Berlin: Springer, 2005.
- [38] S. S. Bhagavatula, S. G. Sanjeevi, D. Kumar and C. K. Yadav, "Multi-Objective Indicator Based Evolutionary Algorithm for Portfolio optimization," in *2014 IEEE International Advance Computing Conference (IACC)*, Gurgaon, India, 2014.
- [39] K. Deb, A. Pratap, S. Agarwal and T. Meyarivan, "A fast and elitist multiobjective genetic algorithm: NSGA-II," *IEEE Transactions on Evolutionary Computation*, vol. 6, no. 2, pp. 182-197, August 2002.
- [40] E. Zitzler, M. Laumanns and L. Thiele, "SPEA2: Improving the strength pareto evolutionary algorithm," ETH Library, 2001.
- [41] R. Shahin and A. Shenfield, "CMA-PAES: Pareto archived evolution strategy using covariance matrix adaptation for Multi-Objective Optimisation," in *2012 12th UK Workshop on Computational Intelligence (UKCI)*, Edinburgh, UK, 2012.
- [42] N. Ghorbani, A. Kasaeian, A. Toopshekan, L. Bahrami and A. Maghami, "Optimizing a

- hybrid wind-PV-battery system using GA-PSO and MOPSO for reducing cost and increasing reliability,” *Energy*, vol. 154, pp. 581-591, 1 July 2018.
- [43] M. Lianbo, C. Shi, W. Xingwei, H. Min, S. Hai, H. Xiaoxian and S. Yuhui, “Cooperative two-engine multi-objective bee foraging algorithm with reinforcement learning,” *Knowledge-Based Systems*, vol. 133, pp. 278-293, October 2017.
- [44] S. Mirjalili, “Dragonfly algorithm: a new meta-heuristic optimization technique for solving single-objective, discrete, and multi-objective problems,” *Neural Computing and Applications*, vol. 27, no. 4, pp. 1053-1073, May 2016.
- [45] B. R. Pereira Junior, A. M. Cossi and J. R. Mantovani, “Multiobjective Short-Term Planning of Electric Power Distribution Systems Using NSGA-II,” *Journal of Control, Automation and Electrical Systems*, vol. 24, no. 3, pp. 286-299, June 2013.
- [46] S. K. A. Attari, M. R. Shakarami and E. S. Pour, “Pareto optimal reconfiguration of power distribution systems with load uncertainty and recloser placement simultaneously using a genetic algorithm based on NSGA-II,” in *2016 21st Conference on Electrical Power Distribution Networks Conference (EPDC)*, Karaj, Iran, 2016.
- [47] D. Buoro, M. Casisi, A. De Nardi, P. Pinamonti and M. Reini, “Multicriteria optimization of a distributed energy supply system for an industrial area,” *Energy*, vol. 58, pp. 128-137, September 2013.
- [48] M. G. Ippolito, M. L. Di Silvestre, E. Riva Sanseverino, G. Zizzo and G. Graditi, “Multi-objective optimized management of electrical energy storage systems in an islanded network with renewable energy sources under different design scenarios,” *Energy*, vol. 64, pp. 648-662, January 2014.
- [49] American Society of Heating, Refrigerating and Air-Conditioning Engineers, Inc, Ashrae handbook of fundamentals, Atlanta, USA: Inch-Pound Edition, 2009, pp. 6-9.
- [50] American Society of Heating, ASHRAE® HANDBOOK FUNDAMENTALS, Atlanta: Refrigerating and Air-Conditioning Engineers, Inc., 2009.
- [51] W. Stoecker and J. Jones, Refrigeration and Air Conditioning, 2 ed., McGraw-Hill, 1983.
- [52] A. Arista, M. Ferraro, F. Sergi and V. Antonucci, “Dynamic Model of High-Performance Li-Ion Cells (LIFEP04, LI-POLYMERS and LIFP6 NBC) in Different Load Conditions,” in *6th International Conference on Experiments/Process/System Modeling/Simulation/Optimization*, Athens, 2015.
- [53] Solar Energy Laboratory, “TRNSYS 17. Volume 4 – Mathematical Reference,” in *Type 47: Shepherd and Hyman Battery models*, vol. 4, University of Wisconsin-Madison, 2012, p. par. 4.2.1.
- [54] Eurostat, 2015. [Online]. Available: [http://ec.europa.eu/eurostat/statistics-explained/images/9/9c/Final\\_energy\\_consumption\\_in\\_the\\_residential\\_sector\\_by\\_type\\_of\\_end-use%2C\\_EU-28%2C\\_2015.png](http://ec.europa.eu/eurostat/statistics-explained/images/9/9c/Final_energy_consumption_in_the_residential_sector_by_type_of_end-use%2C_EU-28%2C_2015.png). [Accessed 2017 11 9].
- [55] G. Andersson and M. Geidl, “A modelling and optimisation approach for multiple energy carrier power flow,” *Power Tech, IEEE 2005*, no. doi:10.1109/PTC.2005.4524640, pp. 1-7, June 2005.
- [56] Elsevier, “ScienceDirect.com | Science, health and medical journals, full text articles and

- books,," November 2015. [Online]. Available: <http://www.sciencedirect.com/>.
- [57] T. Krause, G. Andersson, K. Frohlich and A. Vaccaro, "Multiple-Energy Carriers: Modeling of Production, Delivery, and Consumption," *Proceedings of the IEEE*, vol. 99, no. 1, pp. 15-27, 2011.
- [58] "OPC Foundation," November 2015. [Online]. Available: <https://opcfoundation.org/>.
- [59] "IEC Smart Grid - IEC Standards," November 2015. [Online]. Available: <http://www.iec.ch/smartgrid/standards/>.
- [60] "The Modbus Organization," November 2015. [Online]. Available: <http://www.modbus.org/>.
- [61] "openADR Alliance," November 2015. [Online]. Available: <http://www.openadr.org/>.
- [62] "BACnet Website," November 2015. [Online]. Available: <http://www.bacnet.org/>.
- [63] P. Siano, "Demand response and smart grids - A survey," *Renewable and Sustainable Energy Reviews*, vol. 30, pp. 461-478, February 2014.
- [64] I. S. Bayram and T. S. Ustun, "A survey on behind the meter energy management systems in smart grid," *Renewable and Sustainable Energy Reviews*, vol. 72, pp. 1208-1232, May 2017.
- [65] C. Eid, P. Codani, Y. Perez, J. Reneses and R. Hakvoort, "Managing electric flexibility from Distributed Energy Resources: A review of incentives for market design," *Renewable and Sustainable Energy Reviews*, vol. 64, pp. 237-247, October 2016.
- [66] M. Irfan, J. Iqbal, A. Iqbal, Z. Iqbal, R. A. Riaz and A. Mehm, "Opportunities and challenges in control of smart grids – Pakistani perspective," *Renewable and Sustainable Energy Reviews*, vol. 71, pp. 652-674, May 2017.
- [67] X. Fang, S. Misra, G. Xue and D. Yang, "Smart Grid — The New and Improved Power: Grid A Survey," *IEEE Communications Surveys & Tutorials*, vol. 14, no. 4, pp. 944-980, December 2011.
- [68] M. A. Mohamed, A. M. Eltamaly, H. M. Farh and A. I. Alolah, "Energy management and renewable energy integration in smart grid system," in *2015 IEEE International Conference on Smart Energy Grid Engineering (SEGE)*, Oshawa, ON, Canada, 2015.
- [69] C. Zhang, Y. Ding, J. Ostergaard, H. W. Bindner, N. C. Nordentoft, L. H. Hansen, P. Brath and P. D. Cajar, "A flex-market design for flexibility services through DERs," in *2013 4th IEEE/PES Innovative Smart Grid Technologies Europe (ISGT EUROPE)*, Lyngby, Denmark, 2013.